Topological aspects of
two-dimensional quantum systems

UNIVERSITY OF LEEDS

Suvabrata De

School of Physics and Astronomy

University of Leeds

I confirm that the work submitted in this thesis is my own, except where work which has formed part of jointly authored publications has been included. The contribution of myself and the other authors to this work has been explicitly indicated below. I confirm that appropriate credit has been given within the thesis where reference has been made to the work of others.

Publications

DE LISLE, J., DE, S., ALBA, E., BULLIVANT, A., GARCIA-RIPOLL, J.J., LAHTINEN, V. & PACHOS, J.K. (2014). Detection of Chern numbers and entanglement in topological two-species systems through subsystem winding numbers. *New Journal of Physics*, **16**, 083022. (de Lisle *et al.*, 2014).

Chapter 6 is based on results from this paper. The main new result obtained is the decomposition of the Chern number of topological four-component insulators and superconductors into subsystem winding numbers. A proof of the decomposition for superconductors was done collaboratively with the co-authors, while I independently proved the decomposition for insulators. Numerical verification of the decomposition was provided by Emilio Alba. The idea of measuring the component entanglement spectra of these systems was proposed by myself and developed in collaboration with Dr. Ville Lahtinen. The bottom right plot of figure 6.1 was produced by myself, while the other plots in this figure were produced by Emilio Alba. The top left and bottom right plots of figure 6.2 were produced by Dr. Ville Lahtinen and myself, respectively, while the other plots in this figure were produced by Emilio Alba.

Submitted for publication

DE, S. & SPILLER, T. (2014). A protected vortex exciton qubit. *arXiv preprint arXiv:1405.4446*. (De & Spiller, 2014).

Chapters 3 and 4 are based on a proposal for a protected qubit (and universal fault-tolerant quantum computation with such qubits) described in this paper. The vast majority of this work was done by myself, with input and guidance from Prof. Timothy P. Spiller.

To ma and baba

Acknowledgements

Abstract

In part I, we describe a protected qubit which is realized in a two-dimensional array of Josephson junctions. Our construction is the magnetic analogue of ('dual' to) a suggestion of a superconducting current mirror qubit (Kitaev, 2006b). Our proposal therefore inherits the intrinsic fault-tolerance of the current mirror qubit, but may perform better than it in the laboratory, since magnetic noise is generally less of a problem than electric noise. We adapt the scheme for universal fault-tolerant quantum computation proposed by Kitaev to our construction.

In part II, we describe a method of detecting the Chern number and entanglement properties of topological four-component free-fermion systems in cold atom experiments. We show that the Chern number of these systems decomposes into a sum of subsystem winding numbers which can be measured from time-of-flight images. Such images also enable the degree of subsystem entanglement in, and the component entanglement spectra of, these systems to be measured. The method is applied to the quantum spin-Hall insulator and a staggered topological superconductor. We find that the phase diagrams are accurately reproduced, except when the subsystems are highly entangled.

Abbreviations

2D	Two-dimensional
BCS	Bardeen-Cooper-Schrieffer
BKT	Berezinskii-Kosterlitz-Thouless
BZ	Brillouin zone
CC	Classical computation
CPB	Cooper-pair box
ES	Entanglement spectrum
KCMQ	Kitaev's current mirror qubit
MQC	Macroscopic quantum coherence
RF	Radio frequency
SQUID	Superconducting quantum interference device
QC	Quantum computation
QED	Quantum electrodynamics
QI	Quantum information
QSH	Quantum spin-Hall
QSHI	Quantum spin-Hall insulator
TOF	Time-of-flight
TQC	Topological quantum computation
VEQ	Vortex exciton qubit

Contents

List of Figures

Introduction

The title of this thesis is somewhat generic, and reflects the fact that this work consists of two distinct topics which have overlap only at a broad conceptual level. Both topics are concerned with two-dimensional (2D) many-body quantum systems, and are influenced by topological considerations to varying degrees. The thesis is divided into two parts; below, we say a little about each part.

PART I

Part I of this thesis is entitled 'A protected vortex exciton qubit' and consists of four chapters. The aim in this part is to describe an *intrinsically fault-tolerant* qubit which is realized in a 2D array of Josephson junctions, and the means to perform universal fault-tolerant quantum computation (QC) with such qubits (De & Spiller, 2014). This scheme, in which the suppression of errors is achieved at the hardware level, is inspired by an approach to QC known as *topological QC* (TQC) (Kitaev, 2003). TQC in its 'purest' form consists of storing and processing information using the properties of *anyons* – exotic quasiparticles which can appear in certain 2D many-body systems. Nonetheless, it has become clear that even in the absence of anyons, robust information storage and processing is possible in certain quantum hardware. Superconducting circuits are particularly promising on this front (Douçot & Ioffe, 2012), and our scheme is an example of this.

Chapter 1 provides background material on QC and superconductivity – in particular some elementary aspects of Josephson junctions – which is required to follow the rest of part I. We also take a look at basic 'conventional' superconducting qubits, and touch on the topological approach for contrast.

In chapter 2, we review a protected qubit devised by Kitaev (Kitaev, 2006b). The reason for this is that the qubit that we propose can be regarded as the magnetic analogue or 'dual' of Kitaev's idea, and so by reviewing it we can contrast the two schemes. In particular, the possible shortcomings of Kitaev's qubit with respect to its interaction with its environment – and the possible improvements our construction offers on this matter – are discussed. We examine in detail how a two-fold ground state degeneracy (which can be used to realize a qubit) emerges in the system that Kitaev considers.

Chapter 3 deals with the realization of our proposed qubit in a 2D array of Josephson junctions. We first employ a path integral description to reveal the importance of topological excitations known as *vortices* in the system. A subsequent analysis in terms of a Hamiltonian shows that in an appropriate parameter regime, a protected qubit emerges

which mirrors Kitaev's qubit. This chapter is based on results from (De & Spiller, 2014), and provides extra details of the analysis found therein.

A scheme for universal fault-tolerant QC using our proposed qubit is explained in chapter 4. This scheme was first discussed in (Kitaev, 2006b), and we adapt the gates used by Kitaev to our construction. To this end, we discuss some novel circuit elements, such as a vortex harmonic oscillator. This chapter is based on results from (De & Spiller, 2014), and elaborates on the arguments found therein.

PART II

Part II is entitled 'Detection of the Chern number and entanglement in topological four-component systems through subsystem winding numbers' and consists of two chapters. The aim in this part is to describe a method of measuring a topological invariant known as the *Chern number* which characterizes certain 2D *topological phases of matter* – phases of matter which can only be understood by appealing to topology. Such phases lack local order parameters, which makes the experimental verification of these phases quite challenging in general. The method we propose is tailored for experiments with cold atoms in optical lattices, which is one of the most promising routes for realizing topological phases. We also show how entanglement features – in particular *component entanglement spectra* (Legner & Neupert, 2013; Li & Haldane, 2008) – can be accessed in the 'four-component' systems that we consider. Along with the fundamental interest in topological phases, it is important to have diagnostic tools for topological matter as a first step towards applications, for instance in TQC.

Chapter 5 is an introduction to topological phases of matter. We focus on 2D *free-fermion* systems – namely, topological insulators and superconductors – and discuss two tools which are used to characterize such systems: the (first) Chern number and the entanglement spectrum. As a warm-up for the following chapter, we then describe how the Chern number of 'two-component' insulators (Alba *et al.*, 2011) and superconductors (Pachos *et al.*, 2013) can be extracted in cold atom experiments from time-of-flight images.

In chapter 6, we explain in detail how the Chern number of four-component insulators and superconductors can be detected. We first demonstrate that the Chern number of these systems decomposes into a sum of *subsystem winding numbers* which can be measured using the observables we consider. These observables also allow the degree of subsystem entanglement in, and the component entanglement spectra of, these systems to be measured. We find that the decomposition only fails when the subsystems are maximally entangled, and this is confirmed by numerical studies of the Kane-Mele model (Kane & Mele, 2005) and a recently introduced topological superconductor (Pachos *et al.*, 2013). This chapter is based on, and in places expands on, results published in (de Lisle *et al.*, 2014).

PART I

A protected vortex exciton qubit

CHAPTER 1

Quantum computation with superconductors

Few can possibly disagree with the statement that quantum information (QI) is one of the most dynamic fields of research in physics today. Born out of the need to understand what *quantum* theories of information processing and communication would entail (Bennett *et al.*, 1984; Deutsch, 1985; Schumacher, 1995), its influence has now spread far and wide. QI theoretic concepts are now being used to address problems as diverse as the black hole information paradox (Hayden & Preskill, 2007; Verlinde & Verlinde, 2013), understanding the properties of quantum many-body systems (Amico *et al.*, 2008) and the extent to which quantum coherence is harnessed in biological systems (Lambert *et al.*, 2013).

While a QI way of thinking has been permeating through disparate areas of physics, impressive strides have been made in realizing one of the holy grails of the field: building a large-scale quantum computer (Ladd *et al.*, 2010). By harnessing the laws of quantum mechanics, such computers promise to perform certain tasks – such as factoring large composite integers (Shor, 1994, 1997) and simulating quantum systems (Feynman, 1982; Lloyd, 1996) – far more efficiently than classical computers. However, despite much progress, the prospect of large-scale QC still remains a remote goal. The biggest obstacle to this goal is how to counteract the ever present effects of *decoherence*, and the inevitable errors which occur when attempting to control quantum systems. Almost two decades worth of research into quantum fault-tolerance has taught us that theoretically – and increasingly, experimentally – these problems are not insurmountable. One solution is to employ 'software' error correction, where errors are actively detected and corrected during the computation (Shor, 1995, 1996; Steane, 1996). An alternative method is to find robust or *topologically protected* quantum hardware which is effective in suppressing errors (Kitaev, 2003; Nayak *et al.*, 2008; Pachos, 2012), while hybrids of these two approaches, such as surface codes (Fowler *et al.*, 2012; Raussendorf & Harrington, 2007), are also conceivable.

One of the front runners in the race to provide reliable hardware for QC [1] is *superconducting quantum circuits* (Clarke & Wilhelm, 2008; Devoret & Schoelkopf, 2013). Some of the advantages of such circuits are the relative ease with which they can be 'tuned', the fact that superconducting electronics is already a mature field and the relative ease with which they can be controlled. These circuits are composed of standard circuit elements such as capacitors and *Josephson junctions*, which explains the ease of tunability, while the ability of superconductors to display coherence on macroscopic scales – known as *macroscopic quantum coherence* (MQC) (Leggett, 1980) – is the reason why such circuits can be manipulated with relative ease. Furthermore, the macroscopic nature of superconducting qubits means that they may be easier to scale up than competing microscopic hardware. The spectacular progress in coherence times and quantum nondemolition measurements in recent years clearly indicates the potential of the field (Devoret & Schoelkopf, 2013).

The next section of this chapter deals with the basics of the gate or circuit model of QC. We explain what it means to quantum compute and the necessary and sufficient conditions needed to do so. The standard reference for QC and QI is (Nielsen & Chuang, 2010), while many concise and informative introductions exist, such as (Spiller *et al.*, 2005). Section 1.2 is an introduction to some key aspects of superconductivity that are at the heart of the first part of this thesis. In particular, we explain the nature of the superconducting order parameter and the Josephson junction. Classic references on superconductivity are (Schrieffer, 1999; Tinkham, 2004), while a modern and accessible account (which stresses the importance of MQC) is provided by (Annett, 2004). In section 1.3, we build on the foundations of the first two sections to give a brief overview of some different types of superconducting qubits that exist at present.

1.1 Quantum computation

The following is a brief overview of what QC is and what is needed in practice to achieve it.

1.1.1 The gate model

The gate model of QC [2] is named so due to the features it shares with the gate model of classical computation (CC). Given this, let us take a moment to recap the salient features of the classical model. The building blocks of a classical computer are *bits*, which can take the values 0 or 1. CC consists of a string of bits being mapped to another string, either deterministically or probabilistically, with the map being referred to as an *algorithm*. Any algorithm can be broken down into a series of elementary operations – known as *logic gates*

---

[1] Of course, this is not a race in a sporting sense. Some of the competitors may well 'join forces' to make hybrid architectures in order to cross the line. See for instance (Xiang *et al.*, 2013).

[2] While there are now other models of QC (see (Spiller *et al.*, 2005)), the gate model remains the 'standard' model of QC; it is the only model that we discuss in this thesis.

– on the bits.

The building blocks of a quantum computer are *qubits*, quantum systems that each live in a 2D Hilbert space spanned by $\{|0\rangle, |1\rangle\}$, which is known as the *computational basis*. If the computer consists of a register of N qubits, its state will live in a 2^N-dimensional Hilbert space spanned by $\{|0\rangle, |1\rangle\}^{\otimes N}$. QC consists of an initially prepared state being transformed to a new state by some unitary transformation (belonging to $SU(2^N)$), and then some of the qubits (or all) being measured. The details of the three stage process of preparation, evolution and measurement is determined by the quantum algorithm to be run. Loosely speaking, quantum computers derive an advantage from *quantum parallelism*: the ability to compute simultaneously on many different bit strings, by virtue of their ability to be in a superposition of different bit strings.

Just as any classical algorithm can be decomposed into a series of fundamental gates, in the quantum case, there exists *universal* sets of gates, which can be used to run an arbitrary quantum algorithm. To perform universal QC, it suffices to be able to implement arbitrary single-qubit unitaries and some *entangling* operation on pairs of qubits. For instance, the gate set HADAMARD (H), PHASE (U_P), $\pi/8$ z-rotation ($U_{\pi/8}$) and CNOT (U_CNOT) is universal, and has the matrix representation

$$H = \frac{1}{\sqrt{2}} \begin{pmatrix} 1 & 1 \\ 1 & -1 \end{pmatrix}, U_\mathrm{P} = \begin{pmatrix} 1 & 0 \\ 0 & i \end{pmatrix}, U_{\pi/8} = \begin{pmatrix} 1 & 0 \\ 0 & \exp(i\pi/4) \end{pmatrix}, U_\mathrm{CNOT} = \begin{pmatrix} 1 & 0 & 0 & 0 \\ 0 & 1 & 0 & 0 \\ 0 & 0 & 0 & 1 \\ 0 & 0 & 1 & 0 \end{pmatrix}.$$

(1.1)

The single-qubit gates are written in the computational basis, while CNOT is written in the $\{|00\rangle, |01\rangle, |10\rangle, |11\rangle\}$ basis (the first and second qubits are the control and target, respectively). In practice, the gate set that is chosen is determined by the ease and accuracy of implementation, and is therefore hardware specific. In chapter 4, we discuss an alternative to (1.1) in the context of our proposed superconducting qubit.

1.1.2 The DiVincenzo check-list

While the theoretical requirements to perform QC are relatively easy to state, the practical challenges involved in realizing large-scale QC are daunting. David DiVincenzo proposed the following check-list (DiVincenzo, 2000) (presented below in abbreviated form) which a quantum processor must satisfy if it is to be fully functional:

1. **The system must be scalable and possess well-characterized qubits.** A qubit is well-characterized if its physical parameters are precisely known, for instance, the 'free' Hamiltonian of the qubit. Clearly, it is important to know this since the evolution of the register is determined by the total Hamiltonian of the system. Since useful QC (for tasks such as factoring) requires many ($\mathcal{O}(10^4)$) qubits, the issue of

scalability has to be addressed. The addition of just an extra qubit to the register can introduce potential problems, such as increasing the complexity of gate implementations. Scalability is thus a highly non-trivial problem.

2. **The ability to initialize the register to some desired state.** Clearly, it is important to know the state of the processor at the beginning of the computation. The two main paths to initialization are via cooling to the ground state or by performing a measurement, which projects into the required state or another which differs from it by a unitary rotation.

3. **Coherence must be maintained while gates are being applied.** The inevitable coupling between a quantum computer and its environment will result in a loss of coherence over time – a process known as decoherence. It is therefore important that the system maintains its coherence during the evolution stage, so that the fidelity of the final state (with respect to the final state prescribed by the algorithm) is reasonable. For large-scale computations, unless decoherence is suppressed at the hardware level, this requirement almost certainly calls for software error correction (Shor, 1995, 1996; Steane, 1996) (see section 1.3.3).

4. **Availability of a universal set of gates.** The algorithm to be run has to be physically realizable. The minimum requirement for an arbitrary algorithm to be implemented is a universal set of gates, such as (1.1).

5. **High fidelity qubit-specific measurements.** These are necessary to readout the result of the computation.

1.2 Superconductivity basics

We now give a brief overview of some basic aspects of superconductivity [3] which are needed to follow chapters 2, 3 and 4.

1.2.1 The superconducting order parameter

Certain metals when cooled below a critical temperature undergo a spectacular phase transition and become *superconducting*: upon cooling, the electrons in a sample suddenly pair-up into so-called *Cooper-pairs* which carry charge $-2e$ [4] and zero spin, and the pairs undergo a condensation of sorts. A superconductor can thus be regarded as a condensate, which can be represented by a complex *macroscopic wave function*, $\psi(\vec{r})$. More formally, this is the order parameter of the Ginzburg-Landau theory of superconductivity, which was shown by

---

[3] We restrict our attention here to classic low temperature *s*-wave superconductors.

[4] We adopt the convention that *e* is the elementary charge i.e. it is positive. Some authors prefer to say that Cooper-pairs carry charge 2*e*, and thus treat *e* as a negative quantity.

Figure 1.1: A Josephson junction, which consists of two superconducting regions separated by a thin insulating barrier, or in general, a 'weak link'. The superconductors on the left and right of the junction have condensate phases θ_L and θ_R, respectively.

Gor'kov (Gorkov, 1959) to be derivable from the microscopic Bardeen-Cooper-Schrieffer (BCS) theory of superconductivity (Bardeen *et al.*, 1957) in a suitable limit. Some key features of superconductors are their ability to carry current without dissipation (a so-called *supercurrent*) and the energy gap that exists between the condensed ground state and quasiparticle excitations.

The macroscopic wave function can be written as

$$\psi(\vec{r}) = \sqrt{n(\vec{r})}e^{i\theta(\vec{r})}, \tag{1.2}$$

where $\vec{r}$ is a point in the superconductor, $n(\vec{r})$ is the local density of Cooper-pairs in the condensate and $\theta(\vec{r})$ is the condensate phase. It is the existence of this phase which leads to the appearance of quantum effects on a macroscopic scale, as we shall see below.

1.2.2 The Josephson junction

In 1962, Josephson made a startling discovery regarding electron tunnelling between two different superconductors (Josephson, 1962). He found that a system consisting of two superconductors separated by a thin insulating barrier (see figure 1.1) can support the coherent transfer of Cooper-pairs from one superconductor to the other, even in the *absence* of an applied voltage. Such a system now bears his name and is known as a Josephson junction, while the effect is known as the *DC Josephson effect*. The Cooper-pair current from the superconductor on the left to the one on the right is given by

$$I = I_c \sin\Theta, \tag{1.3}$$

where I_c is the critical current of the junction (the maximum dissipation-less current that the junction can sustain) and Θ is the gauge invariant phase difference across the junction. Θ is defined to be

$$\Theta \equiv \theta_R - \theta_L + \frac{2e}{\hbar}\int_L^R \vec{A} \cdot d\vec{r}, \tag{1.4}$$

where θ_L and θ_R are the condensate phases of the superconductors on the left and right, respectively, and $\vec{A}$ is the vector potential in the system. The line integral above is taken along a path through the insulating barrier, from its left edge to its right edge.

One way to set up a phase difference between two superconducting regions is to thread an external flux Φ_{ex} through a superconducting ring which is interrupted by a tunnel junc-

1. Quantum computation with superconductors
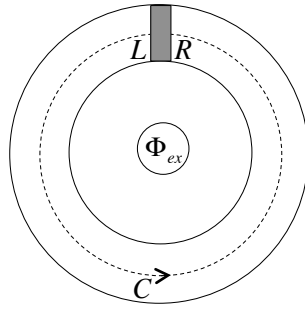
Figure 1.2: A superconducting ring interrupted by an insulating barrier is threaded by an external flux, Φ_{ex}. The flux induces a phase difference across the junction.

tion, as shown in figure 1.2. From Ginzburg-Landau theory, we know that the current inside a superconductor is proportional to $\vec{\nabla}\theta + (2e/\hbar)\vec{A}$, which means that $\vec{\nabla}\theta = -(2e/\hbar)\vec{A}$ in the bulk of a superconductor, since there is no current there [5]. Non-zero Φ_{ex} (a finite vector potential) therefore gives rise to a phase twist within the superconducting ring, so that the phases on either side of the junction must be different. The phase difference is simply

$$\theta_R - \theta_L = \int_C \vec{\nabla}\theta \cdot d\vec{r} = -\frac{2e}{\hbar}\int_C \vec{A}\cdot d\vec{r}, \tag{1.5}$$

where the path C (the dashed contour in figure 1.2) goes through the bulk of the superconductor. The gauge invariant phase difference is thus

$$\Theta = -\frac{2e}{\hbar}\int_C \vec{A}\cdot d\vec{r} + \frac{2e}{\hbar}\int_L^R \vec{A}\cdot d\vec{r} = -\frac{2e}{\hbar}\oint \vec{A}\cdot d\vec{r} = 2\pi\frac{\Phi_{\text{ex}}}{\Phi_0}, \tag{1.6}$$

where $|\Phi_0| = h/(2e)$ is the *flux quantum* [6]. In general, the total flux through the ring will contain a contribution from the supercurrent induced flux, but assuming that the self-inductance of the ring is negligible (which is true for small enough rings), this contribution can be neglected so that the total flux is Φ_{ex}. The Cooper-pair tunnelling current is thus

$$I = I_c \sin\left(\frac{2\pi\Phi_{\text{ex}}}{\Phi_0}\right). \tag{1.7}$$

A Josephson junction acts as a perturbation which couples two superconducting regions, and the energy associated with this coupling can be derived by looking at the split-ring geometry introduced above. From Faraday's law, we know that as the external flux through the ring is increased from zero to Φ_{ex}, an emf is induced around the ring. The work done by the induced emf is thus equal to the energy of the junction, since there is no dissipation for currents less than I_c. The rate at which work is done (the power) is given by the product of

---

[5]This is due to the *Meissner effect*: electromagnetic fields are screened in the bulk of a superconductor.

[6]For a superconducting ring with no interruptions, the fact that the macroscopic wave function is single-valued – i.e. $\oint \vec{\nabla}\theta \cdot d\vec{r} = -(2e/\hbar)\oint \vec{A}\cdot d\vec{r} = 2\pi n$, where n is an integer – implies that the total flux enclosed by the ring must be quantized in units of the flux quantum.

the emf and the Josephson current, and so using (1.6) and (1.7) the junction energy is seen to be

$$\int I \frac{d\Phi}{dt} \, dt = \frac{\hbar I_c}{2e} \int_0^\Theta \sin\theta \, d\theta = E_J \left(1 - \cos\Theta\right), \tag{1.8}$$

where $E_J \equiv \Phi_0 I_c / (2\pi)$ is the *Josephson coupling energy*. The constant E_J is often dropped from the above expression, and this will be the case throughout this thesis, unless stated otherwise.

The DC Josephson effect forms the basis for superconducting quantum interference devices (SQUIDs) (Tinkham, 2004). In the simplest SQUID, a ring threaded by an external flux is split into two halves by two junctions, with current being able to enter one half and leave the other half. The currents through the two junctions display interference, which is reminiscent of Young's slits in optics. Here, the interference arises due to the path dependent phases picked up by Cooper-pairs, which depends on the external flux. Such SQUIDS enable a tunable Josephson energy to be realized, which often comes in handy in superconducting circuits.

The second effect that Josephson predicted is known as the *AC Josephson effect*: a constant voltage V across a junction gives rise to a phase difference which varies linearly with time

$$\frac{d\Theta}{dt} = \frac{2eV}{\hbar}. \tag{1.9}$$

The above relation implies (via (1.3)) that the Josephson current alternates sinusoidally with frequency $2eV/\hbar$. Furthermore, the appearance of Planck's constant indicates that quantum mechanics is at work, which demonstrates that the phenomenon is an example of MQC, which was mentioned in the introduction. The non-linear and non-dissipative properties of a Josephson junction make it a unique circuit element and a key building-block of superconducting qubits, which we discuss next.

1.3 Superconducting qubits

In describing the Josephson effects, the phase difference Θ was treated as a semi-classical variable. However, under suitable conditions, its quantum mechanical nature becomes evident. From (1.6), one can see that Θ is essentially a dimensionless flux, and it turns out that its conjugate variable is electric charge – the charge on a junction [7]. Indeed, in the previous section, the capacitive nature of a junction was not considered; the capacitance was taken to be so large that Cooper-pairs could move freely across the junction with very little energy penalty. As a result, the junction charge would have large fluctuations, and so from the uncertainty principle, Θ would have small fluctuations, which justifies the semi-classical treatment. However, for low capacitance junctions, the charging energy associated with charge transfer across a junction becomes sizeable. Such junctions exist in an 'insulat-

---

[7]In section 1.3.2 where we discuss flux qubits, we show that flux and charge are conjugate variables by looking at the Lagrangian of a superconducting circuit.

ing' state where the charge has small fluctuations, with the phase difference now possessing large fluctuations.

The quantum behaviour of the charge and flux degrees of freedom is exploited in the design of superconducting qubits. Originally, three basic types known as charge (Bouchiat *et al.*, 1998; Nakamura *et al.*, 1999), flux (Chiorescu *et al.*, 2003; Friedman *et al.*, 2000; Mooij *et al.*, 1999; Van der Wal *et al.*, 2000) and phase (Martinis *et al.*, 2002) qubits were proposed. From these, new generations of qubits with improved coherence have evolved, such as the Quantronium (Vion *et al.*, 2002), Transmon (Koch *et al.*, 2007a) and Fluxonium (Manucharyan *et al.*, 2009) qubits. The advent of circuit quantum electrodynamics (QED) (Blais *et al.*, 2004; Wallraff *et al.*, 2004) – named due to the similarities with the field of cavity QED – where superconducting qubits are coupled to transmission line resonators offers a promising route to scalable QC. In topologically protected superconducting circuits (Gladchenko *et al.*, 2008; Ioffe & Feigelman, 2002; Ioffe *et al.*, 2002; Kitaev, 2006b), information is stored in robust global degrees of freedom, in contrast to the local encoding of information employed by 'conventional' superconducting qubits.

In sections 1.3.1 and 1.3.2, we discuss the most basic charge and flux qubits, respectively, while in section 1.3.3, we provide some motivation for the study of topologically protected superconducting qubits. Reviews of conventional superconducting qubits – and schemes to couple qubits, which we will not discuss – can be found in (Clarke & Wilhelm, 2008; Girvin, 2011; Makhlin *et al.*, 2001; Zagoskin & Blais, 2008), while (Douçot & Ioffe, 2012) reviews the implementation of protected qubits in superconducting circuits.

1.3.1 Charge qubits

Charge qubits operate in the regime where charge fluctuations are small, so that charge is the relevant variable and is manipulated. The key element in such qubits is a low capacitance junction, which possesses not only a Josephson energy, but also a non-negligible electrostatic charging energy. This latter energy scale corresponds to the energy needed to place charges $\pm e$ on the junction 'plates'.

The most basic charge qubit is realized by a small superconducting island – known as a Cooper-pair 'box' (CPB), as shown in figure 1.3 – coupled by a junction with capacitance C_J and coupling energy E_J to a superconducting electrode. This electrode acts as a reservoir, from which n Cooper-pairs can tunnel onto the CPB, and back again. The island has to be small, so that its capacitance is small enough to result in a charging energy which is much larger than the thermal energy, kT. A control gate voltage V_g is also coupled to the system, with the help of a gate capacitor with capacitance C_g. This polarizes the CPB and sets up a bias, i.e. it induces an offset (or gate) charge of $C_g V_g \equiv 2en_g$ [8]. For the system to function as a charge qubit, the (single electron) charging energy $E_C \equiv e^2/(2C_\Sigma) - C_\Sigma \equiv C_g + C_J$ is the total capacitance of the CPB – must dominate E_J. This is a consequence of the uncertainty

---

[8]A pictorial depiction of a classical charge configuration in this system can be found in (Büttiker, 1987).
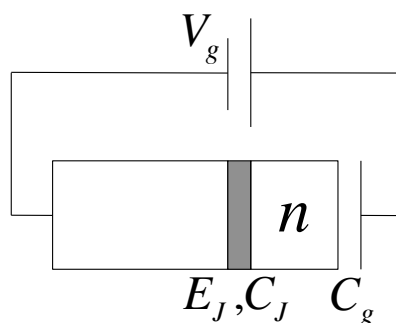
Figure 1.3: A CPB, characterized by a gate voltage V_g and capacitance C_g, and a Josephson junction energy E_J and capacitance C_J. n denotes the number of excess Cooper-pairs on the CPB.

principle and can be understood heuristically as follows: E_C sets the kinetic energy scale, and when it is much larger than the potential energy scale E_J, the junction is free to explore all values of the phase difference, which results in small charge fluctuations.

As mentioned in section 1.2.1, superconductors are characterized by an energy gap Δ between the ground state and quasi-particle excitations. It is crucial that both the superconducting electrode and CPB possess an energy gap $\Delta \gg E_C$. This condition is needed so that quasi-particle tunnelling is effectively suppressed, which means that one may assume that the CPB is free from quasi-particle 'poisoning'. We will show below that, since only Cooper-pairs can tunnel through the junction, the Hamiltonian describing the system is

$$\mathcal{H}_{\mathrm{CPB}} = 4E_C(n - n_{\mathrm{g}})^2 - E_J \cos\Theta, \tag{1.10}$$

where the dimensionless gate charge n_{g} is a continuous classical control parameter, and n and Θ are canonically conjugate operators satisfying $[\Theta, n] = i$. In contrast to the phase difference of the superconducting ring in figure 1.2, Θ is compact: it lives on a circle with the eigenvalues Θ and $\Theta + 2\pi$ being identified. The reason for this is that in the CPB circuit in figure 1.3, there is no continuous superconducting path from one side of the junction to the other. There is thus no way of tracking how the phase winds from one side to the other; all one can ascertain is the phase difference modulo 2π. Since Θ lives on a circle, the spectrum of n is automatically restricted to the integers.

The first term in (1.10) captures the charging energy stored in the junction and gate capacitors, as well as the energy of the battery. In terms of the gate and junction charges, q_{g} and q_J, respectively, this contribution is given by

$$\frac{q_{\mathrm{g}}^2}{2C_{\mathrm{g}}} + \frac{q_J^2}{2C_J} - V_{\mathrm{g}} q_{\mathrm{g}}, \tag{1.11}$$

where the last term reflects the fact that the battery has done work $V_{\mathrm{g}} q_{\mathrm{g}}$, so that its energy has decreased by this amount. Kirchoff's voltage law requires that $V_{\mathrm{g}} = q_{\mathrm{g}}/C_{\mathrm{g}} + q_J/C_J$, and the junction charge differs from the gate charge by n excess Cooper pairs i.e. $q_J = q_{\mathrm{g}} - 2ne$.

Substituting the charges in terms of n and V_g, (1.11) can be rewritten as

$$4E_C(n-n_g)^2 - \frac{1}{2}C_g V_g^2, \tag{1.12}$$

which agrees with the first term of (1.10), except for a constant. This constant can be neglected since we are interested in the energies of different charge states at a fixed gate voltage.

Given $E_C \gg E_J$, it is convenient to work in the number basis $\{|n\rangle\}$, where $|n\rangle$ is a charge eigenstate with n excess Cooper-pairs on the CPB. Since $\cos\Theta = \left(e^{i\Theta} + e^{-i\Theta}\right)/2$ and $e^{\pm i\Theta}|n\rangle = |n\mp 1\rangle$, the Hamiltonian (1.10) can be represented as

$$\mathcal{H}_{CPB} = \sum_{n=-\infty}^{\infty} \left[4E_C(n-n_g)^2 |n\rangle\langle n| - \frac{1}{2}E_J\left(|n\rangle\langle n+1| + |n+1\rangle\langle n|\right) \right]. \tag{1.13}$$

The spectrum of $\mathcal{H}_{CPB}$ is dominated by the charging contribution, except in the vicinity of n_g being a half-odd-integer. For a given n, the charging energy is a parabola centred at $n_g = n$, and adjacent parabolae touch at half-odd-integer values of n_g. At such voltages, the degeneracy of two adjacent states – for instance, $n=0$ and $n=1$ at $n_g = 1/2$ – is lifted by the Josephson coupling, so that the charge states become superposed. Near these voltages, all other charge states by virtue of their much higher energies ($\mathcal{O}(E_C)$ or more) can be ignored. The CPB circuit thus effectively realizes a qubit, with the two logical states corresponding to states which differ by a Cooper-pair on the CPB. Explicitly, we approximate the tunnelling and charging contributions to (1.13) as

$$-\frac{E_J}{2}\left(|n\rangle\langle n+1| + |n+1\rangle\langle n|\right)$$

and

$$2E_C\left\{\left(2n_g - [2n+1]\right)|n\rangle\langle n| - \left(2n_g - [2n+1]\right)|n+1\rangle\langle n+1|\right\},$$

respectively, where the deviation about the degeneracy point $n_g = n + 1/2$ is assumed to be small. To be concrete, let us look at the region near $n_g = 1/2$ $(n=0)$, in which case the circuit can be viewed as a spin-1/2 particle in a magnetic field:

$$\mathcal{H}_{CPB} = B_z Z + B_x X. \tag{1.14}$$

Above, $X = \begin{pmatrix} 0 & 1 \\ 1 & 0 \end{pmatrix}$ and $Z = \begin{pmatrix} 1 & 0 \\ 0 & -1 \end{pmatrix}$ are the Pauli-x and z matrices, respectively, which act on the space spanned by $\{|0\rangle \equiv |\uparrow\rangle, |1\rangle \equiv |\downarrow\rangle\}$, while $B_x \equiv -E_J/2$ and $B_z \equiv 2E_C(2n_g - 1)$ are the x and z components of the magnetic field, respectively. The avoided energy level crossing at a degeneracy point was first shown in (Nakamura *et al.*, 1997).

While it is desirable to be able to control B_x – and this can indeed be achieved by replacing the junction with a DC SQUID – (1.14) is nonetheless sufficient to perform an arbitrary single-qubit unitary. Such gates can be realized by switching the gate voltage. For instance,

by starting out far to the left of the degeneracy point (so that the eigenstates of (1.14) are essentially the charge eigenstates) and then switching quickly to the degeneracy point (so that $\mathcal{H}_{\text{CPB}} = B_x X$) for some time produces a rotation about the *x*-axis of the Bloch sphere. Such coherent oscillations were first demonstrated in (Nakamura *et al.*, 1999). Nowadays, AC voltage is usually used to implement gates, although switching still has its uses in qubit initialization and measurement.

CPBs – and charge qubits in general – are affected by low-frequency $1/f$ electric field noise (Paladino *et al.*, 2014) due to electrons hopping between traps in the local environment. Such traps are always present in the substrate material on which superconducting circuits are built. This noise, along with the noise that can arise from fluctuations in the gate voltage, can lead to sudden large jumps in the gate charge. To maximise insensitivity to these kinds of fluctuations, CPBs are usually operated at the degeneracy point $n_{\text{g}} = 1/2$ (the so-called 'sweet spot' or optimal working point (Vion *et al.*, 2002)) where the effects of low-frequency noise vanish to first-order. Another $1/f$ source of dephasing which affects all superconducting qubits is critical current fluctuations (Paladino *et al.*, 2014), which leads to fluctuations in the Josephson energy.

1.3.2 Flux qubits

We have seen that when the charging energy dominates the Josephson energy, quantum information can be stored and manipulated in the charge degree of freedom. In the opposite regime, charge fluctuations become pronounced while the phase becomes a good quantum number. Flux or persistent current qubits function in this latter regime, and take the form of a superconducting ring interrupted by a number of junctions, with flux threading the ring. The simplest member of this family of qubits is the radio frequency (RF) SQUID (Friedman *et al.*, 2000), which makes use of a ring interrupted by a single junction, as shown in figure 1.2.

To find the quantum Hamiltonian of the RF SQUID, we start by looking at its classical Lagrangian (Annett *et al.*, 2002):

$$\mathcal{L}_{\text{RF}}(\Phi, \dot{\Phi}) = \frac{1}{2} C_J \dot{\Phi}^2 + E_J \cos\left(\frac{2\pi\Phi}{\Phi_0}\right) - \frac{(\Phi - \Phi_{\text{ex}})^2}{2L}. \tag{1.15}$$

The total flux through the ring, $\Phi = \Phi_{\text{ex}} - LI$, consists of an external flux Φ_{ex} which biases the system, and a contribution from a supercurrent I (L is the effective ring inductance). The first two terms of (1.15) represent the charging and Josephson coupling energies of the junction, with C_J and E_J being the junction capacitance and Josephson energy, respectively. The momentum conjugate to Φ is the charge on the capacitor

$$\frac{\partial \mathcal{L}_{\text{RF}}}{\partial \dot{\Phi}} = C_J \dot{\Phi} = Q, \tag{1.16}$$

and thus the classical Hamiltonian is

$$\mathcal{H}_{\mathrm{RF}}(\Phi, Q) = Q\dot{\Phi} - \mathcal{L}_{\mathrm{RF}}$$
$$= \frac{Q^2}{2C_J} - E_J \cos\left(\frac{2\pi\Phi}{\Phi_0}\right) + \frac{(\Phi - \Phi_{\mathrm{ex}})^2}{2L}. \tag{1.17}$$

Upon canonical quantization, whereby flux and charge become operators which satisfy $[\Phi, Q] = i\hbar$, we arrive at the quantum Hamiltonian

$$\mathcal{H}_{\mathrm{RF}} = -\frac{\hbar^2}{2C_J}\frac{\partial^2}{\partial\Phi^2} - E_J \cos\left(\frac{2\pi\Phi}{\Phi_0}\right) + \frac{(\Phi - \Phi_{\mathrm{ex}})^2}{2L}, \tag{1.18}$$

where the replacement $Q = -i\hbar\partial/\partial\Phi$ has been made. The junction phase difference – which is proportional to Φ – can be determined by how the phase winds along a continuous superconducting path in the ring. In other words, the phase difference is not a compact variable as was the case for CPB circuits: the spectrum of Φ (and Q) is the real line.

Given a large enough ring inductance and an external flux which is approximately a half-odd-integer multiple of the flux quantum ($\Phi_{\mathrm{ex}} \approx (n + 1/2)\Phi_0$), the potential of (1.18) forms a double-well structure near $\Phi = (n + 1/2)\Phi_0$ with nearly degenerate minima, which is exact for $\Phi_{\mathrm{ex}} = (n + 1/2)\Phi_0$. This can be seen by setting the derivative of the potential $-E_J \cos(2\pi\Phi/\Phi_0) + (\Phi - \Phi_{\mathrm{ex}})^2/2L$ to zero, which yields the equation

$$\sin\left(\frac{2\pi\Phi}{\Phi_0}\right) = \frac{\Phi_0^2}{4\pi^2 L E_J}\left[\frac{2\pi}{\Phi_0}(\Phi_{\mathrm{ex}} - \Phi)\right]. \tag{1.19}$$

A double-well potential has three stationary points, and therefore, in order for at least three solutions to exist for the above equation for $\Phi_{\mathrm{ex}} \approx (n + 1/2)\Phi_0$, the gradient of the right-hand side must be less than one, since the magnitude of the slope at $\sin[(2n+1)\pi]$ is equal to one:

$$\frac{\Phi_0^2}{4\pi^2 L E_J} < 1. \tag{1.20}$$

As long as condition (1.20) is well satisfied, superpositions of the two lowest energy eigenstates can be used to create two orthonormal states which are localized at either minima. These states correspond to oppositely circulating persistent current states – or equivalently, flux up and down states – and can be used as the basis for a qubit, with the (anti)-clockwise state being denoted $(|\uparrow\rangle)\ |\downarrow\rangle$. It should be noted that these states are not flux eigenstates – they are not 'sharp' in flux, but rather are flux wavepackets. The Hamiltonian of this effective two-level system is of the same form as the CPB Hamiltonian (1.14): the bias B_z depends on Φ_{ex} and controls the asymmetry of the double-well, while B_x is the inter-well tunnelling amplitude. It depends on the barrier height, which is controlled by E_J, and the mass of the system, C_J. B_x can also be made tunable by replacing the junction with a DC SQUID, allowing arbitrary single-qubit unitaries to be realized.

Motivated by the inability to observe MQC by the late 90's, improved flux qubit de-

16

signs were proposed, making use of smaller rings – possessing therefore much smaller inductances than typical RF SQUID values – interrupted by three (Mooij *et al.*, 1999) or four (Feigel'man *et al.*, 2000) junctions. The problem with the RF SQUID is that, condition (1.20) requires both the loop inductance and E_J to be large. Larger inductances lead to greater system-environment coupling, while larger Josephson energies raise the double-well barrier height, which is detrimental to flux tunnelling. As a result, the RF SQUID experiment in (Friedman *et al.*, 2000) was only able to create superpositions of excited states near the top of the barrier, which was inferred from the level repulsion near the degeneracy point, $\Phi_{ex} = \Phi_0/2$. It was estimated that the two superimposed flux states differed in magnetic moment by $10^{10}\mu_B$, and were thus macroscopically distinct quantum states. The negligible inductance of the three junction design offers longer coherence times, due to weaker system-environment coupling, and tunnelling between the lowest states in this system has been demonstrated (Van der Wal *et al.*, 2000). Furthermore, Rabi oscillations were realized by irradiating such a qubit with microwave pulses (Chiorescu *et al.*, 2003).

Flux qubits suffer from $1/f$ magnetic field noise (Paladino *et al.*, 2014) due to fluctuating magnetic moments, the origin of which has been a puzzle for over 20 years. In (Koch *et al.*, 2007b), a model of electrons hopping stochastically between traps with different preferential spin orientations is proposed, while (Faoro & Ioffe, 2008) suggests that the noise results from electron spin diffusion at superconductor-insulator (substrate) boundaries. Magnetic noise also arises from fluctuations in external fluxes and current sources connected to qubits. As with charge qubits, by working at the degeneracy point, the first order effects of $1/f$ noise can be negated.

1.3.3 Topologically protected qubits

As mentioned in the introduction to this chapter, the biggest obstacle to realizing large-scale QC is the debilitating effect of noise on qubits, either through coupling to an environment or processing errors. To meet this challenge, ingenious *error correcting codes* have been concocted (Shor, 1995, 1996; Steane, 1996), wherein information is encoded redundantly and errors are detected and corrected actively, without destroying the encoded information. While classical error correcting codes also employ redundancy by utilizing many copies of a bit string, quantum codes are fundamentally different since QI cannot be cloned (Wootters & Zurek, 1982). In the quantum case, information is encoded non-locally: the information stored in a logical qubit is 'spread' over many 'physical' qubits. As a result, errors – which are typically local in nature – can be detected and corrected without harming the encoded information.

The large overhead required for quantum error correction however places stringent demands on the coherence times of qubits and the fidelities of elementary operations (gates and measurements). Indeed, for *fault-tolerant QC* (Shor, 1996) to be possible in principle, coherence times must be many orders of magnitude greater than the typical time needed for an elementary operation, while the probability of error of these operations must be smaller

than a certain *threshold* probability. While the exact value of the error threshold depends on the code and noise model employed, values around 10^{-4} were quoted in the literature for some years (Gottesman, 2009). Recently, significantly higher (and experimentally attainable) thresholds around 10^{-2} have been found in the surface code (Fowler *et al.*, 2012; Raussendorf & Harrington, 2007; Wang *et al.*, 2011), an approach which marries the software and topological approaches to error correction. Moreover, the surface code only requires qubits to be arranged on a 2D square lattice and interact with nearest neighbours, and therefore naturally suggests an implementation with high quality superconducting circuits (Barends *et al.*, 2014).

In a pioneering paper (Kitaev, 2003), Kitaev proposed a radically different solution to combating errors [9]. The basic idea of this topological approach to error correction is to find robust quantum hardware which is effective at suppressing errors. A spin lattice model known as the toric code (Kitaev, 2003) is the canonical example of this: it can be regarded as a Hamiltonian realization of an error correcting code. In particular, the ground states of the Hamiltonian can be viewed as code states (logical basis states), whereas excited states correspond to errors being present, and thus live outside of the code space. As a result, at temperatures well below the energy gap between ground and excited states, errors will be energetically suppressed, and so the system possesses an intrinsic fault-tolerance. Intriguingly, excitations in the toric code are (Abelian) anyons – quasiparticles which are neither fermionic or bosonic and which possess fractional (braiding) statistics (Leinaas & Myrheim, 1977; Wilczek, 1982). In fact, variants of the toric code can support *non-Abelian* anyons (Kitaev, 2003; Nayak *et al.*, 2008; Pachos, 2012), which when braided with each other can produce unitary transformations in a ground state manifold and thus process encoded information. Such operations are inherently robust since all that matters is the topological class or nature of braids – their geometrical details are irrelevant. This scheme, which uses the properties of anyons to store and manipulate information, is known as TQC, which was mentioned in the introduction to the thesis.

Topological protection has been sought in superconducting circuits for some time (Ioffe & Feigelman, 2002; Ioffe *et al.*, 2002). Unfortunately, both these examples (and similar schemes) would be difficult to realize with current fabrication technology, due to problems such as sensitivity to random offset charges ($1/f$ electric noise) and magnetic field non-uniformities. Encouragingly though, intrinsic fault-tolerance in an array of Josephson junctions has recently been demonstrated in the laboratory (Gladchenko *et al.*, 2008). The two-fold ground state degeneracy of the array in (Gladchenko *et al.*, 2008) was found to be protected against local flux noise well beyond linear order, while conventional approaches – which as discussed above, rely on tuning control parameters – offer only linear order protection (Chiorescu *et al.*, 2003; Vion *et al.*, 2002; Wallraff *et al.*, 2004). Furthermore, recent design improvements which reduce sensitivity to offset charge fluctuations (Bell *et al.*,

---

[9]This idea had actually been around since 1997! (Kitaev, 1997)

2014) are expected to lead to further progress. In the next chapter, we examine in detail another protected superconducting circuit which possesses a doubly degenerate ground state (Kitaev, 2006b), while in chapter 3 we discuss our proposal of the magnetic analogue of this circuit.

CHAPTER 2

Kitaev's current mirror qubit

In chapter 1, we introduced the idea that fault-tolerant QC can be performed by manipulating anyons. While this idea is undeniably elegant, finding *and* harnessing anyons in systems, be they natural or 'man-made', remains a highly non-trivial task which is likely to keep experimentalists busy for many years to come. While various 'sightings' of anyons have been made (Camino *et al.*, 2005; Mourik *et al.*, 2012; Willett *et al.*, 2009), to date, information storage and processing has not been achieved with anyons.

Despite these difficulties, TQC suggests another intriguing question: Can we find or engineer systems that might not possess anyons, but still enable information to be encoded and processed in a robust and global manner? This question probably inspired Kitaev to devise a protected superconducting 'current mirror' qubit, and a scheme for universal fault-tolerant computation using such qubits (Kitaev, 2006b). While the qubit possesses many microscopic degrees of freedom, information can be robustly encoded in a global phase degree of freedom. This chapter deals with the emergence of this qubit from microscopic degrees of freedom. In chapter 4, we examine the scheme for QC, in the context of our dual construction of Kitaev's qubit, which is discussed in chapter 3.

2.1 Co-tunnelling transport in coupled Josephson junction chains

Kitaev's idea builds on (Choi *et al.*, 1998), in which quantum phase transitions in a system consisting of two capacitively coupled chains of Josephson junctions (see figure 2.1) were studied. In section 2.1.1, we discuss the parameters of the array and build some intuition for the phases that the system admits. We then verify this intuition in section 2.1.2 by deriving an effective Hamiltonian.
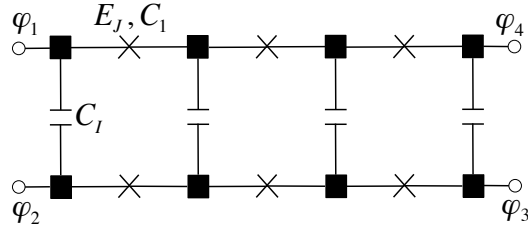
Figure 2.1: Schematic diagram of the superconducting current mirror array, which consists of two capacitively coupled chains of Josephson junctions. The superconducting islands or grains are denoted by black squares, while the Josephson junctions are denoted by crosses. Each junction has a Josephson energy E_J and a capacitance C_1, while the chains are coupled by a capacitance C_I. The phases of the order parameters of the four corner grains are φ_i, and superconducting leads are attached to these grains.

2.1.1 Array parameters

The array consists of identical junctions possessing a Josephson energy E_J [10] and a charging energy $E_1 \equiv e^2/(2C_1)$, which is associated with the junction capacitance, C_1. There is also another characteristic energy, $E_I \equiv e^2/(2C_I)$, which corresponds to the inter-chain capacitance C_I, which couples the chains. It is assumed that no tunnelling – Cooper-pair or otherwise – is allowed between the chains. In (Choi *et al.*, 1998), the effect of a finite self-capacitance (capacitance to ground) and an external gate voltage applied to each island was examined. Such a setup results in an external (polarization) charge being induced on the islands, frustrating the system. Sizeable frustration pushes the array into phases which would be unsuitable for realizing a qubit, and so Kitaev assumes a frustration-free system.

The junctions are assumed to be 'ultra-small', which implies that C_1 is extremely small. Junction charging energies therefore dominate the Josephson energies, $E_J \ll E_1$, and thus the island charges are highly localized. As a result, without inter-chain coupling, each chain would be in the insulating phase. Now let us consider a finite inter-chain coupling; the coupling capacitance is assumed to be much larger than the junction capacitance, $C_I \gg C_1$, which means that $E_I \ll E_1$. While uncorrelated individual currents cannot flow, it is energetically much more favourable for Cooper-pairs to propagate in one chain, while Cooper-pairs propagate simultaneously in the other chain in the opposite direction. In other words, for large enough E_J, the system should possess a phase where *excitons* – Cooper-pair and 'Cooper-hole' pairs – can propagate along the array. This is the reason why Kitaev dubbed the system a 'current mirror' qubit; we refer to this qubit as 'Kitaev's current mirror qubit' (KCMQ).

---

[10]We use the notation employed in (Choi *et al.*, 1998), which is different from Kitaev's notation.

2.1.2 Array Hamiltonian

The Hamiltonian of the system is

$$\mathcal{H}_{\text{KCMQ}} = \frac{(2e)^2}{2} \sum_{l,l';x,x'} n_l(x) \mathcal{C}_{ll'}^{-1}(x,x') n_{l'}(x') - E_J \sum_{l,x} \cos\left[\varphi_l(x+1) - \varphi_l(x)\right], \qquad (2.1)$$

where the conjugate variables $n_l(x)$ and $\varphi_l(x)$ satisfy $[\varphi_l(x), n_m(y)] = i\delta_{lm}\delta_{xy}$, and refer to the excess number of Cooper-pairs on, and the (superconducting) phase of, the island at discrete position x and on chain l ($l = 1,2$), respectively. We take the system to be of length L and assume periodic boundary conditions, so that the sums over x and x' in (2.1) run from 1 to L [11]. The first term in (2.1) captures the charging energy of the array, while the second term reflects the Josephson energies of the junctions. The capacitance matrix, $\mathcal{C}$, encapsulates the electrostatic interactions between charges, and is defined by

$$\mathcal{C}_{ll'}(x,x') \equiv C(x,x') \otimes \delta_{ll'} + C_I \delta_{xx'} \otimes \begin{pmatrix} 1 & -1 \\ -1 & 1 \end{pmatrix}, \qquad (2.2)$$

where the intra-chain capacitance matrix is

$$C(x,x') \equiv C_1 \left(2\delta_{xx'} - \delta_{x,x'+1} - \delta_{x,x'-1}\right). \qquad (2.3)$$

$\mathcal{C}$ is defined such that, given the potential of the island at (x,l) is $V_l(x)$, the charge on an arbitrary island, $2en_l(x) = \sum_{l',x'} \mathcal{C}_{ll'}(x,x') V_{l'}(x')$, should agree with what circuit theory predicts. This is indeed the case:

$$\begin{aligned}
2en_l(x) &= \sum_{l',x'} \mathcal{C}_{ll'}(x,x') V_{l'}(x') \\
&= 2C_1 V_l(x) - C_1 V_l(x-1) - C_1 V_l(x+1) + C_I V_l(x) - C_I V_{l'\neq l}(x) \\
&= C_1(V_l(x) - V_l(x-1)) + C_1(V_l(x) - V_l(x+1)) + C_I(V_l(x) - V_{l'\neq l}(x)).
\end{aligned}$$

To make progress, it is useful to cast the charging energy contribution into a form which is easier to analyse. If we write this contribution as $2e^2 \vec{n}^T \mathcal{C}^{-1} \vec{n}$, where $\vec{n} \equiv \begin{pmatrix} n_1(1) & n_2(1) & n_1(2) & \dots \end{pmatrix}^T$, we can effect a unitary transformation with the matrix $H = \delta_{xx'} \otimes \frac{1}{\sqrt{2}} \begin{pmatrix} 1 & 1 \\ 1 & -1 \end{pmatrix}$ (a Hadamard matrix acting on 'chain-space'), satisfying $H^2 = \delta_{xx'} \otimes \delta_{ll'}$, by writing

$$2e^2 \vec{n}^T \mathcal{C}^{-1} \vec{n} = 2e^2 \vec{n}^T HH \mathcal{C}^{-1} HH \vec{n} = e^2 \vec{n}'^T \mathcal{C}'^{-1} \vec{n}'. \qquad (2.4)$$

---

[11]We are assuming that an analysis of this periodic array will capture the behaviour of an array with open boundary conditions (as shown in figure 2.1), which is ultimately what we are interested in.

2. Kitaev's current mirror qubit

The transformed capacitance matrix is

$$\mathcal{C}' \equiv H\mathcal{C}H = C(x,x') \otimes \delta_{ll'} + 2C_I \delta_{xx'} \otimes \begin{pmatrix} 0 & 0 \\ 0 & 1 \end{pmatrix}, \qquad (2.5)$$

while the transformed vector is $\vec{n}' \equiv \sqrt{2}H\vec{n} = \begin{pmatrix} n_+(1) & n_-(1) & n_+(2) & ... \end{pmatrix}^T$, where $n_\pm(x) \equiv n_1(x) \pm n_2(x)$. The transformation reveals that the '+' and '−' degrees of freedom are decoupled, which should be clear to see below.

Let us simplify $\mathcal{C}'$ by making use of $C_I \gg C_1$:

$$\mathcal{C}' \approx 2\delta_{xx'} \otimes \begin{pmatrix} C_1 & 0 \\ 0 & C_I \end{pmatrix} - C_1(\delta_{x,x'+1} + \delta_{x,x'-1}) \otimes \begin{pmatrix} 1 & 0 \\ 0 & 1 \end{pmatrix}. \qquad (2.6)$$

While an exact solution for $\mathcal{C}'^{-1}$ is possible by 'hand', its complexity would render it difficult to use. This motivates us to use mathematical software to invert $\mathcal{C}'$ for different sized systems and extract the salient features of $\mathcal{C}'^{-1}$. Some examples of (2.6) and its inverse are collected in appendix A. As noted there, the elements of $\mathcal{C}'^{-1}$ which couple the '+' components only fall off arithmetically with distance, while those which couple the '−' components fall off geometrically with distance. These features – which hold for arrays of modest size and should remain for arrays of arbitrary size – allow us to approximate (2.1) as

$$\mathcal{H}_{\mathrm{KCMQ}} \approx \mathcal{O}(E_1)\sum_x n_+(x)^2 + E_I\sum_x n_-(x)^2 + \mathcal{O}(E_1)\sum_{x;y>0} n_+(x)n_+(x+y)$$
$$- 2E_J\sum_x \cos\left[\varphi_+(x+1) - \varphi_+(x)\right]\cos\left[\varphi_-(x+1) - \varphi_-(x)\right], \qquad (2.7)$$

where $\varphi_\pm(x) = [\varphi_1(x) \pm \varphi_2(x)]/2$ are the coordinates conjugate to the momenta $n_\pm(x)$ i.e. $[\varphi_\pm(x), n_\pm(y)] = i\delta_{xy}$, and terms $\mathcal{O}(C_1/C_I)E_I$ or smaller have been dropped. Strictly speaking, the terms which are of order E_1 should be written as, for example, $E_1\sum_x \mathcal{O}(1)(x)n_+(x)^2$, but as we will see below, this is inessential.

Employing degenerate perturbation theory, it is possible to find an *effective Hamiltonian* which describes the low energy dynamics of the system. The method of finding an effective Hamiltonian is sketched in appendix B, and since the calculation for the problem at hand is lengthy, we relegate it to appendix C. Treating the Josephson term in (2.7) as a perturbation and projecting into the subspace $n_+(x) = 0, n_-(x) = 0, \pm 2$, one arrives at an effective Hamiltonian, $\mathcal{H}_{\mathrm{KCMQ}}^{\mathrm{eff}}$, which describes the system as a single chain of junctions with excitons as the tunnelling objects instead of Cooper-pairs (see figure 2.2):

$$\mathcal{H}_{\mathrm{KCMQ}}^{\mathrm{eff}} = 4E_I\sum_x n'_-(x)^2 - E_J^{\mathrm{ex}}\sum_x \cos\left[\varphi'_-(x+1) - \varphi'_-(x)\right]. \qquad (2.8)$$

$\varphi'_-(x) \equiv 2\varphi_-(x)$ and $n'_-(x) \equiv n_-(x)/2$ are the phase of the macroscopic exciton wavefunc-
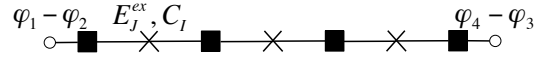
Figure 2.2: $\mathcal{H}_{\text{KCMQ}}^{\text{eff}}$ in (2.8) describes a single chain of junctions with excitons as the tunnelling objects.

tion and the number of excitons, at position x, respectively, and are conjugate variables: $[\varphi_-'(x), n_-'(y)] = i\delta_{xy}$. The junctions have a Josephson energy of $E_J^{\text{ex}} \equiv E_J^2/E_1$, while their charging energy is set by E_I. In the regime where E_I is much less than E_J^{ex} (which requires $E_J \gg E_I$, given that $E_1 \gg E_J$), the excitons form a condensate. This is equivalent to saying that the excitonic junctions are in the 'superfluid' regime, so that excitons can move freely along the chain. Assuming that this is so, the exciton condensate phase has small quantum fluctuations.

2.2 Low energy behaviour of the array and the emergence of a qubit

Given that in the low energy limit, the system is effectively described by a single chain of excitonic junctions, its properties can be determined by appealing to results known from the study of conventional chains of Josephson junctions (Pop *et al.*, 2010). It turns out that the ground state of such a chain can in fact be described by a single degree of freedom: the number of *phase slips* in the chain. Consider a chain of L junctions (with open boundary conditions) with a phase drop of γ across the chain, in a regime where the Josephson energy E_J dominates the charging energy. If we neglect the charging energy for the moment, the classical ground state consists of γ being equally distributed amongst all the junctions: $\theta_i = \gamma/L$, where θ_i is the phase difference across junction i. The assumption here is that γ/L is small enough, so that $\theta_i = \gamma/L$ is the minimum energy configuration. Given this, the potential of the chain is simply $E_0 = E_J \sum_{i=1}^{L} 1 - \cos\theta_i \approx E_J\gamma^2/2L$.

However, this is not the end of the story. Phase slips can occur, where the phase of one junction, say the jth, changes as $\theta_j \to \theta_j + 2\pi$. Assuming that the phase bias is constant (i.e. $\sum_i \theta_i = \gamma$ must always be satisfied), the phases of the other junctions must change a little to accommodate the phase slip. As a result, the energy of the chain changes to $E_1 = E_J(\gamma - 2\pi)^2/2L$, and after m phase slips, the energy is $E_m = E_J(\gamma - 2\pi m)^2/2L$. These energies correspond to parabolae centred at $\gamma = 2\pi m$, and the curves E_m and E_{m+1} are degenerate at $\gamma = (2m+1)\pi$. Restoring the charging energy – which introduces quantum phase fluctuations which can give rise to phase slips – lifts these degeneracies. A tight-binding model proposed in (Matveev *et al.*, 2002) gives rise to energy bands which are 2π periodic; the lowest band was confirmed in (Pop *et al.*, 2010).

Applying these ideas to Kitaev's device, we see that the lowest energy band can be written primarily as a function of the phase difference at the ends, $(\varphi_4 - \varphi_3) - (\varphi_1 - \varphi_2)$:

$$E = F(\varphi_4 - \varphi_3 + \varphi_2 - \varphi_1) + \text{error term}, \tag{2.9}$$
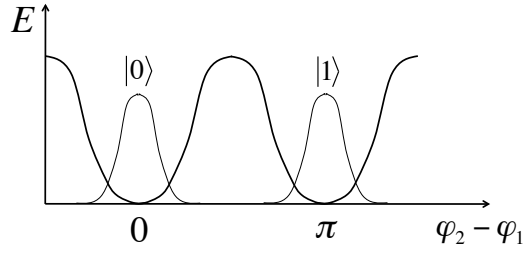
Figure 2.3: The circuit's energy, E, becomes almost exactly π-periodic in $\varphi_2 - \varphi_1$ once the boundary conditions $\varphi_1 = \varphi_3$ and $\varphi_2 = \varphi_4$ are imposed. The two states localized near the minima at $\varphi_2 - \varphi_1 = 0, \pi$ can be used as the basis states of a qubit. These states are degenerate, up to an exponentially small correction.

where F is 2π periodic. The 'error term' arises from uncorrelated currents, i.e. currents which are non-excitonic in nature, and is predicted to decrease exponentially as the number of junctions increases [12] (Brooks *et al.*, 2013; Kitaev, 2006b). If the first and third leads are connected so that $\varphi_1 = \varphi_3$, and similarly the second and fourth, the energy becomes π periodic in $\varphi_2 - \varphi_1$, up to an exponentially small correction: $E \approx F\left(2(\varphi_2 - \varphi_1)\right)$. The two *distinct* minima of $F\left(2(\varphi_2 - \varphi_1)\right)$ are located at $\varphi_2 - \varphi_1 = 0$ and $\varphi_2 - \varphi_1 = \pi$ [13], and as long as the barrier separating the minima is large enough, there are two ground states localized around these minima. These states can be identified with the logical states of a qubit (say, $\varphi_2 - \varphi_1 = 0 \leftrightarrow |0\rangle$, $\varphi_2 - \varphi_1 = \pi \leftrightarrow |1\rangle$), as shown in figure 2.3.

The error term in (2.9) leads to an exponentially small (in the length of the device) difference in the energy of the minima, which would inhibit dephasing. Encouragingly, this degeneracy has been shown to be robust to modest disorder in circuit parameters (Dempster *et al.*, 2014). One may think that since the barrier height is $\mathcal{O}(E_J^{\text{ex}}/L)$ (L is the length of the device), in order to prevent bit flips or tunnelling between the wells, one cannot arbitrarily increase the length of the device. However, as long as the 'mass' of the system – which scales with C_I (see the 'kinetic' or charging energy term of $\mathcal{H}_{\text{KCMQ}}^{\text{eff}}$ in (2.8)) – is made sufficiently large, the system cannot easily tunnel between the wells. As Kitaev notes, if we take the kinetic energy scale of the system to be $e^2/(LC_I)$ (LC_I can be regarded as the total inter-chain capacitance), then to suppress bit flips it is necessary to have

$$\frac{E_J^{\text{ex}}}{L} \gg \frac{e^2}{LC_I}. \tag{2.10}$$

$[E_J^{\text{ex}}/L]/[e^2/(LC_I)]$ is independent of L, and it can be increased by increasing C_I. The suppression of errors at the hardware level is what makes Kitaev's qubit 'protected'.

---

[12] We further discuss this error term in section 3.3, since it also arises in our dual construction.

[13] If the leads are not connected as described, then $F\left(\varphi_4 - \varphi_3 + \varphi_2 - \varphi_1\right)$ has minima at $\varphi_4 - \varphi_3 + \varphi_2 - \varphi_1 = 0, 2\pi$ which are equivalent, since the phases are 2π periodic variables.

2.3 Summary and discussion

In this chapter, we have explained how a qubit, namely KCMQ, can be realized in two capacitively coupled chains of Josephson junctions. An effective Hamiltonian (2.8) reveals that, with the right choice of array parameters, the system can be regarded as a chain of junctions which is superconducting with respect to excitons – composite objects consisting of a Cooper-pair and a Cooper-pair hole. With the right choice of boundary conditions, the energy of the circuit becomes π-periodic in a global phase difference, and possesses two distinct minima. The two states localized at these minima can be used to realize a qubit, and are degenerate up to an exponentially small correction in the length of the array. This near degeneracy would inhibit dephasing, while bit flips can be minimized by making the interchain capacitance large enough. Hence, KCMQ has all the ingredients one would expect to find in an intrinsically fault-tolerant qubit; it belongs to a family of protected superconducting '0-π qubits' (Douçot & Vidal, 2002; Gladchenko *et al.*, 2008; Ioffe & Feigelman, 2002). We note that a realization of Kitaev's qubit in a bilayer exciton condensate contacted by superconducting leads has been suggested in (Peotta *et al.*, 2011).

We have yet to discuss the interaction between KCMQ and its environment; a consideration of electric field fluctuations reveals that they may change the behaviour of the system qualitatively, and no longer allow a qubit to be realized. While Kitaev took the self-capacitance of the islands to be zero, in practice these capacitances will be finite, albeit small. Charge fluctuations in the form of electrons hopping back and forth between traps (see section 1.3.1) would effectively result in an external AC voltage being applied to the islands. With finite self-capacitances, such fluctuations could result in uncorrelated currents flowing along the system, thus destroying the current mirror effect.

Conventional wisdom says that in the laboratory, electric noise is generally worse than magnetic noise: the relaxation and dephasing times for a flux qubit outperform those for a charge qubit (Clarke & Wilhelm, 2008). Thus, it seems reasonable to guess that a qubit analogous to KCMQ, based on *magnetic* degrees of freedom, would perform better than KCMQ in the laboratory. Furthermore, the magnetic analogue of Cooper-pair excitons – *vortex-antivortex pairs* – can arise naturally in a suitable 2D array of junctions. This provides another motivation for looking for a protected qubit which is dual to KCMQ, and this is the topic of the next chapter.

CHAPTER 3

A protected vortex exciton qubit

In this chapter, we explain our construction of a magnetic analogue of KCMQ. As mentioned earlier, there are a couple of reasons for why one would attempt to construct a qubit dual to KCMQ. One motivation is the problem that electric field noise may pose to KCMQ in an experimental realization. An analogue based on magnetic degrees of freedom would have an advantage over KCMQ since magnetic field noise is less problematic than its electric counterpart. Another motivating factor is that the magnetic analogue of Cooper-pair excitons, namely, vortex-antivortex pairs, arise naturally in arrays where Josephson energies dominate at low temperatures. This chapter is based on results from (De & Spiller, 2014).

3.1 Vortices

A *vortex* – in the context of Josephson junction arrays – is a configuration of the phases which can be regarded as a topological excitation. Let us flesh out what is meant by this. Arrays in which junction capacitances are so large that charging energies are negligible are known as classical arrays. The physics of these arrays can be described by one of the work-horses of classical statistical mechanics: the *2D XY model* (Herbut, 2007). This model describes ferromagnetically coupled classical planar spins of unit length, confined to two dimensions. Clearly, this model is equivalent to a model of a 2D array of superconducting islands which are Josephson coupled to their neighbours.

At low temperatures, the spins or phases of the islands will tend to align, in order to minimize the energy. Such phase configurations can be decomposed in terms of long wavelength oscillations known as spin-waves. However, at higher temperatures, the 2π periodicity of the phases leads to the appearance of configurations which cannot be captured by spin-waves, namely, vortices. An example of a vortex is shown in figure 3.1. Let us pick a closed contour encircling the central plaquette in figure 3.1, which we can think of as

29
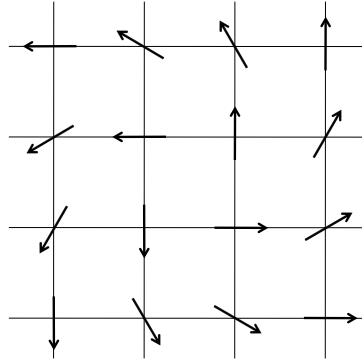
Figure 3.1: A vortex on a square lattice. The spins or phases are represented by the arrows.

where the vortex 'lives'. If we track the change in phase as we traverse this contour in an anti-clockwise fashion, we find that the phase changes by 2π. In fact, this is true for *any* contour surrounding the position of the vortex.

Mathematically, distinct vortex configurations are classified according to their *winding number*

$$n = \frac{1}{2\pi} \oint d\vec{r} \cdot \vec{\nabla}\phi(\vec{r}), \tag{3.1}$$

which is an integer. A continuum notation has been adopted in (3.1) for clarity. The fact that the integral in (3.1) is an integer follows from the periodicity of the phases; it measures the number of times the phase winds by 2π along a closed loop. n is said to be a *topological invariant*: it is impossible to change the winding of a configuration through smooth deformations of the phases [14], and it is for this reason that vortices are known as topological excitations.

Vortices in the 2D XY model lead to a profound phase transition which is not accompanied by a breaking of a symmetry, known as the *Berezinskii-Kosterlitz-Thouless (BKT) transition* (Berezinskii, 1971; Kosterlitz & Thouless, 1973). This transition describes the unbinding of vortices: below the critical temperature T_{BKT}, any vortices in the system are strongly bound to an antivortex partner (a configuration with opposite winding), while above it, the vortex-antivortex pairs disassociate into free entities. Vortices also play a key role in arrays in which charging energies, while smaller than Josephson energies, are not negligible. In such cases, quantum fluctuations of the junctions must be taken into account. We will see in the remainder of this chapter that in doing so, vortices emerge as massive *quantum mechanical* point-like charges. Let us now turn our attention to our dual construction of KCMQ.

---

[14]More precisely, it is impossible to construct a function $\phi(\vec{r},t)$ ($t \in [0,1]$) which is continuous in t and for which the winding of $\phi(\vec{r},0)$ is n and the winding of $\phi(\vec{r},1)$ is $m \neq n$. Configurations with different windings are said to belong to different *homotopy classes*.
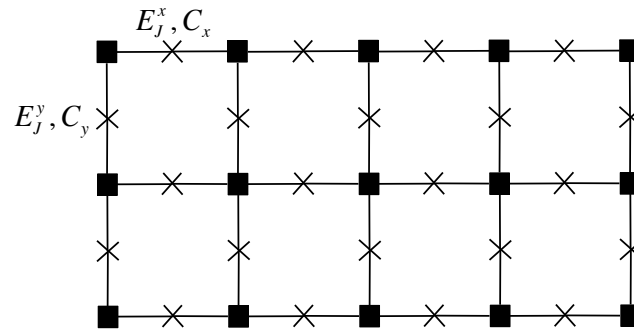
Figure 3.2: The Josephson junction array which gives rise to a protected vortex exciton qubit.

3.2 Path integral representation of the array

Our strategy for finding the dual of Kitaev's qubit is to employ a rectangular array which has anisotropic junction capacitances as well as anisotropic Josephson couplings, as shown in figure 3.2. For the moment, let us focus on the Josephson couplings; we will discuss our choice of capacitances below in section 3.3. We assume that the coupling in the y-direction dominates that in the x-direction: $E_J^y \gg E_J^x$. The reason for assuming this is that in a classical array with isotropic couplings, vortices when sufficiently far apart behave as a 2D Coulomb gas of charges, with the strength of their interaction set by the Josephson energy. With $E_J^y \gg E_J^x$, it turns out that it costs more energy for a vortex-antivortex pair ('vortex exciton') to line up horizontally rather than vertically (see figure 3.4 and the discussion in section 3.3), in analogy with the allowed configurations of charge excitons in KCMQ.

The existence of vortices in the array [15] is seen by analysing the partition function of the system (Fazio & Schön, 1991), which is

$$\mathcal{Z} = \text{tr} e^{-\mathcal{H}/(kT)} = \prod_i \int_0^{2\pi} d\phi_i \langle \{\phi_i\}| e^{-\mathcal{H}/(kT)} |\{\phi_i\}\rangle , \qquad (3.2)$$

where $\mathcal{H}$ is the Hamiltonian of the system, $\{\phi_i\}$ denotes the configuration of phases of the array and T is the temperature. The matrix elements in (3.2) have the following path integral representation (Swanson, 1992) ($\hbar = 1$)

$$\langle \{\phi_i\}| e^{-\mathcal{H}/(kT)} |\{\phi_i\}\rangle = \int_{\{\phi_i\}}^{\{\phi_i\}} D\{Q_j\}D\{\phi_j\}e^{-\mathcal{S}[\{Q_j(\tau)\},\{\phi_j(\tau)\}]} , \qquad (3.3)$$

---

[15]For theoretical convenience, we shall consider an infinite square array in what follows and assume that what we learn holds for the rectangular array shown in figure 3.2.

3. A protected vortex exciton qubit

where the Euclidean action is

$$\mathcal{S}[\{Q_j(\tau)\},\{\phi_j(\tau)\}] \equiv \int_0^{(kT)^{-1}} d\tau \left(\frac{(2e)^2}{2} \sum_{i,j} Q_i(\tau) C_{ij}^{-1} Q_j(\tau) - i \sum_i Q_i(\tau) \dot{\phi}_i(\tau) \right.$$
$$\left. - \sum_{\langle i,j \rangle} E_J^{ij} \cos \phi_{ij}(\tau) \right). \tag{3.4}$$

In (3.3), $\int D\{\phi_j\}$ denotes integration over all paths satisfying $\phi_i(0) = \phi_i((kT)^{-1}) = \phi_i$, and $\int D\{Q_j\} \equiv \prod_j \int DQ_j$ where

$$\int DQ_j \equiv \lim_{N\to\infty} \frac{1}{(2\pi)^N} \sum_{Q_{j,0}=-\infty}^{\infty} \cdots \sum_{Q_{j,N-1}=-\infty}^{\infty}, \tag{3.5}$$

with $Q_{j,k}$ representing the dimensionless charge on island j at discrete time $\tau_k = \varepsilon k$ (the time spacing ε is defined below). In the action (3.4), $\phi_{ij} \equiv \phi_i - \phi_j$, $\langle i,j \rangle$ denotes nearest neighbour sites i and j while C_{ij}^{-1} denotes the inverse of the capacitance matrix.

The presence of vortices can be seen by applying the *Villain approximation* (José *et al.*, 1977; Villain, 1975) to the Josephson energy term in $\mathcal{Z}$. This approximation – which is presented in appendix D – consists of trading the cosine Josephson potential for a form which is quadratic in the phases and a summation over integers. As a result, the phases can be integrated out, while the summation preserves the fundamental 2π periodicity of the phases. To make the approximation, we must consider the imaginary-time integral (3.4) in its discretized form, with time spacing ε. For isotropic arrays, this is chosen to be of the order of the inverse Josephson plasma frequency, $\omega_J^{-1} = (8E_J E_C)^{-1/2}$, which can be regarded as an ultraviolet cutoff. For an anisotropic array, there are in general two different plasma frequencies, and we choose ε to be of the order of $\omega_{J,x}^{-1} = (8E_J^x E_C^x)^{-1/2}$. This choice is motivated by the fact that the Villain approximation

$$\exp\left(\varepsilon E_J^{ij} \cos \phi_{ij,\tau} \right) \approx \sum_{m_{ij,\tau}=-\infty}^{\infty} \exp\left(-\frac{\varepsilon E_J^{ij}}{2} (\phi_{ij,\tau} - 2\pi m_{ij,\tau})^2 \right), \tag{3.6}$$

holds for $E_J^{ij}\varepsilon \gtrsim 1$ and improves in accuracy as $E_J^{ij}\varepsilon$ increases (Stern, 1994).

Using Villain's approximation, $\exp\left(\varepsilon \sum_{\langle i,j \rangle,\tau} E_J^{ij} \cos \phi_{ij,\tau} \right)$ can be written as

$$\sum_{\{\vec{m}_{i,\tau}\}} \exp\left[-\frac{\varepsilon}{2} \sum_{i,\tau} E_J^x (\phi_{i+\hat{x},\tau} - \phi_{i,\tau} - 2\pi m_{i,\tau}^x)^2 + E_J^y (\phi_{i+\hat{y},\tau} - \phi_{i,\tau} - 2\pi m_{i,\tau}^y)^2 \right], \tag{3.7}$$

where $\vec{m}_{i,\tau} = (m_{i,\tau}^x, m_{i,\tau}^y)$ is an integer-valued vector field associated with the links emerging from site i in the $+\hat{x}$ and $+\hat{y}$ directions, with $\hat{x}, \hat{y}$ being the two lattice unit vectors. (3.7) can in turn be rewritten in terms of another integer-valued vector field $\vec{J}_{i,\tau}$ (its components have

the same interpretation as the components of $\vec{m}_{i,\tau}$)

$$\sum_{\{\vec{J}_{i,\tau}\}} \exp\left[-\sum_{i,\tau}\left(\frac{1}{2\varepsilon E_J^x}J_{i,\tau}^{x\,2} + \frac{1}{2\varepsilon E_J^y}J_{i,\tau}^{y\,2} + i\vec{J}_{i,\tau}\cdot\vec{\nabla}\phi_{i,\tau}\right)\right],\qquad(3.8)$$

where $\vec{\nabla}\phi_{i,\tau} = (\phi_{i+\hat{x},\tau} - \phi_{i,\tau}, \phi_{i+\hat{y},\tau} - \phi_{i,\tau})$. The details of this step are outlined in appendix D. After noting that

$$i\sum_i \int d\tau Q_i(\tau)\dot{\phi}_i(\tau) \to i\varepsilon\sum_{i,\tau} Q_{i,\tau}\frac{\phi_{i,\tau+\varepsilon} - \phi_{i,\tau}}{\varepsilon} = i\sum_{i,\tau} Q_{i,\tau}\partial_\tau\phi_{i,\tau},\qquad(3.9)$$

where $\partial_\tau\phi_{i,\tau} \equiv \phi_{i,\tau+\varepsilon} - \phi_{i,\tau}$, we see that we can evaluate the phase integral

$$\prod_i \int_0^{2\pi} d\phi_i \sum_{\{\phi_{i,\tau}\}} \exp\left[i\sum_{i,\tau}\left(Q_{i,\tau}\partial_\tau\phi_{i,\tau} - \vec{J}_{i,\tau}\cdot\vec{\nabla}\phi_{i,\tau}\right)\right],\qquad(3.10)$$

since it is linear in the phases. The argument of the exponent above can be written as

$$i\sum_{i,\tau}\left(\underbrace{-Q_{i,\tau} + Q_{i,\tau-\varepsilon}}_{-\partial_\tau Q_{i,\tau}} + \underbrace{J_{i,\tau}^x - J_{i-\hat{x},\tau}^x + J_{i,\tau}^y - J_{i-\hat{y},\tau}^y}_{\vec{\nabla}\cdot\vec{J}_{i,\tau}}\right)\phi_{i,\tau},\qquad(3.11)$$

and since the Qs and Js above are integers, each integral over the phases yields a Kronecker delta, $\delta_{\vec{\nabla}\cdot\vec{J}_{i,\tau}-\partial_\tau Q_{i,\tau},0}$, up to a constant. We will not keep track of such constants since they do not yield any information about the degrees of freedom that the system possesses.

The partition function is now subject to the constraints $\vec{\nabla}\cdot\vec{J}_{i,\tau} - \partial_\tau Q_{i,\tau} = 0$ at each lattice site (i,τ). Introducing the rescaling $\tilde{J}_{i,\tau}^\mu = J_{i,\tau}^\mu/\sqrt{E_J^\mu}$ and $\tilde{\nabla}_\mu = \sqrt{E_J^\mu}\nabla_\mu$, the constraints become $\vec{\tilde{\nabla}}\cdot\vec{\tilde{J}}_{i,\tau} - \partial_\tau Q_{i,\tau} = 0$, and the enforcement of these constraints is indicated by the $'$ on top of $\sum_{\{\vec{\tilde{J}}_{i,\tau}\}}$:

$$\mathcal{Z} = \sum_{\{Q_{i,\tau}\}}\sum_{\{\vec{\tilde{J}}_{i,\tau}\}}' \exp\left[-2\varepsilon e^2\sum_{i,j,\tau} Q_{i,\tau}C_{ij}^{-1}Q_{j,\tau} - \frac{1}{2\varepsilon}\sum_{i,\tau}|\vec{\tilde{J}}_{i,\tau}|^2\right].\qquad(3.12)$$

The original constraints are solved by

$$J_{i,\tau}^\mu = n^\mu\left(\vec{n}\cdot\vec{\nabla}\right)^{-1}\partial_\tau Q_{i,\tau} + \varepsilon^{\mu\nu}\nabla_\nu A_{i,\tau},\qquad(3.13)$$

where repeated indices are summed over and $\left(\vec{n}\cdot\vec{\nabla}\right)^{-1}$ is the line integral on the lattice, with the unit vector $\vec{n}$ specifying the direction of the integral [16]. Furthermore, $\varepsilon^{\mu\nu}$ is the antisymmetric tensor ($\varepsilon^{12} = -\varepsilon^{21} = 1$), $A_{i,\tau}$ is an integer-valued field which lives on the

---

[16]For instance, for a function f_j living on a one-dimensional lattice in the $\hat{x}$ direction, $\left(\hat{x}\cdot\vec{\nabla}\right)^{-1}f_j \equiv \sum_{i=1}^j f_i$.

3. A protected vortex exciton qubit

dual lattice [17], $\nabla_\nu A_{i,\tau} \equiv A_{i+\hat{\nu},\tau} - A_{i,\tau}$ and $\nabla_\nu \partial_\tau Q_{i,\tau} \equiv \partial_\tau Q_{i,\tau} - \partial_\tau Q_{i-\hat{\nu},\tau}$. As a result, the transformed constraints are solved by

$$\tilde{J}^\mu_{i,\tau} = \tilde{n}^\mu \left(\vec{n} \cdot \vec{\nabla} \right)^{-1} \partial_\tau Q_{i,\tau} + \varepsilon^{\mu\nu} \tilde{\nabla}_\nu \tilde{A}_{i,\tau}, \tag{3.14}$$

where $\tilde{n}^\mu = n^\mu / \sqrt{E^\mu_J}$ and $\tilde{A}_{i,\tau} = A_{i,\tau} / \sqrt{E^x_J E^y_J}$. $A_{i,\tau}$ is summed over without any constraints, and so $\mathcal{Z}$ becomes

$$\mathcal{Z} = \sum_{\{Q_{i,\tau}\}} \sum_{\{A_{i,\tau}\}} \exp\left(-\varepsilon 2 e^2 \sum_{i,j,\tau} Q_{i,\tau} C^{-1}_{ij} Q_{j,\tau} - \frac{1}{2\varepsilon} \sum_{i,\tau} \underbrace{\left[\tilde{n}^x \left(\vec{n} \cdot \vec{\nabla} \right)^{-1} \partial_\tau Q_{i,\tau} + \tilde{\nabla}_y \tilde{A}_{i,\tau} \right]^2}_{\triangle} \right.$$

$$\left. + \underbrace{\left[\tilde{n}^y \left(\vec{n} \cdot \vec{\nabla} \right)^{-1} \partial_\tau Q_{i,\tau} - \tilde{\nabla}_x \tilde{A}_{i,\tau} \right]^2}_{\square} \right), \tag{3.15}$$

and since $\sum_{\{A_{i,\tau}\}} = \prod_{i,\tau} \sum^\infty_{A_{i,\tau}=-\infty}$, we can use the Poisson resummation formula (D.5) to rewrite $\sum_{\{A_{i,\tau}\}} \exp\left(-\frac{1}{2\varepsilon} \sum_{i,\tau} [\triangle + \square] \right)$ as

$$\prod_{i,\tau} \left[\sum^\infty_{V_{i,\tau}=-\infty} \sqrt{E^x_J E^y_J} \int^\infty_{-\infty} d\tilde{A}_{i,\tau} \exp\left(i 2\pi \sqrt{E^x_J E^y_J} V_{i,\tau} \tilde{A}_{i,\tau} - \frac{1}{2\varepsilon} (\triangle + \square) \right) \right]. \tag{3.16}$$

In the above, $V_{i,\tau}$ is another integer-valued field living on the dual lattice, which we will eventually interpret as representing vortex degrees of freedom [18]. The integrals in (3.16) can be cast into the form of a multi-dimensional Gaussian integral, which can be evaluated in the following manner

$$\prod^N_{i=1} \left(\int^\infty_{-\infty} dA_i \right) \exp\left(-\frac{1}{2} \vec{A}^T \cdot M \cdot \vec{A} + \vec{B} \cdot \vec{A} \right) = \left(\frac{(2\pi)^N}{\det M} \right)^{1/2} \exp\left(\frac{1}{2} \vec{B}^T \cdot M^{-1} \cdot \vec{B} \right), \tag{3.17}$$

where A_i is the ith component of $\vec{A}$ and M is an $N \times N$ positive definite real symmetric matrix. I.e., (3.16) can be rewritten as (upon relabelling $\tilde{A}_{i,\tau} \to A_{i,\tau}$)

$$\exp\left(-\frac{1}{2\varepsilon} \sum_{i,\tau,\mu} \left[\tilde{n}^\mu \left(\vec{n} \cdot \vec{\nabla} \right)^{-1} \partial_\tau Q_{i,\tau} \right]^2 \right) \prod_{i,\tau} \left[\left(\sum^\infty_{V_{i,\tau}=-\infty} \sqrt{E^x_J E^y_J} \int^\infty_{-\infty} dA_{i,\tau} \right) \right.$$

$$\left. \times \exp\left(-\frac{1}{2} \vec{A}^T \cdot M \cdot \vec{A} + \vec{A} \cdot \vec{B} \right) \right], \tag{3.18}$$

---

[17] The dual lattice consists of the set of points at the centres of the elementary squares of the original lattice.

[18] We will spell out why $V_{i,\tau}$ represent vortices when we come to (3.44), but in the meantime still refer to them as vortices.

where the components of $\vec{A}$ are $A_{i,\tau}$ and the components of $\vec{B}$ are

$$B_{i,\tau} \equiv i2\pi\sqrt{E_J^x E_J^y} V_{i,\tau} + \frac{1}{\varepsilon}\varepsilon^{\mu\nu}\tilde{n}^\mu (\vec{n}\cdot\vec{\nabla})^{-1}\tilde{\nabla}_\nu \partial_\tau Q_{i,\tau}. \tag{3.19}$$

The fact that the eigenvalues of M in (3.18) are strictly positive is seen from the following: the trace of M is positive (see (3.21)), and since M is infinite in extent, by symmetry, its eigenvalues must be equal and therefore positive.

The partition function is now thus (up to constants)

$$\mathcal{Z} = \sum_{\{Q_{i,\tau}\}}\sum_{\{V_{i,\tau}\}} \exp\left(-\varepsilon 2e^2 \sum_{i,j,\tau} Q_{i,\tau}C_{ij}^{-1}Q_{j,\tau} - \frac{1}{2\varepsilon}\sum_{i,\tau,\mu}\left[\tilde{n}^\mu\left(\vec{n}\cdot\vec{\nabla}\right)^{-1}\partial_\tau Q_{i,\tau}\right]^2 + \frac{1}{2}\vec{B}^T\cdot M^{-1}\cdot\vec{B}\right).$$
$$\tag{3.20}$$

To determine M^{-1}, we must look at the form of M: it couples only nearest neighbour (in space) components of $\vec{A}$ and is symmetric. The elements of M can be determined by expanding out $\triangle$ and $\square$. Letting $k \equiv (i,\tau)$, we see that its diagonal elements are

$$-\frac{E_J^x}{\varepsilon}A_k^2 - \frac{E_J^y}{\varepsilon}A_k^2 = -\frac{E_J^x + E_J^y}{\varepsilon}A_k^2 \equiv -\frac{1}{2}A_k M_{kk}A_k$$

$$\rightarrow M_{kk} = \frac{2}{\varepsilon}\left(E_J^x + E_J^y\right). \tag{3.21}$$

In a similar vein, the element which couples nearest neighbours in the y-direction, $M_{kl} = M_{lk}$ ($l \equiv (i+\hat{y},\tau)$), is given by

$$\frac{E_J^y}{\varepsilon}A_k A_l \equiv -\frac{1}{2}A_k M_{kl}A_l - \frac{1}{2}A_l M_{lk}A_k = -A_k A_l M_{kl}$$

$$\rightarrow M_{kl} = -\frac{E_J^y}{\varepsilon}, \tag{3.22}$$

while the element which couples nearest neighbours in the x-direction, $M_{kl} = M_{lk}$ ($l \equiv (i+\hat{x},\tau)$), is given by

$$M_{kl} = -\frac{E_J^x}{\varepsilon}. \tag{3.23}$$

In summary, the elements of M' – which for convenience is defined via $M = \frac{2}{\varepsilon}(E_J^x + E_J^y)M' = \frac{2E_J^x}{\varepsilon}(1+\beta)M'$, where $\beta = E_J^y/E_J^x$ is the Josephson energy anisotropy – are (suppressing the time dependence)

$$M'_{kl} = M'_{lk} = \begin{cases} 1 & \text{if } k = l \\ -\frac{\beta}{2(1+\beta)} & \text{if } k = i \text{ and } l = i+\hat{y} \\ -\frac{1}{2(1+\beta)} & \text{if } k = i \text{ and } l = i+\hat{x} \\ 0 & \text{otherwise} \end{cases}. \tag{3.24}$$

3. A protected vortex exciton qubit

We can express M'_{kl} as a Fourier transform [19]

$$M'_{kl} \equiv M'(\vec{r}_k - \vec{r}_l) = \int d^2\vec{q}\, M'(\vec{q}) e^{i\vec{q}\cdot(\vec{r}_k - \vec{r}_l)}, \qquad (3.25)$$

where $\int d^2\vec{q} \equiv \int_{-\pi}^{\pi} \frac{dq_x}{2\pi} \int_{-\pi}^{\pi} \frac{dq_y}{2\pi}$, from which we find

$$M'(\vec{q}) = \sum_{\vec{r}_k - \vec{r}_l} M'(\vec{r}_k - \vec{r}_l) e^{-i\vec{q}\cdot(\vec{r}_k - \vec{r}_l)} = 1 - \frac{\beta}{2(1+\beta)}\left(e^{-iq_y} + e^{iq_y}\right) - \frac{1}{2(1+\beta)}\left(e^{-iq_x} + e^{iq_x}\right)$$

$$\to M'(\vec{q}) = 1 - \frac{1}{(1+\beta)}\left(\cos(q_x) + \beta\cos(q_y)\right). \qquad (3.26)$$

Let us call the inverse of M' the matrix G. This implies that the Fourier transform of G – $G(\vec{q})$ – satisfies $M'(\vec{q})G(\vec{q}) = 1$, and so

$$G_{kl} \equiv G(\vec{r}_k - \vec{r}_l) = \int d^2\vec{q}\, \frac{e^{i\vec{q}\cdot(\vec{r}_k - \vec{r}_l)}}{1 - \frac{1}{(1+\beta)}\left(\cos(q_x) + \beta\cos(q_y)\right)}. \qquad (3.27)$$

It can be shown using the methods outlined in (Cserti, 2000) that

$$G(\vec{r}) = 2(1+\beta)\int_0^{\pi} \frac{dq_y}{2\pi} \frac{e^{-|n|s}\cos(mq_y)}{\sinh(s)}, \qquad (3.28)$$

where $\vec{r} = (n, m)$ and $\sinh(s) = \sqrt{(1 + \beta[1 - \cos(q_y)])^2 - 1}$. Defining the matrix I to be [20]

$$G(\vec{r}) \equiv \frac{2(1+\beta)}{2\pi} I(n, m; \beta), \qquad (3.29)$$

we can thus give an expression for M^{-1}:

$$M^{-1} = \frac{\varepsilon}{2E_J^x(1+\beta)} G = \frac{\varepsilon}{2\pi E_J^x} I. \qquad (3.30)$$

$\frac{1}{2}\vec{B}^T \cdot M^{-1} \cdot \vec{B}$ is now

$$\frac{1}{2}\vec{B}^T \cdot M^{-1} \cdot \vec{B} = -\frac{\varepsilon}{4\pi E_J^x} \sum_{i,j,\tau} \left(2\pi\sqrt{E_J^x E_J^y} V_{i,\tau} - \frac{i}{\varepsilon}\varepsilon^{\mu\nu}\tilde{n}^\mu(\vec{n}\cdot\vec{\nabla})^{-1}\tilde{\nabla}_\nu\partial_\tau Q_{i,\tau}\right) I_{ij}(\beta) \times$$

$$\left(2\pi\sqrt{E_J^x E_J^y} V_{j,\tau} - \frac{i}{\varepsilon}\varepsilon^{\alpha\beta}\tilde{n}^\alpha(\vec{n}\cdot\vec{\nabla})^{-1}\tilde{\nabla}_\beta\partial_\tau Q_{j,\tau}\right). \qquad (3.31)$$

Since M is block diagonal, with all blocks being the same and each block corresponding to a certain time 'slice', the inverse also has the same structure, so we need not label the elements of $I(\beta)$ above with time indices. The cross terms in (3.31) can be summed by

---

[19] We work with dimensionless units, so that the lattice spacing is of unit length.

[20] The dependence of I on β is made explicit here for what follows below.

parts (Fazio & Schön, 1991)

$$\sum_{i,j} V_{i,\tau} I_{ij} \varepsilon^{\alpha\beta} \tilde{n}^{\alpha} (\vec{n} \cdot \vec{\nabla})^{-1} \tilde{\nabla}_{\beta} \partial_{\tau} Q_{j,\tau} = -\sum_{i,j} V_{i,\tau} \underbrace{\varepsilon^{\alpha\beta} \left[\tilde{n}^{\alpha} (\vec{n} \cdot \vec{\nabla})^{-1} \tilde{\nabla}_{\beta} I_{ij} \right]}_{\Theta_{ij}} \partial_{\tau} Q_{j,\tau}, \qquad (3.32)$$

where the charge-vortex interaction potential Θ_{ij} has been introduced, and since $I_{ij} = I_{ji}$ ($I(n,m;\beta) = I(-n,-m;\beta)$), the cross terms contribute the following in (3.31)

$$-i\sqrt{\beta} \sum_{i,j,\tau} V_{i,\tau} \Theta_{ij} \partial_{\tau} Q_{j,\tau}. \qquad (3.33)$$

To analyse the coupling between the time derivative of the charges, we require the identity $\varepsilon^{\mu\nu} \varepsilon^{\alpha\beta} = \delta^{\mu\alpha} \delta^{\nu\beta} - \delta^{\mu\beta} \delta^{\nu\alpha}$, using which

$$\varepsilon^{\mu\nu} \varepsilon^{\alpha\beta} \tilde{n}^{\mu} (\vec{n} \cdot \vec{\nabla})^{-1} \tilde{\nabla}_{\nu} \partial_{\tau} Q_{i,\tau} I_{ij} \tilde{n}^{\alpha} (\vec{n} \cdot \vec{\nabla})^{-1} \tilde{\nabla}_{\beta} \partial_{\tau} Q_{j,\tau} =$$
$$\underbrace{\tilde{n}^{\mu} (\vec{n} \cdot \vec{\nabla})^{-1} \tilde{\nabla}_{\nu} \partial_{\tau} Q_{i,\tau} I_{ij} \tilde{n}^{\mu} (\vec{n} \cdot \vec{\nabla})^{-1} \tilde{\nabla}_{\nu} \partial_{\tau} Q_{j,\tau}}_{(a)} \underbrace{- \tilde{n}^{\mu} (\vec{n} \cdot \vec{\nabla})^{-1} \tilde{\nabla}_{\nu} \partial_{\tau} Q_{i,\tau} I_{ij} \tilde{n}^{\nu} (\vec{n} \cdot \vec{\nabla})^{-1} \tilde{\nabla}_{\mu} \partial_{\tau} Q_{j,\tau}}_{(b)}.$$
$$(3.34)$$

Since $\tilde{n}^{\mu}$ and $\tilde{n}^{\nu}$ can be moved about freely, (b) in (3.34) becomes

$$-(\vec{n} \cdot \vec{\nabla})^{-1} \tilde{n}^{\nu} \tilde{\nabla}_{\nu} \partial_{\tau} Q_{i,\tau} I_{ij} (\vec{n} \cdot \vec{\nabla})^{-1} \tilde{n}^{\mu} \tilde{\nabla}_{\mu} \partial_{\tau} Q_{j,\tau} = -\partial_{\tau} Q_{i,\tau} I_{ij} \partial_{\tau} Q_{j,\tau}, \qquad (3.35)$$

yielding the following contribution to (3.31)

$$-\frac{1}{4\pi\varepsilon E_J^x} \sum_{i,j,\tau} \partial_{\tau} Q_{i,\tau} I_{ij} \partial_{\tau} Q_{j,\tau}. \qquad (3.36)$$

It is known from (Fazio & Schön, 1991) that (a) in (3.34) produces the following contribution to (3.31)

$$\frac{1}{2\varepsilon} \sum_{i,\mu,\tau} \left[\tilde{n}^{\mu} (\vec{n} \cdot \vec{\nabla})^{-1} \partial_{\tau} Q_{i,\tau} \right]^2, \qquad (3.37)$$

which therefore cancels the term of opposite sign which exists in (3.20). The last term to be examined in (3.31) is the vortex-vortex coupling, which is simply

$$-\pi\varepsilon E_J^y \sum_{i,j,\tau} V_{i,\tau} I_{ij}(\beta) V_{j,\tau}. \qquad (3.38)$$

An inspection of I (see (3.27) and (3.29)) reveals that it is infrared divergent (the integrand diverges as $\vec{q} \to 0$). This motivates the decomposition of I into an infrared divergent part and a finite part (Kogut, 1979):

$$I(\vec{r}) = I'(\vec{r}) + I(0), \qquad (3.39)$$

3. A protected vortex exciton qubit

where

$$I'(\vec{r}) = \frac{2\pi}{2(1+\beta)} \int d^2\vec{q} \frac{e^{i\vec{q}\cdot\vec{r}} - 1}{1 - \frac{1}{(1+\beta)}(\cos(q_x) + \beta \cos(q_y))} \qquad (3.40)$$

and $I(0) \sim \ln(R)$, where R is the linear size of the array. This means that in

$$\exp\left(-\pi\varepsilon E_J^y \sum_{i,j,\tau} V_{i,\tau} I_{ij} V_{j,\tau}\right) = \exp\left(-\pi\varepsilon E_J^y I(0) \sum_\tau \left[\sum_i V_{i,\tau}\right]^2\right) \exp\left(-\pi\varepsilon E_J^y \sum_{i,j,\tau} V_{i,\tau} I'_{ij} V_{j,\tau}\right),$$
$$(3.41)$$

as $R \to \infty$ (and so $I(0) \to \infty$), configurations $\{V_{i,\tau}\}$ which are not 'neutral' are suppressed. In other words, only configurations satisfying

$$\sum_i V_{i,\tau} = 0 \quad \forall \tau \qquad (3.42)$$

contribute to the partition function. $\mathcal{Z}$ thus now reads

$$\mathcal{Z} = \sum_{\{Q_{i,\tau}\}} \sum_{\{V_{i,\tau}\}}' e^{-\mathcal{S}_{\text{CCG}}(\{Q_{i,\tau}\},\{V_{i,\tau}\})}, \qquad (3.43)$$

where the prime on the sum means that only neutral configurations $\{V_{i,\tau}\}$ enter the sum, and the *coupled Coulomb gas action* is given by

$$\mathcal{S}_{\text{CCG}}(\{Q_{i,\tau}\},\{V_{i,\tau}\}) = \varepsilon \sum_{i,j,\tau} 2e^2 Q_{i,\tau} C_{ij}^{-1} Q_{j,\tau} + \pi E_J^y V_{i,\tau} I'_{ij} V_{j,\tau} + i\frac{\sqrt{\beta}}{\varepsilon} V_{i,\tau} \Theta_{ij} \partial_\tau Q_{j,\tau}$$

$$+ \frac{1}{4\pi\varepsilon^2 E_J^x} \partial_\tau Q_{i,\tau} I_{ij} \partial_\tau Q_{j,\tau}. \qquad (3.44)$$

For an isotropic array ($\beta = 1$), I'_{ij} implies a logarithmic interaction between vortices [21]. This agrees with a heuristic derivation of the form of the interaction between a vortex and an antivortex (Tinkham, 2004). We are thus led to interpret the variables $V_{i,\tau}$ as representing vortex degrees of freedom. For arrays in which the two charging energies are equal, C_{ij}^{-1} also assumes a logarithmic form (in the limit of vanishing self capacitance). This is precisely the nature of the Coulomb interaction between electric charges confined to a 2D world, and so this motivates the name of the action. Having seen how vortices emerge from a path integral description of the system, let us now examine a Hamiltonian description of the array. Such a description will allow us to fine tune the parameters of the array, so that a dual of KCMQ can be constructed.

---

[21] The interaction is asymptotically logarithmic (i.e. as $|\vec{r}_i - \vec{r}_j| \to \infty$), although the logarithmic form is not a bad approximation even when $|\vec{r}_i - \vec{r}_j|$ is $\mathcal{O}(1)$ (Kogut, 1979).

3.3 Hamiltonian description of the array

The emergence of vortices and the almost perfect symmetry that exists between charges and vortices in $\mathcal{S}_{\text{CCG}}$ suggests that a *dual description* of the system exists. In other words, a representation in terms of vortices $\{V_i\}$ and phases $\{\theta_i\}$ (residing on the dual lattice), conjugate to the vortices, ought to exist. Indeed, when charging energies are small compared to the corresponding Josephson energies (as is the case in the array we consider – see below in this section), charge fluctuations become pronounced while the phases of the islands become ordered. In such regimes, vortices, rather than Cooper-pairs, become the relevant dynamical degrees of freedom, and it can be more convenient to analyse a Hamiltonian defined in terms of vortices and their conjugate phases (Choi, 1994; van Wees, 1991). The Hamiltonian describing our array is

$$\mathcal{H}^v = \pi E_J^y \sum_{i,j} V_i I'_{ij} V_j - \frac{2}{\pi^2} E_C^y \sum_i \cos\left(\theta_{i+\hat{x}} - \theta_i\right) - \frac{2}{\pi^2} E_C^x \sum_i \cos\left(\theta_{i+\hat{y}} - \theta_i\right), \qquad (3.45)$$

where the sums are over the dual lattice sites, and vortices and phases satisfy the commutation relation $[\theta_i, V_j] = i\delta_{ij}$.

Let us justify (3.45). Just as vortices emerged from the Villain approximation of the phases $\{\phi_i\}$, it is clear that a Villain approximation of the dual phases $\{\theta_i\}$ in (3.45) would yield the electric charging energy contribution to $\mathcal{S}_{\text{CCG}}$. C_{ij} – in particular, the charging energies associated with the junction capacitances – fixes the dual Josephson couplings to be $E_{JD}^y \equiv \frac{2}{\pi^2} E_C^x = \frac{2}{\pi^2} \frac{e^2}{2C_x}$ and $E_{JD}^x \equiv \frac{2}{\pi^2} E_C^y = \frac{2}{\pi^2} \frac{e^2}{2C_y}$. To see this, we first examine the capacitance matrix, which is

$$C_{ij} = \begin{cases} 2(C_x + C_y) & \text{if } i = j \\ -C_x & \text{if } i = j \pm \hat{x} \\ -C_y & \text{if } i = j \pm \hat{y} \\ 0 & \text{otherwise} \end{cases} . \qquad (3.46)$$

We have omitted the self-capacitances of the islands (which would contribute to the diagonal of the matrix) since experiments show that they are negligible compared to the junction capacitances (Fazio & Van der Zant, 2001). C_{ij} agrees with circuit theory, since we expect the charge on island i, Q_i, to equal $\sum_j C_{ij}\Phi_j$ (Φ_j being the potential of island j), and indeed it does:

$$Q_i = C_x(\Phi_i - \Phi_{i+\hat{x}}) + C_x(\Phi_i - \Phi_{i-\hat{x}}) + C_y(\Phi_i - \Phi_{i+\hat{y}}) + C_y(\Phi_i - \Phi_{i-\hat{y}})$$
$$= 2(C_x + C_y)\Phi_i - C_x(\Phi_{i+\hat{x}} + \Phi_{i-\hat{x}}) - C_y(\Phi_{i+\hat{y}} + \Phi_{i-\hat{y}})$$
$$= \sum_j C_{ij}\Phi_j .$$

In section 3.2, we saw that anisotropic Josephson couplings of the phases $\{\phi_i\}$ give rise to the form of the vortex-vortex interaction I'_{ij}. Similarly, anisotropic Josephson couplings of

3. A protected vortex exciton qubit
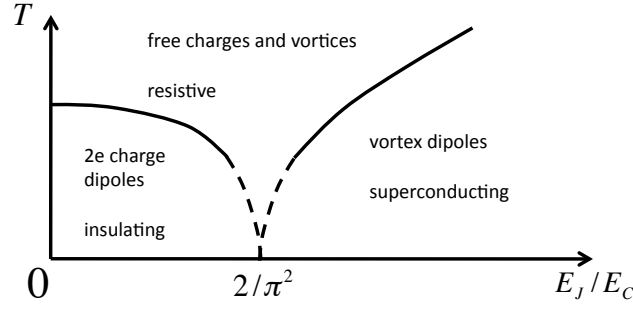
Figure 3.3: The phase diagram for an isotropic array (see (Fazio & Schön, 1991)).

the dual phases $\{\theta_i\}$ would give rise to C_{ij}^{-1}. Comparing with how $\vec{B}^T \cdot M^{-1} \cdot \vec{B}/2$ gives rise to the vortex-vortex interaction term, we see that we should make the identification (see (3.19))

$$\frac{1}{2}\left(i2\pi\sqrt{E_{JD}^x E_{JD}^y}Q_i\right)(M^{-1})_{ij}\left(i2\pi\sqrt{E_{JD}^x E_{JD}^y}Q_j\right) = -\varepsilon 2e^2 Q_i (C^{-1})_{ij}Q_j$$

$$\rightarrow M_{ij} = \frac{\pi^2}{\varepsilon e^2}E_{JD}^x E_{JD}^y C_{ij}. \qquad (3.47)$$

(3.22), (3.23) and (3.46) tell us that

$$-\frac{E_{JD}^y}{\varepsilon} \equiv -\frac{\pi^2}{\varepsilon e^2}E_{JD}^x E_{JD}^y C_y$$

$$\rightarrow E_{JD}^x \equiv \frac{2}{\pi^2}\frac{e^2}{2C_y} = \frac{2}{\pi^2}E_C^y, \qquad (3.48)$$

and similarly $E_{JD}^y \equiv \frac{2}{\pi^2}E_C^x$.

Of course, the last term in (3.44) cannot be represented in (3.45). This term breaks the perfect symmetry between charges and vortices, and reflects the spin-wave excitations of the superconducting phases. In general, spin-waves are a source of dissipation for vortices. However, since we are assuming that self-capacitances are negligible, the spin-wave dispersion only has an optical branch (Fazio & Van der Zant, 2001). As a result, the spin-wave-vortex coupling is irrelevant at low temperatures, and so (3.45) should be an effective description of the array.

We are now in a position to see how the physics of KCMQ can be mirrored in the system, with the right choice of parameters in $\mathcal{H}^v$ and appropriate boundary conditions. Here, the analogue of the charge excitons in KCMQ are vortex-antivortex pairs (vortex excitons), which, as mentioned in section 3.1, can bind naturally in a classical array when the temperature is below T_{BKT}. The phase diagram for an isotropic 'quantum array' (i.e. when the charging energies are not negligible), was established in (Fazio & Schön, 1991) and is shown in figure 3.3. In such arrays, there are two different BKT transitions, namely, a vortex-unbinding transition when $E_J \gg E_C$, and a charge-unbinding transition when $E_C \gg E_J$. These two transitions therefore compete when $E_J \sim E_C$ and meet at the quantum critical
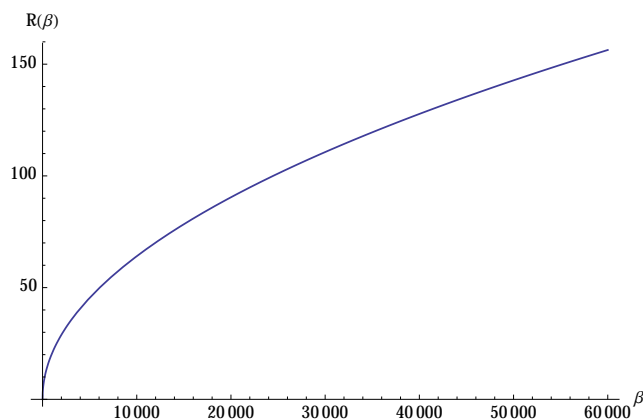
Figure 3.4: Ratio of energies required for a nearest neighbour vortex exciton to form in the x-direction compared to the y-direction, $R(\beta)$, as a function of the Josephson coupling anisotropy, $\beta = E_J^y / E_J^x$.

point $E_J / E_C \approx 2/\pi^2$.

Since we are considering an array with anisotropies in both the Josephson and charging energies, the phase diagram of the array will acquire 'extra dimensions'. For instance, one extra dimension will be the Josephson energy anisotropy parameter, β, since it is known that the critical temperature in the anisotropic 2D XY model depends on the strength of the anisotropy (Spišák, 1993). We will assume that whatever our required array parameters, we can place the system in an area of the phase diagram where vortices and antivortices are bound together. In the next chapter, we will discuss arrays of junctions for measurements and gates, in which we will require the existence of free vortices. Figure 3.3 informs us that it is thus undesirable to run the qubit in an ultra-low temperature environment, since the only two phases available to arrays at $T \approx 0$ are the vortex dipole and charge dipole phases. The fact that an ultra-low temperature environment is not required may make an experimental realization of the qubit easier to come by.

In KCMQ, the charge excitons are arranged in the vertical (y) direction. Similarly, vortex excitons also orient themselves in this manner since, as mentioned in section 3.2, we assume that $E_J^y \gg E_J^x$. This can be seen by considering the ratio of the energies required to form nearest neighbour vortex dipoles in the x-direction ('$+-$' or '$-+$') and in the y-direction ('$\pm$' or '$\mp$'). We denote this ratio by [22]

$$R(\beta) \equiv \frac{I'(1,0;\beta)}{I'(0,1;\beta)}, \tag{3.49}$$

and it is plotted in figure 3.4. Clearly, for large enough anisotropy (i.e. $\beta = E_J^y / E_J^x \gg 1$), it is energetically much more favourable for vortex excitons to orient themselves vertically rather than horizontally.

---

[22] $I_{ij}(\beta) \equiv I(x_i - x_j, y_i - y_j; \beta)$, where distances are measured in units of the lattice spacing.

3. A protected vortex exciton qubit

The absence of Josephson tunnelling between the two chains of KCMQ means that the motion of Cooper-pairs is restricted to one dimension. Likewise, to ensure that vortices only move along the length of the array, we require the Josephson tunnelling of the vortices in the y-direction to be inhibited. Such motion can be achieved by taking the inertia of the vortices in the y-direction to dominate the inertia in the x-direction i.e. by enforcing $C_x \gg C_y \rightarrow E_C^y \gg E_C^x$. Furthermore, since we want the array to be in the regime of phase coherence where vortices are the relevant degrees of freedom, the Josephson energies must dominate the corresponding charging energies, i.e. $E_J^i \gg E_C^i, i \in \{x,y\}$. In particular, the condition $E_J^y \gg E_C^y$ ensures that uncorrelated vortex hopping is too costly, although correlated motion of vortex excitons is possible, as we shall explain below.

Upon neglecting tunnelling in the y-direction, Hamiltonian (3.45) becomes

$$\mathcal{H}^v \approx \pi E_J^y \sum_{i,j} V_i I_{ij}' V_j - \frac{2}{\pi^2} E_C^y \sum_i \cos\left(\theta_{i+\hat{x}} - \theta_i\right), \qquad (3.50)$$

and using the notation employed in (Choi *et al.*, 1998), this can be rewritten as

$$\mathcal{H}^v = \pi E_J^y \sum_{l,l',x,x'} V_l(x) I_{ll'}'(x,x') V_{l'}(x') - \frac{2}{\pi^2} E_C^y \sum_{l,x} \cos\left(\theta_l(x+1) - \theta_l(x)\right). \qquad (3.51)$$

In the above, $l = 1,2$ denotes the y-coordinate of the dual lattice sites, while x denotes the coordinate along the length of the array. Given the one-to-one correspondence between the essential features of KCMQ and the system we are considering, $\mathcal{H}^v$ is well approximated by (compare with (2.7) in the previous chapter)

$$\begin{aligned}
\mathcal{H}^v \approx &\ \mathcal{O}[-I'(1,0;\beta)] E_J^y \sum_x V_+(x)^2 + \mathcal{O}[-I'(0,1;\beta)] E_J^y \sum_x V_-(x)^2 \\
&+ \mathcal{O}[-I'(1,0;\beta)] E_J^y \sum_{x;y>0} V_+(x) V_+(x+y) \\
&- \frac{4}{\pi^2} E_C^y \sum_x \cos\left[\theta_+(x+1) - \theta_+(x)\right] \cos\left[\theta_-(x+1) - \theta_-(x)\right], \qquad (3.52)
\end{aligned}$$

where $V_\pm(x) = V_1(x) \pm V_2(x)$ and $\theta_\pm(x) = [\theta_1(x) \pm \theta_2(x)]/2$.

We are interested in the low energy dynamics of the system, and given that the energy scale for horizontal excitons ($\mathcal{O}[-I'(1,0;\beta)] E_J^y$) dominates the other energy scales, we can project (3.52) into the subspace $V_+(x) = 0$, $V_-(x) = 0, \pm 2$. This projection yields the effective Hamiltonian (in complete analogy to how the effective Hamiltonian (2.8) of KCMQ is derived)

$$\mathcal{H}_{\text{eff}}^v \approx \mathcal{O}\left[-4I'(0,1;\beta)\right] E_J^y \sum_x V_-'(x)^2 - E_C^{\text{ex}} \sum_x \cos\left[\theta_-'(x+1) - \theta_-'(x)\right], \qquad (3.53)$$

where $\theta_-'(x) = 2\theta_-(x)$, $V_-'(x) = V_-(x)/2$ and $E_C^{\text{ex}} \equiv \frac{4}{\pi^4} \frac{E_C^{y\,2}}{\mathcal{O}[-I'(1,0;\beta)] E_J^y}$. $\mathcal{H}_{\text{eff}}^v$ describes a one-dimensional chain of junctions in which vertically aligned vortex excitons can tunnel. In
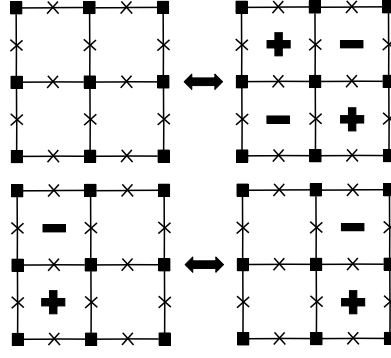
Figure 3.5: Examples of vortex exciton tunnelling.

other words, the effective low energy degrees of freedom are vortex-antivortex pairs at position x – characterized by the quantum number $V'_-(x)$ – which can tunnel due to a Josephson coupling energy E_C^{ex}, as shown schematically in figure 3.5. This is precisely the scenario in KCMQ, with vortices replaced by Cooper-pairs. For the system to be in the superfluid phase where the fluctuations of the phases θ'_- are small and the dipoles tunnel freely, the tunnelling strength must dominate the vortex 'charging energy', i.e. $E_C^{\text{ex}} \gg \mathcal{O}\left[-4I'(0,1;\beta)\right]E_J^y$. This leads to the requirement

$$\left(\frac{E_C^y}{E_J^y}\right)^2 \gg \underbrace{\pi^4 \mathcal{O}\left[I'(0,1;\beta)\right]\mathcal{O}\left[I'(1,0;\beta)\right]}_{X}. \tag{3.54}$$

It is possible to see that there are parameter regimes which satisfy the condition immediately above and the condition [23]

$$\left(\frac{E_C^y}{E_J^y}\right)^2 \ll \underbrace{\frac{\pi^4}{16}\left(\mathcal{O}\left[I'(1,0;\beta)\right]\right)^2}_{Y}, \tag{3.55}$$

which is needed so that the projection into the subspace $V_+(x) = 0, V_-(x) = 0, \pm 2$ is valid. If we demand that (3.54) satisfies $(E_C^y/E_J^y)^2 = \gamma X$ and (3.55) satisfies $(E_C^y/E_J^y)^2 = \gamma^{-1}Y$, where $\gamma > 1$, then dividing these two equations yields [24]

$$R(\beta) = 16\gamma^2. \tag{3.56}$$

Choosing $\gamma = 3$ leads to $\beta \sim 5 \times 10^4$, which means that $(E_C^y/E_J^y)^2 \sim 10^{-4}$. These conditions do not fix the lowest energy scale, E_C^x, and we are free to choose it so that the junctions in the x-direction are phase coherent, just like their counterparts in the y-direction. Thus, all necessary conditions can be satisfied, although it is clear that there are many orders of

---

[23]This condition is equivalent to $\mathcal{O}\left[-I'(1,0;\beta)\right]E_J^y \gg (4/\pi^2)E_C^y$.

[24]We make the replacements $\mathcal{O}\left[I'(1,0;\beta)\right] \to I'(1,0;\beta)$ etc.
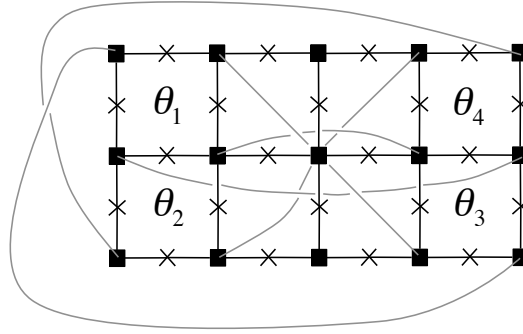
Figure 3.6: The superconducting wires that should be attached to establish the boundary conditions needed for a π-periodic energy landscape.

magnitude separating the highest and lowest energy scales. This separation increases for larger choices of γ, which would be ideal so that the inequalities in (3.54) and (3.55) are well satisfied. In practice, it may be difficult to realize a sufficiently broad range of energies.

The energy of the system is described by an equation with exactly the same form as (2.9), but with the replacements $\varphi_i \to \theta_i$, where θ_i are the dual phases at the corners of the array (see figure 3.6). The error term identified by Kitaev also has a counterpart here, and can be justified as follows. In addition to the tunnelling of vortex excitons, rare uncorrelated tunnelling of individual vortices may also occur. For such a process to provide a net contribution to vortex current (and hence a contribution to the energy, since the derivative of the energy with respect to suitable phases yields a current), a vortex must move from one end of the array to the other. If the length of the array is N and the probability for a vortex to hop to an adjacent site is p – where p is small – then the probability for a vortex to make its way from one end to the other is p^N. Hence, the error term decreases exponentially in the length of the array.

As explained in the previous chapter, Kitaev arrived at a π-periodic energy with two degenerate minima by connecting the leads of his device diagonally. To establish a π-periodicity here, the phases of the top left plaquette and the bottom right plaquette must be identified, and similarly, the bottom left and the top right phases must be set equal too. Attaching superconducting wires between the islands in the manner depicted in figure 3.6 will do the job. The wires equalize the phases of the superconducting islands that they connect. Hence, if one were to track the winding of the superconducting phases of the top left and bottom right plaquettes, one would find that the windings (or vorticities) would be the same, which implies $\theta_1 = \theta_3$ (and similarly $\theta_2 = \theta_4$). The π-periodic energy (up to an exponentially small correction) that results from the boundary conditions, and the states localized around the two minima to be used as the computational basis for the qubit, will be as shown in figure 2.3 (with the replacements $\varphi_i \to \theta_i$).

As with KCMQ, the exponentially small difference in the energy of the minima (due to the error term) would suppress dephasing. Furthermore, owing to the one-to-one correspondence between the essential features of KCMQ and its dual, we expect the degeneracy to be little affected by modest disorder in the array parameters, as has been shown for KCMQ (Dempster *et al.*, 2014). The condition which guarantees that bit flips are suppressed in KCMQ, (2.10), has an analogy here as well – (3.54). As explained above, this condition can be met in principle, although in practice it may be difficult to realize. These features thus protect the qubit from errors at the hardware level.

3.4 Summary and discussion

In this chapter, we have demonstrated how a protected qubit – a magnetic analogue of KCMQ – emerges in a suitable array of junctions. A path integral representation of the array reveals that a dual description exists in terms of vortices and dual phases. This motivates the analysis of a Hamiltonian in a vortex and dual phase representation, to see how to mirror the physics of KCMQ. With an appropriate choice of parameters, one can arrive at an effective Hamiltonian, (3.53). (3.53) tells us that the system can be viewed as a chain of junctions which is superconducting with respect to vortex excitons (vortex-antivortex pairs). We note that quantum coherent behaviour of vortices (which is needed for our qubit and gates to function) has been observed in arrays for many years (Elion *et al.*, 1993).

By implementing certain conditions on the boundary phases, the array energy becomes π-periodic in a global phase difference – a difference of phases at the ends of the system. Two distinct minima are positioned at phase differences of 0 and π, and the states localized at these minima can be identified with the computational basis of a qubit. Since the minima are degenerate up to an exponentially small correction in the length of the array, dephasing would be inhibited. Bit flips can also be suppressed in principle with the right choice of array parameters. Hence, the qubit should be well protected from errors at the hardware level and is an addition to the family of protected 0-π qubits (Douçot & Vidal, 2002; Gladchenko *et al.*, 2008; Ioffe & Feigelman, 2002; Kitaev, 2006b).

In practice, the system will be subject to stray external magnetic fields, which will act analogously to external gate charge in KCMQ. However, as noted in section 2.3, magnetic noise is generally less of a headache than electric noise in a laboratory, and we expect the qubit to be resilient to a small amount of noise. Furthermore, the problem of random offset charges on the islands due to electric noise is non-existent since Josephson energies in our array dominate the corresponding charging energies, which means that charge fluctuations are strong anyway. In the next chapter, we adapt Kitaev's proposal for universal fault-tolerant QC to our dual construction.

CHAPTER 4

Fault-tolerant universal quantum computation using protected vortex exciton qubits

Kitaev proposed a scheme for universal QC (Kitaev, 2006b), suitable for use with 0-π superconducting qubits [25]. This scheme is attractive due to its intrinsic fault-tolerance. In attempting to control qubits (say, to perform single qubit gates), errors inevitably crop up (over or under-rotations). This is due to unavoidable imperfections in the timing of the protocol or the coupling strength between the qubit and the external system. Clearly, the suppression of such errors at the hardware level is desirable, since it saves the experimentalist from resorting to costly error correction procedures, and this is precisely what Kitaev's scheme promises.

The measurements and gates proposed by Kitaev are:

1. Measurement in the computational basis ('Z measurement')

2. Measurement in the dual basis ('X measurement')

3. The one-qubit unitary $R_1(\pi/8) = \exp(i(\pi/8)Z)$ and its inverse

4. The one-qubit unitary $R_1(\pi/4) = \exp(i(\pi/4)Z)$ and its inverse

5. The two-qubit unitary $R_2(\pi/4) = \exp(i(\pi/4)Z \otimes Z)$ and its inverse

This set of measurements and gates was shown by Kitaev to be universal. A computation using this set would be adaptive: the outcomes of intermediate measurements fix the gates to be applied in the future. The X and Z measurements for KCMQ are believed to be

---

[25]To be precise, it is suitable for use with superconducting qubits whose microscopic degrees of freedom are Cooper-pairs and superconducting phases. Physically, the scheme has to be altered for qubits which utilise vortices and dual phases. The current chapter addresses this problem.

Figure 4.1: Scheme for measurement in the computational basis.

fault-tolerant [26] (Kitaev, 2006b), while the phase gates $R_{1/2}(\pi/4)$ have been shown to be fault-tolerant (Brooks *et al.*, 2013) if certain conditions are met (see section 4.5). If these measurements and phase gates are exact, then $R_1(\pi/8)$ can be afforded to be 'noisy': it only needs to be realized with a fidelity of $F > 0.93$ to enable fault-tolerant computations (Bravyi & Kitaev, 2005). Of course, in practice, some noise is likely to be associated with the measurements, although it has been noted that repetition and majority voting or repetition coding can improve reliability (Brooks *et al.*, 2013).

In this chapter, we adapt Kitaev's measurement and gate set to our qubit. We explain how fault-tolerant computation with current mirror qubits can be mimicked with vortex exciton qubits (VEQs). To this end, we present two novel circuit elements: a vortex DC SQUID and a vortex harmonic oscillator. This chapter is based on results in (De & Spiller, 2014).

4.1 Computational basis measurement

A method of measuring in the computational basis $\{|0\rangle, |1\rangle\}$ is sketched in figure 4.1. Two 'tracks' of junctions are connected onto the ends of the qubit, and the finite but small temperature [27] implies that free vortices can exist in the tracks if the charging and Josephson energies are similar. We take the top loop to enclose an external electric charge, Q. It is well known that electrons circling around magnetic flux acquire a phase due to the

---

[26]I.e. it is believed that they can be performed non-destructively and with little probability of changing the measured observable.

[27]Recall from figure 3.3 in the previous chapter that a finite temperature is needed for free vortices to exist in principle.

Aharonov-Bohm effect (Aharonov & Bohm, 1959). Similarly, vortices traversing around electric charge acquire a phase due to a dual phenomena known as the *Aharonov-Casher effect* (Aharonov & Casher, 1984; Reznik & Aharonov, 1989), which has already been seen in arrays (Elion *et al.*, 1993). An electric charge vector potential, $\vec{A}_Q$, can therefore be introduced (Van Wees, 1990) satisfying

$$\oint_C d\vec{r} \cdot \vec{A}_Q = Q, \tag{4.1}$$

where the closed contour C encloses Q. The gauge invariant phase difference between plaquettes j and i is thus (compare for (1.4))

$$\theta_j - \theta_i - \frac{\Phi_0}{\hbar} \int_i^j d\vec{r} \cdot \vec{A}_Q. \tag{4.2}$$

As a result, the top loop will be subject to the constraint

$$2\pi \frac{Q}{2e} = \chi + \sum_i \Delta\theta_i, \tag{4.3}$$

where

$$\chi = \theta_2 - \theta_1 - \frac{\Phi_0}{\hbar} \int_1^2 d\vec{r} \cdot \vec{A}_Q = 0, \pi, \tag{4.4}$$

and $\{\Delta\theta_i\}$ are the gauge invariant phase drops across the qubit and the rest of the loop, respectively.

Say the ground state corresponds to all the phase drops $\{\Delta\theta_i\}$ being equal. This being the case, the vortex current in the top loop $\sim \sin\Delta\theta_i$ will depend on Q and χ. If $Q/(2e) = 1/4$, then a measurement of the vortex current [28] – which through the AC Josephson effect is equivalent to a voltage measurement (see figure 4.1 and (1.9)) – would reveal the state of the qubit.

As with the analogous measurement for KCMQ, this protocol should be fault-tolerant, since χ is as protected during the measurement as when the qubit is 'idle'. Noise in the measurement can be overcome by applying the CPHASE gate [29] to the target qubit and an ancilla qubit in the state $|+\rangle = (|0\rangle + |1\rangle)/\sqrt{2}$, and then performing an X measurement (see section 4.2) on the ancilla. Repeating this procedure and using majority voting will yield a reliable Z measurement (Brooks *et al.*, 2013).

4.2 Dual basis measurement

Before we discuss a dual basis $\{|\pm\rangle = (|0\rangle \pm |1\rangle)/\sqrt{2}\}$ measurement, we will first discuss the dual protocol for KCMQ. Such a measurement for VEQs will require a 'vortex charge qubit' (discussed below in 4.2.2), which to the best of our knowledge has not been discussed

---

[28] With $Q/(2e) = 1/4$, if $\chi = 0$ then $\sin\Delta\theta_i > 0$, while if $\chi = \pi$ then $\sin\Delta\theta_i < 0$.

[29] CPHASE can be decomposed in terms of the protected phase gates $R_1(\pi/4)$ and $R_2(\pi/4)$ (Brooks *et al.*, 2013).
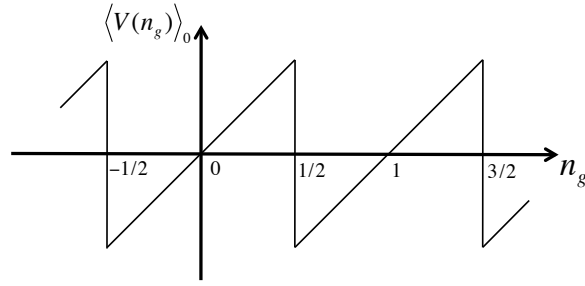
Figure 4.2: The ground state expectation value of the voltage as a function of n_g.

in the literature. Thus, it will be helpful to first consider the method for KCMQ which utilises a conventional charge qubit.

4.2.1 Dual measurement for KCMQ

As explained in section 2.2, the basis states of KCMQ have the following interpretation: $|0\rangle$ corresponds to the state peaked about $\Theta \equiv \varphi_2 - \varphi_1 = 0$, while $|1\rangle$ corresponds to the state peaked about $\Theta = \pi$. If $|0,1\rangle$ are ideal 'spikes' at $\Theta = 0, \pi$, then $|+,-\rangle$ are superpositions of either even or odd number states, respectively. This is easily seen be expanding the basis in terms of the number states $\{|n\rangle\}$

$$|\Theta\rangle = \sum_{n=-\infty}^{\infty} e^{in\Theta} |n\rangle \,, \tag{4.5}$$

where $\{|n\rangle\}$ are eigenstates of n, the number operator conjugate to Θ. $|+,-\rangle$ can thus be thought of as even or odd parity states, respectively. A dual basis measurement therefore corresponds to a parity measurement of n.

Attaching a charge measurement device – say a charge qubit (an elementary CPB, as described in section 1.3.1) – to the terminals of the qubit is no good for measuring the parity of n. This is because charge qubits respond with unit period i.e. they have the same response to n and $n+1$ offset or gate charge (in dimensionless units). This motivates the following observation by Kitaev: If the wire connecting terminals 1 and 3 is cut, then $2\varphi_2 - \varphi_3 - \varphi_1 = 0 \,(\mathrm{mod}\,2\pi)$, from which it follows that the phase drop across these terminals becomes $\varphi_3 - \varphi_1 = 2(\varphi_2 - \varphi_1) \equiv 2\Theta$. The operator conjugate to the phase difference 2Θ is $n/2$. If we now connect terminals 1 and 3 across a charge qubit, the charge qubit can now tell the difference between even and odd n i.e. it can tell whether $n/2$ is an integer or half-odd integer.

The Hamiltonian for a charge qubit is

$$\mathcal{H}_{\mathrm{ch}} = 4E_C(N - n_g)^2 - E_J \cos\phi \,, \tag{4.6}$$

where $[\phi, N] = i$, E_C and E_J are the charging and Josephson energies, respectively, and n_g is the dimensionless external bias applied to the charge qubit. Attaching terminals 1 and

3 across the charge qubit leads to a bias of $n_g = n/2$. The voltage across the charge qubit is given by $V = \frac{1}{2e}\frac{\partial \mathcal{H}}{\partial n_g}$, which leads to (using the Hellmann-Feynman theorem) the ground state expectation value of the voltage to be

$$\langle V(n_g)\rangle_0 = \frac{1}{2e}\frac{\partial E_0}{\partial n_g}, \tag{4.7}$$

where $E_0(n_g)$ is the ground state energy. This expectation value is periodic in n_g with unit period, and resembles a 'sawtooth', as shown in figure 4.2.

Adding a further bias of about $1/4$ leads to a total bias of $n_g \approx 1/4 + n/2$. A voltage measurement of the charge qubit subsequently needs to be performed. If the measured voltage is positive, then n is even, whereas if it is negative, then n is odd. Since we are considering an elementary charge qubit operating in the regime where E_C dominates E_J, its eigenstates are effectively charge eigenstates (except near the 'sweet spots' where n_g is a half-odd integer). As a result, the measured voltage would be to a very good approximation equal to $\langle V\rangle_0$, and so the measurement is essentially one-shot. This scheme thus realises a parity measurement of n.

4.2.2 Dual measurement for VEQs

As with the dual basis measurement for KCMQ, a dual measurement on a VEQ is tantamount to a parity measurement of m, the operator conjugate to χ, defined in (4.4). Such a measurement requires a 'vortex charge qubit'. Similar to a conventional charge qubit, two equal and oppositely charged vortices sitting next to each other will store some 'vortex charging energy'. The device we have in mind is similar to a dual DC SQUID, which is discussed in section 4.3 and sketched in figure 4.3 [30]. To be concrete, let us take the vortex on the left plaquette to have charge $-M$, while its neighbour has charge $+M$. The precise form of the charging energy is given by the vortex-vortex interaction, which is discussed in section 3.2. For short distances, the interaction is not easy to work with. Nonetheless, the fact that the charging energy is symmetric under $M \to -M$ and vanishes as $M \to 0$ are the only pieces of information that we need for our purposes.

Since the energy is symmetric and is not simply constant, this device has properties reminiscent of a conventional charge qubit. Applying a charge bias of $1/2$ (in units of the flux quantum) to one of the plaquettes and $-1/2$ to the other plaquette will result in the states $M = 0$ and $M = 1$ becoming degenerate. However, vortex tunnelling, which can be controlled by external electric charge (see figure 4.3) will break the degeneracy, resulting in a spectrum that should be qualitatively similar to that of a charge qubit, at least for the lowest band. Hence, we call this device a 'vortex charge qubit'.

A parity measurement now follows in complete analogy to the scheme for KCMQ. The

---

[30]In our discussion of a dual DC SQUID in section 4.3, we are interested in the regime where the vortex tunnelling strength dominates the interaction energy, whereas the opposite regime interests us here.
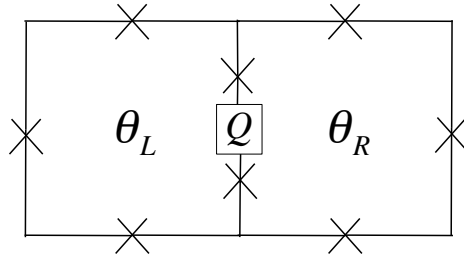
Figure 4.3: A vortex DC SQUID.

first step is to cut the wires that equalize the phases θ_1 and θ_3. This results in a phase difference of $\theta_3 - \theta_1 = 2(\theta_2 - \theta_1) = 2\chi$ between the free ends, which is conjugate to $m/2$. The next step is to take a vortex charge qubit and apply the free ends of the VEQ across it. Since the charge qubit has a unit period energy (with respect to bias charge), so does the ground state vortex voltage, which is physically an electrical current [31]. This means that if a bias of $\sim 1/4$ is applied, then measurement of the vortex charge qubit voltage will yield the parity of m.

This measurement should be fault-tolerant, for the same reason given for the fault-tolerance of the Z measurement. Given this, noise in the measurement procedure can again be overcome by using the trick mentioned at the end of section 4.1 (Brooks *et al.*, 2013). In fact, (Brooks *et al.*, 2013) notes that even if there is some probability for the measurement to flip the parity of m, this can be negated by employing repetition coding.

4.3 $R_1(\pi/8)$ gate

An unprotected rotation $R_1(\pi/8)$ can be realized using the setup in figure 4.1 with some modifications: external charge and voltage measurement are not needed, while a switch of some sort should be inserted in the top track. This switch could be a dual or vortex DC SQUID, a realization of which we now sketch.

We envisage a device which consists of two adjacent vortex sites with phases $\theta_{L/R}$, as shown in figure 4.3. Tunnelling can occur between the two sites across two junctions which both have charging energy E_C. Charge $Q(t)$ (which we assume can be controlled with time t) sitting on the island between these two junctions can control tunnelling, in the same way that external flux piercing a conventional DC SQUID (Tinkham, 2004) controls charge tunnelling via parallel paths. The two gauge invariant phase differences are

$$\theta_{L \to R} = \theta_R - \theta_L - \frac{\Phi_0}{\hbar} \int_L^R d\vec{r} \cdot \vec{A}_Q \;, \;\; \theta_{R \to L} = \theta_L - \theta_R - \frac{\Phi_0}{\hbar} \int_R^L d\vec{r} \cdot \vec{A}_Q \;, \qquad (4.8)$$

with $\vec{A}_Q$ satisfying (4.1). The energy of this component has the form expected for a DC

---

[31] The equation $Q = CV$ which describes a conventional capacitor is 'dual' to the equation $\Phi = LI$ which describes a conventional inductor or a 'flux capacitor'. Hence, 'flux voltage' corresponds to electrical current.
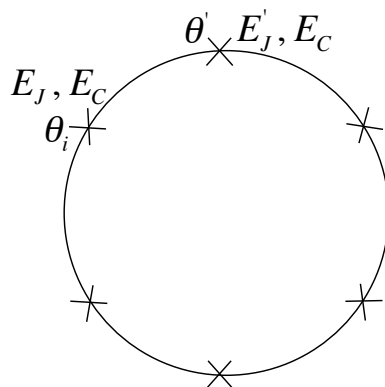
Figure 4.4: A ring of Josephson junctions.

$$-E_C \left(\cos \theta_{L \to R} + \cos \theta_{R \to L} \right) = -2E_C \cos \left(\frac{\pi Q(t)}{2e} \right) \cos \left(\theta_R - \theta_L \right)$$

$$\equiv -E_C(t) \cos \left(\theta_R - \theta_L \right), \tag{4.9}$$

where $E_C(t)$ is the time-dependent coupling energy of the dual DC SQUID.

When the switch is turned on, an interaction term proportional to $\cos \chi = Z$ is generated. This can be seen easily by noting that $\cos \chi |0\rangle = |0\rangle$ and $\cos \chi |1\rangle = -|1\rangle$ if $|0\rangle$ and $|1\rangle$ are ideal spikes located at $\chi = 0, \pi$, respectively. The switch pulse should thus satisfy $\frac{1}{\hbar} \int_0^T E_C(t) \, dt = \frac{\pi}{8}$, for some time T to implement the gate $R_1(\pi/8) = \exp \left(i(\pi/8)Z \right)$. We assume that when the switch is inserted into the top track, dual phase locking occurs, so that the term $-E_C(t)Z$ is the only addition to the qubit Hamiltonian.

Clearly, the fidelity of this gate will suffer from timing errors and fluctuations in the coupling strength $2E_C \cos \left(\frac{\pi Q}{2e} \right)$. However, as mentioned in the introduction to this chapter, a moderate loss of fidelity can be tolerated as long as the other gates and measurements are highly accurate.

4.4 A dual *LC* oscillator

The protected phase gates first described by Kitaev and elaborated on in (Brooks *et al.*, 2013) require the 0-π qubit to be coupled to a high impedance electrical *LC* oscillator. Implementing these protected phase gates on a VEQ therefore demands the construction of a high impedance vortex or dual *LC* oscillator. We now turn our attention to this.

---

[32]We are assuming that E_C dominates the Josephson energies of the device, so that the vortex-vortex interaction term can be neglected. Clearly, E_C cannot be made too big, since this will push the device into the insulating regime.

4.4.1 A toy model

Let us first consider a simple toy model to establish the kind of phenomenology we would like to see in a vortex oscillator. Consider a ring of Josephson junctions, as shown in figure 4.4. The junction at the 'top' is characterised by junction energy E_J' and charging energy E_C, while all other junctions (which we refer to as the array junctions) are characterised by a junction energy E_J and E_C. We work with the assumption that $E_J \gg E_C \gg E_J'$, which means that the top junction effectively looks like a capacitor, while the array junctions effectively look like inductors or semi-classical junctions.

Let us denote the number of charges on the top junction as n' and the phase drop across it as θ', while the charges and phases of the array junctions are $\{n_i\}$ and $\{\theta_i\}$, respectively. Therefore, the Hamiltonian of the ring is effectively

$$\mathcal{H}_{\text{ring}} \approx 4E_C n'^2 + \underbrace{4E_C \sum_i n_i^2 - E_J \sum_i (\cos\theta_i - 1)}_{f(-\theta')} . \tag{4.10}$$

The fact that the array terms in (4.10) can be represented as $f(-\theta')$ follows from two facts. First, there is a loop constraint $\theta' + \sum_i \theta_i = 2\pi k$ (k is an integer), which implies that $\sum_i \theta_i = -\theta' + 2\pi k$. Second, as discussed in section 2.2, the energy of a chain of junctions in the superfluid phase is a 2π periodic function ($f(\theta)$) of the phase drop across the chain. Expanding about the minimum at zero (i.e. $\theta' = 0$) where f is quadratic, we can write $f(-\theta') \sim \theta'^2$. As a result, the system looks like a harmonic oscillator. We note the similarity between our toy model and the Fluxonium circuit (Manucharyan *et al.*, 2009). The Fluxonium Hamiltonian agrees with our analysis, in the limit that the Josephson energy of the 'black-sheep' junction (which corresponds to the top junction in our model) is dominated by all other energies [33].

4.4.2 Vortex electrostatics

Before we discuss our construction of a vortex oscillator, we must consider the 'electrostatics' of vortices. As mentioned in chapter 3, when vortices in an isotropic array have a separation which is much greater than the lattice constant, they can be considered to be point 'charges' which interact via a 2D Coulomb interaction. In a 2D world, the electric field due to a point charge Q is simply $\frac{Q}{2\pi\varepsilon_0 r}$, which can be derived from Gauss's law in two dimensions. As a result, the energy stored in a $\pm Q$ charge configuration separated by a distance r, relative to the energy stored at a distance a, is

$$\frac{Q^2}{2\pi\varepsilon_0} \ln\left(\frac{r}{a}\right) . \tag{4.11}$$

---

[33] We mention in passing that θ' corresponds to the 'superinductance mode' of the Fluxonium circuit in (Ferguson *et al.*, 2013), which is decoupled from all other degrees of freedom in the low energy limit.
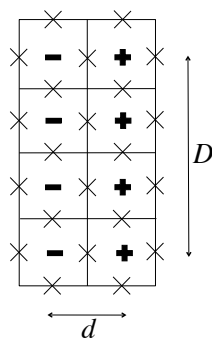
Figure 4.5: A 2D vortex capacitor.

The vortex-vortex interaction term in an isotropic array is $\pi E_J V_i I'_{ij} V_j$ (see (3.44)), which motivated by (4.11) can be rewritten as $\frac{1}{2\pi\varepsilon_0} 2\pi^2 \varepsilon_0 E_J V_i I'_{ij} V_j$. From this, we identify the unit of vortex charge to be

$$e_{\mathrm{v}} \equiv \sqrt{2\pi^2 \varepsilon_0 E_J} \,. \tag{4.12}$$

Treating vortices as Coulombic charges, one can perform a simple calculation of the energy stored in a 2D 'vortex capacitor', along the lines of a calculation for electric charges in three dimensions. For a capacitor storing a $\pm Q$ charge configuration, the energy still has the form $Q^2/(2C_{\mathrm{c}})$, where the capacitance is $C_{\mathrm{c}} = \varepsilon_0 D/d$ (the subscript 'c' in C_{c} denotes that C_{c} is the capacitance in conventional units). Here, D is the length of the 'plates' (in units of the dual lattice spacing) and $d = 1$ is the distance between the plates, as shown in figure 4.5. The energy stored is thus

$$\frac{Q^2}{2C_{\mathrm{c}}} = \frac{[(D+1)e_{\mathrm{v}}]^2}{2C_{\mathrm{c}}} = \pi^2 E_J \frac{(D+1)^2}{D} \,. \tag{4.13}$$

However, vortices only behave as Coulombic charges when the separation between them becomes large. One ought to check whether the simple $Q^2/(2C_{\mathrm{c}})$ energy of the setup in figure 4.5 actually matches up with an exact calculation of the energy stored using $\pi E_J V_i I'_{ij} V_j$. It turns out that for small D, there is a large mismatch between the energies calculated via the two methods. Nonetheless, the ratio of the energies calculated via the '$Q^2/(2C_{\mathrm{c}})$ way' and the 'exact way' tends to unity as D increases: for $D = 20$ this ratio is approximately 1.2. Therefore, for large enough D, the energy of the configuration shown in figure 4.5 should approximately be given by $Q^2/(2C_{\mathrm{c}})$.

4.4.3 A vortex oscillator

We are now in a position to discuss our construction of a vortex oscillator. The array for such an oscillator is sketched in figure 4.6. We assume that the Josephson energies E_J are isotropic, and chosen (in conjunction with the charging energies to be discussed) such that free vortices and antivortices can exist in the array. Now, we take the charging energies of 'the capacitive bit' (the junctions along the thick black line in figure 4.6) and of junctions
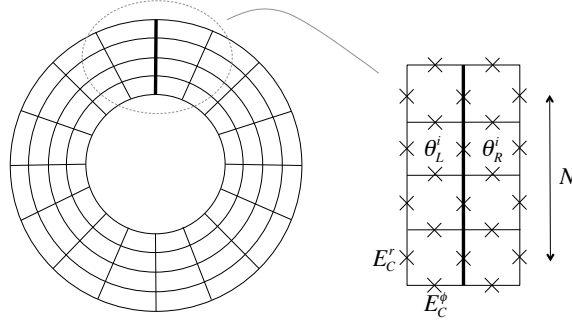
Figure 4.6: The array for a vortex oscillator (left) and 'the capacitive bit' of the oscillator (right).

in the angular direction (except for the angular junctions right next to the thick black line, which have energy E_C^ϕ) as being negligible. As a result, we can neglect vortex tunnelling across these junctions. If vortices and antivortices can accumulate on either side of the thick black line, which behaves as a barrier for vortices, then this part of the array would resemble a vortex capacitor, as in figure 4.5.

We would like each 'track' of the array at a constant radius (starting from one side of the barrier and ending on the other side) to resemble a chain of dual junctions in the superfluid phase, as in the toy model discussed in section 4.4.1. To achieve this, we need the charging energy in the radial direction to be as large as possible relative to E_J such that a description in terms of vortices remains sensible: $E_C^r \gtrsim E_J$. Similarly, we also require $E_C^\phi \gtrsim E_J$, so that all the dual phases on one side of the barrier (right next to the barrier) become phase locked: $\theta_{L/R}^i \approx \theta_{L/R}^{i+1}$.

Starting from the commutation relation $[\theta_i, V_j] = i\delta_{ij}$, we can make the change of variables

$$[\underbrace{\theta_R^i - \theta_L^i}_{\gamma^i}, \underbrace{\frac{1}{2}(V_R^j - V_L^j)}_{Q^j/e_v}] = i\delta_{ij}, \tag{4.14}$$

where e_v is the unit of vortex charge defined in (4.12). With the above conditions in place, the Hamiltonian describing the array is approximately

$$\mathcal{H}_{VO} \approx \frac{1}{2C_c}Q_{Tot}^2 + \frac{E_C^r}{2M}\sum_{i=1}^{N+1}\gamma^{i2} + E_C^\phi\sum_{i=1}^{N}\sum_{X=L,R}[1 - \cos(\theta_X^{i+1} - \theta_X^i)]. \tag{4.15}$$

In (4.15), $C_c = \varepsilon_0 N$, $Q_{Tot} = \sum_{i=1}^{N+1} Q^i$ and M is the number of junctions (with hopping amplitude E_C^r) in each track. The second term reflects the fact that each track resembles a chain of junctions in the superfluid phase (see the discussion of the toy model above and the chain of superfluid junctions in section 2.2). If E_C^ϕ is strong enough such that $\theta_{L/R}^i \approx \theta_{L/R}^{i+1}$, then all the phase drops across the barrier are nearly the same, say $\gamma^i \approx \gamma$. As a result,

$$\mathcal{H}_{VO} \approx \frac{1}{2C_c}Q_{Tot}^2 + \frac{E_C^r(N+1)}{2M}\gamma^2, \tag{4.16}$$
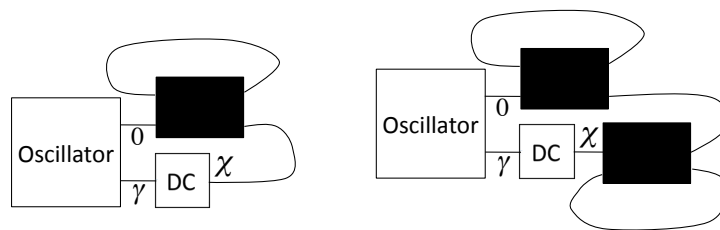
Figure 4.7: *Left*: Circuit for implementing $R_1(\pi/4)$. *Right*: Circuit for implementing $R_2(\pi/4)$. γ is the phase of the oscillator and χ is the phase drop across the qubit(s).

with γ and Q_{Tot} being conjugate variables since

$$\left[\underbrace{\frac{1}{N+1}\sum_{i=1}^{N+1}\gamma^i}_{\gamma}, \underbrace{\frac{1}{e_{\text{v}}}\sum_{i=1}^{N+1}Q^i}_{Q_{\text{Tot}}}\right] = i. \tag{4.17}$$

The system we have described is thus effectively a vortex harmonic oscillator.

We can rewrite (4.16) in the form

$$\mathcal{H}_{\text{VO}} \approx \frac{q_{\text{Tot}}^2}{2C} + \frac{\gamma^2}{2L}, \tag{4.18}$$

where $q_{\text{Tot}} = Q_{\text{Tot}}/e_{\text{v}}$, and $C = C_{\text{c}}/e_{\text{v}}^2$ and $L = \frac{M}{(N+1)E_C^r}$ are the capacitance and inductance of the oscillator, respectively. Both L and C have dimensions of inverse energy. For the gates $R_{1/2}(\pi/4)$ to be fault-tolerant, the impedance of the oscillator, $\sqrt{L/C}$, should be large (Brooks *et al.*, 2013). We can express L/C in terms of array parameters:

$$\frac{L}{C} = \frac{M}{(N+1)E_C^r} \cdot \frac{e_{\text{v}}^2}{C_{\text{c}}} = \frac{M}{(N+1)E_C^r} \cdot \frac{2\pi^2\varepsilon_0 E_J}{\varepsilon_0 N} = \frac{2\pi^2 M E_J}{N(N+1)E_C^r}. \tag{4.19}$$

Since M scales with the radius of the 'hole' of the array, by making this radius arbitrarily large compared to the length of the capacitor plate, the impedance can be made arbitrarily large.

4.5 Protected phase gates

The central idea behind the protected phase gates is to use a continuous-variable error-correcting code (Gottesman *et al.*, 2001), in which switching on a coupling between a qubit and a harmonic oscillator results in the qubit becoming encoded into the Hilbert space of the oscillator. The oscillator then picks up a qubit-state dependent phase factor, which is resilient to experimental imperfections such as timing errors or perturbations in the coupling, due to the properties of the code (Brooks *et al.*, 2013). When the coupling is switched off, the qubit and oscillator become disentangled, with $R_1(\pi/4)$ having been applied to the qubit.
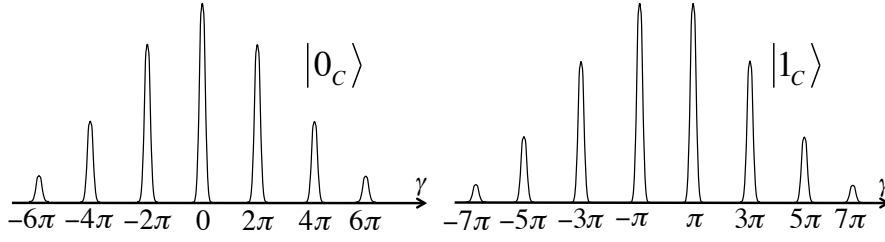
Figure 4.8: *Left*: The grid state $|0_C\rangle$ forms when the qubit is in state $|0\rangle$ ($\chi = 0$). *Right*: The grid state $|1_C\rangle$ forms when the qubit is in state $|1\rangle$ ($\chi = \pi$).

The circuit for implementing $R_1(\pi/4)$ on a VEQ is shown on the left in figure 4.7. The elements labelled 'Oscillator' and 'DC' correspond to a dual *LC* oscillator and a dual DC SQUID, respectively, while the black box denotes the VEQ. With time-dependent control over the external charge of the vortex DC SQUID (see section 4.3), the device can function as a switch. When $Q = 0$ it is switched on, and so the qubit and the oscillator are Josephson coupled, whereas when $Q = e$, the device is switched off and so the qubit and oscillator are uncoupled. The circuit is thus described by the Hamiltonian

$$\mathcal{H}_{\text{ph}} = \frac{q_{\text{Tot}}^2}{2C} + \frac{\gamma^2}{2L} - E_C(t)\cos(\gamma - \chi),\tag{4.20}$$

where $E_C(t)$ is defined in (4.9).

To implement the gate, the coupling energy has to be turned on from zero and held at its maximum value of $2E_C$ for a duration of L/π, and then turned off again [34]. The sign of the additional cosine potential that the oscillator 'sees' depends on the state of the qubit. For $\chi = 0$, this term is $-E_C(t)\cos\gamma$, whereas for $\chi = \pi$ it is $E_C(t)\cos\gamma$. If the oscillator is prepared in its ground state (a Gaussian wave function), then as $E_C(t)$ is turned on, the oscillator evolves into one of two 'grid states', conditioned on the qubit's state. As shown in figure 4.8, the grid states $|0_C\rangle$ and $|1_C\rangle$ [35] are superpositions of 'spike' like functions governed by a broad Gaussian envelope. The spikes are at even multiples of π if the qubit's state is $|0\rangle$, which reflects the positions of the local minima of the potential due to the cosine term. On the other hand, the spikes reside at odd multiples of π if the qubit's state is $|1\rangle$. Therefore, if the qubit is initially in the state $\alpha|0\rangle + \beta|1\rangle$, then as the coupling pulses on to its maximum value, the qubit and oscillator evolve as

$$(\alpha|0\rangle + \beta|1\rangle)|\psi_i\rangle \rightarrow \alpha|0\rangle|0_C\rangle + \beta|1\rangle|1_C\rangle,\tag{4.21}$$

where the initial state of the oscillator, $|\psi_i\rangle$, is assumed to be the ground state.

Having prepared the grid states, the coupling $E_C(t)$ needs to be held at its maximum

---

[34] There are some constraints on the form of $E_C(t)$ in order for the gate to be well protected, which are discussed in (Brooks *et al.*, 2013). We simply note that these constraints can be satisfied by the circuit parameters.

[35] The subscript '*C*' denotes that these states can be thought of as a basis for an error-correcting code.

value of $2E_C$ for a time L/π. During this time, the oscillator is subject to the effective Hamiltonian $\gamma^2/(2L)$, which can be justified as follows. The kinetic term $q_{\text{Tot}}^2/(2C)$ can be neglected, since it is assumed that the height of the local wells and the 'mass' of the oscillator (C) suppress tunnelling into neighbouring wells. Furthermore, the term $-2E_C \cos \gamma$ acting on the peaks at even multiples of π and the term $2E_C \cos \gamma$ acting on the peaks at odd multiples of π both lead to the same phase factor, i.e. the cosine term generates a global phase factor. The spikes in the grid state $|0_C\rangle$ therefore undergo the evolution

$$|2\pi k\rangle \rightarrow e^{-it\gamma^2/(2L)} |2\pi k\rangle = |2\pi k\rangle\,, \tag{4.22}$$

for $t = L/\pi$ and where k is an integer. On the other hand, the peaks of $|1_C\rangle$ pick up a phase of $-i$:

$$|2\pi(k+1/2)\rangle \rightarrow e^{-it\gamma^2/(2L)} |2\pi(k+1/2)\rangle = -i|2\pi(k+1/2)\rangle\,. \tag{4.23}$$

As a result, the qubit and oscillator evolve as

$$\alpha |0\rangle |0_C\rangle + \beta |1\rangle |1_C\rangle \rightarrow \alpha |0\rangle |0_C\rangle - i\beta |1\rangle |1_C\rangle\,. \tag{4.24}$$

To complete the gate, the coupling has to be turned off to zero. During this process, $|0_C\rangle$ evolves to $|\psi_f^0\rangle$ while $|1_C\rangle$ evolves to $|\psi_f^1\rangle$, and so the final state of the qubit and oscillator is

$$\alpha |0\rangle |\psi_f^0\rangle - i\beta |1\rangle |\psi_f^1\rangle\,. \tag{4.25}$$

If $|\psi_f^0\rangle = |\psi_f^1\rangle$, then $R_1(\pi/4)$ is implemented perfectly on the qubit, while the gate fidelity is reduced from unity if $\langle\psi_f^0|\psi_f^1\rangle \neq 1$. It is argued in (Brooks *et al.*, 2013) that under appropriate conditions $\langle\psi_f^0|\psi_f^1\rangle \approx 1$ to a very high degree, which implies that the gate is almost perfect. The intrinsic gate error [36] is found to scale favourably as $\exp\left(-\frac{1}{4}\sqrt{L/C}\right)$, which is the reason for demanding a high impedance oscillator. In fact, as alluded to above, (Brooks *et al.*, 2013) find that small timing errors (i.e. if the coupling remains at its maximum value for some time longer than L/π) do not change the exponential scaling of the error, and that the gate remains robust in the presence of a small non-zero temperature and against small perturbations in the Hamiltonian (4.20). Finite temperature robustness is key for our dual scheme, since, as we have explained above, our scheme would have to operate in a finite temperature environment.

$R_2(\pi/4)$ can be applied to two VEQs by coupling them in series to an oscillator – as shown on the right in figure 4.7 – and implementing exactly the same steps described for $R_1(\pi/4)$. The total phase drop across the two qubits is 0 for the states $|00\rangle$ and $|11\rangle$, and so the oscillator evolves to the final state $|\psi_f^0\rangle$. On the other hand, the total phase drop is π for the states $|01\rangle$ and $|10\rangle$, and hence the oscillator evolves to the final state $|\psi_f^1\rangle$. As with

---

[36] This intrinsic error arises because the spikes of the code states will in practice have a finite width, resulting in a small overlap between the states.

$R_1(\pi/4)$, if $|\psi_f^0\rangle = |\psi_f^1\rangle$, then $R_2(\pi/4)$ is implemented perfectly, up to a global phase.

4.6 Summary and discussion

In this chapter, we have explained how Kitaev's scheme for fault-tolerant universal QC using current mirror qubits can be adapted for protected VEQs. Each measurement and gate in Kitaev's universal set can be realized with appropriate arrays of junctions. Furthermore, the fault-tolerance of the measurements and the gates $R_{1/2}(\pi/4)$ implies that even with a slightly noisy $R_1(\pi/8)$, fault-tolerant computations can be guaranteed. To realize this scheme, we have presented some novel circuit elements, namely, a vortex DC SQUID and a vortex harmonic oscillator. In particular, we have seen that the impedance of the vortex oscillator can in principle be made arbitrarily large, which is promising with respect to ensuring the intrinsic fault-tolerance of $R_{1/2}(\pi/4)$.

Conclusions

In the first part of this thesis, we have described a protected qubit which is dual to a 0-π qubit (KCMQ) proposed in (Kitaev, 2006b). Our construction – which utilises vortex and dual phase degrees of freedom – mirrors the key features of KCMQ and therefore inherits its intrinsic fault-tolerance. More precisely, with suitable array parameters and boundary conditions, a nearly doubly degenerate ground state emerges which can be used to robustly store information, since bit flips and dephasing would be suppressed. We have also adapted the scheme for universal fault-tolerant QC proposed by Kitaev to our qubit. This has required the construction of novel circuit elements, such as a vortex harmonic oscillator.

One motivation for our construction is that the magnetic analogue of Cooper-pair excitons (present in KCMQ), namely vortex-antivortex pairs, can arise naturally in low temperature arrays in which Josephson energies are dominant. Another motivation is that electric field noise may impair the current mirror effect which KCMQ relies on, while the analogous magnetic field noise which would affect our qubit is generally less of an issue in the laboratory.

Interesting next steps to further investigate this scheme include assessing the impact of realistic noise on both KCMQ and its dual, in order to verify our claim that the dual would perform better in practice. It would also be interesting to examine the effect of the dissipative vortex-spin-wave coupling on both the qubit and gates and measurements. While we argued in section 3.3 that this coupling should be irrelevant at low temperatures, it should be remembered that our scheme cannot run in an ultra-low temperature environment, and so future work would reveal the possible effects of the coupling. On a similar note, the gap to excited states must be determined (as has been determined for KCMQ (Dempster *et al.*, 2014)) in order to gauge the effect of thermal fluctuations. Finally, we noted in section 3.3 that the ideal required array parameters may be difficult to realize experimentally; examining the extent to which our qubit retains its desirable features in practical parameter regimes is therefore a worthwhile problem for future study.

PART II

Detection of the Chern number and entanglement in topological four-component systems through subsystem winding numbers

CHAPTER 5

Topological phases of matter

5.1 Introduction

Since its introduction in 1937, the Landau theory of phase transitions (Landau, 1937) has been fruitful in the effort to understand the various phases that matter can assume (Anderson, 1984; Landau & Lifshitz, 1958). The central idea of this theory is that phases of matter can be classified by the symmetries that they break, while the associated local order parameters contain information about how the phases are ordered. Given its success in explaining the behaviour of systems as disparate as ferromagnets, superfluids and nematic liquid crystals, it was thought that Landau theory (along with the renormalization group and Landau Fermi liquid theory (Wen, 2004)) could in principle account for all states of matter. Indeed, it took the discovery of the integer quantum Hall effect (Klitzing *et al.*, 1980) – more than forty years after Landau theory was introduced – to show that Landau theory could not be the be-all and end-all in the classification of phases of matter. It turns out that the mathematics of topology is key to understanding integer quantum Hall (IQH) states (Avron *et al.*, 2003; Kohmoto, 1985; Thouless *et al.*, 1982), and a new paradigm known as *topological order* (Wen, 1995, 2004) has emerged to understand topological phases of matter. Research into topological order continues at great pace today, with the recent discovery of topological insulators and superconductors (Bernevig & Hughes, 2013; Hasan & Kane, 2010; Qi & Zhang, 2011). This effort is spurred on by the prospect of using topological matter for QC (Nayak *et al.*, 2008; Pachos, 2012).

As of yet, no complete framework for classifying topological phases of matter has been found, and inequivalent notions of topological order exist. The term is used most commonly (Wen, 1995, 2004) in the context of fractional quantum Hall states (Tsui *et al.*, 1982), which emerge from strong electronic interactions (Laughlin, 1983). Nonetheless, there are non-interacting phases of matter – namely topological insulators (for instance IQH states) and

superconductors – which cannot be understood without appealing to topology, and are thus regarded as being topologically ordered. Such free-fermion systems have in fact been classified according to their symmetries and dimensionality (Kitaev, 2009; Schnyder *et al.*, 2008). Some examples of current interest are topological *p*-wave superconductors in one (Kitaev, 2001) and two dimensions (Read & Green, 2000), which are both predicted to support localized Majorana modes at defects. Such emergent Majorana fermions are the subject of intense theoretical investigation (Alicea, 2012), partly motivated by the prospect of using them to perform TQC, by virtue of their non-Abelian statistics (Ivanov, 2001) (see section 1.3.3). The search for them in the laboratory has been no less intense, and some (inconclusive) evidence of their existence in solid-state systems has been found (Das *et al.*, 2012; Deng *et al.*, 2012; Mourik *et al.*, 2012; Rokhinson *et al.*, 2012). Another topical class of free-fermion systems are $\mathbb{Z}_2$ topological insulators (Kane & Mele, 2005), which was the first example of an experimentally observed time-reversal symmetric topological phase (König *et al.*, 2007).

A number of theoretical signatures of topological order exist. Examples include robust ground state degeneracies which are sensitive to the topology of the surface that the system resides on (Wen & Niu, 1990), and the ability of a system to support anyons. These two signatures are closely related, with the latter implying a ground state degeneracy if the system is placed on a torus (Einarsson, 1990). Topological insulators and superconductors are characterized by bulk topological invariants such as *Chern numbers* (Bernevig & Hughes, 2013; Kohmoto, 1985; Stone, 1992; Thouless *et al.*, 1982). A remarkable feature of these systems is the *bulk-boundary correspondence*: bulk topological invariants yield information about gapless boundary modes, and vice versa (Hatsugai, 1993; Ryu & Hatsugai, 2002). More recently, entropic measures (Kitaev & Preskill, 2006; Levin & Wen, 2006; Li & Haldane, 2008) have been shown to successfully capture aspects of topological order. However, accessing such signatures experimentally is generally challenging: topological ordering lacks local order parameters, which makes it difficult to infer from local measurements. An exception is the Chern number characterizing IQH states, which can be determined from measurements of the conductivity.

While the domain of topological matter has traditionally been solid-state systems, much attention is currently focused on preparing and detecting topological states with cold atoms in optical lattices. This route holds much promise, due to the inherently clean nature of cold atom experiments and the recent implementation of topological insulating Hamiltonians (Aidelsburger *et al.*, 2013; Miyake *et al.*, 2013). Still, the detection of topological signatures in 2D optical lattices remains an outstanding challenge [37], although much progress has been made recently on this front using various physical observables. Examples include extracting topological invariants from time-of-flight (TOF) measurements (Alba *et al.*, 2011;

---

[37] An invariant known as the Zak phase (Zak, 1989) has recently been measured in a one-dimensional setup (Atala *et al.*, 2013).

Goldman *et al.*, 2013; Pachos *et al.*, 2013; Wang *et al.*, 2013), analysis of wave packet dynamics (Price & Cooper, 2012) and centre-of-mass measurements (Dauphin & Goldman, 2013), interferometric measurements of the Berry phase (Abanin *et al.*, 2013) and measurement of the entanglement entropy using a 'quantum switch' (Abanin & Demler, 2012). Some of these schemes are however tailored for particular systems, and require idealistic conditions that can be unrealistic in actual experiments. We note that there are other architectures which offer promising routes to realize or simulate topological phases, such as superconducting circuits (Gladchenko *et al.*, 2008; Roushan *et al.*, 2014).

In the next two sections, we introduce the first Chern number [38] and the *entanglement spectrum* (ES) (Li & Haldane, 2008) – one of the entropic measures of topological order mentioned above – while in section 5.4, we discuss how the Chern number of the simplest free-fermion systems can be measured in cold atom experiments [39]. These sections will set the stage for chapter 6, where we discuss a method to measure the Chern number and ES of 'four-component' topological insulators and superconductors.

5.2 The first Chern number

The Chern number is an integer topological invariant which characterizes the many-body ground state of a *gapped* non-interacting system of fermions. Historically, it emerged as a defining property of 2D time-reversal breaking band insulators ever since their Hall conductance was proved to be proportional to the Chern number (i.e. quantized) (Thouless *et al.*, 1982), and has since been used to classify topologically non-trivial superconductors as well (Read & Green, 2000; Volovik, 2009).

A common representation of the Chern number is in terms of the total Berry flux or curvature of the occupied single-particle states in the Brillouin zone (BZ) (Bernevig & Hughes, 2013; Kohmoto, 1985; Stone, 1992). An equivalent representation is [40] (Avron *et al.*, 1983)

$$\nu = -\frac{i}{2\pi} \int_{\text{BZ}} d^2 p \, \text{tr} \left(\mathcal{P}_{\vec{p}} \left[\partial_{p_x} \mathcal{P}_{\vec{p}}, \partial_{p_y} \mathcal{P}_{\vec{p}} \right] \right), \tag{5.1}$$

where for insulators, $\mathcal{P}_{\vec{p}}$ is the projector onto the occupied single-particle states labelled by $\vec{p} \in \text{BZ}$, while for superconductors, $\mathcal{P}_{\vec{p}}$ projects onto the negative energy quasiparticle states labelled by $\vec{p} \in \text{BZ}$. ν is well defined for projectors which vary smoothly across the BZ, and is a topological invariant in the following sense: Say we pick a reference Hamiltonian and an associated ground state; a smooth interpolation or deformation to another Hamiltonian and its associated ground state cannot change the Chern number, and the two ground states are said to be *adiabatically connected* to each other. ν thus defines an *equivalence class* of Hamiltonians or ground states. The Chern number can only change at a phase transition,

---

[38]For brevity, we will hereafter speak of the Chern number rather than the first Chern number.

[39]Hereafter, our focus is on 2D free-fermion systems.

[40]The system is assumed to possess periodic boundary conditions i.e. we place it on a torus.

i.e. when the system becomes gapless and $\mathcal{P}_{\vec{p}}$ no longer varies smoothly across the BZ. For insulators, this occurs when the valence and conduction bands become degenerate, while for superconductors, this happens when one of the quasiparticle bands touches zero energy, so that the band becomes degenerate with its particle-hole symmetric partner [41]. We explicitly discuss the steps required to calculate the Chern number of the simplest free-fermion systems in section 5.4.

As mentioned in the introduction to this chapter, ν – despite being a bulk quantity (i.e. it is calculated for a system with no edges) – remarkably contains information about the edge physics of a 'real' finite-size system (Bernevig & Hughes, 2013; Hasan & Kane, 2010; Hatsugai, 1993). A system characterized by $\nu \neq 0$ possesses *chiral gapless edge states*. In other words, such a system with edges, while still possessing bulk states (i.e. states with support only in the bulk of the system) and a bulk energy gap, will also possess gapless edge states (i.e. states with support only on the edge of the system) which traverse or fill the bulk gap. These states are chiral in the sense that they propagate in one direction only along an edge, due to broken time-reversal symmetry (e.g. the application of a magnetic field giving rise to an IQH state). The number of 'branches' of chiral fermions per edge is equal to $|\nu|$, while the chirality is determined by $\mathrm{sgn}(\nu)$. Furthermore, such edge states are topologically protected – they persist under smooth changes of the Hamiltonian which do not change the Chern number – and are insensitive to disorder since there are no states available for back-scattering. We note in passing that the Chern number also contains information about the properties of anyons which may exist in free-fermion systems (Kitaev, 2006a; Read & Green, 2000).

5.3 The entanglement spectrum

In 2006, Kitaev and Preskill (Kitaev & Preskill, 2006) and simultaneously Levin and Wen (Levin & Wen, 2006) made the startling proposal that, by examining the entanglement entropy of a 2D ground state wave function, one can glean information about whether the system is topologically ordered or not. The basic idea (Pachos, 2012) is to partition the system into two spatial regions – which are assumed to possess typical length scales which are much larger than the correlation length [42] of the system – and calculate the entanglement entropy with respect to this bipartition. Say we call one of the regions $\mathcal{A}$ and its complement $\mathcal{B}$; by tracing out the degrees of freedom in $\mathcal{B}$, for instance, one arrives at a reduced density matrix for $\mathcal{A}$, $\rho_{\mathcal{A}}$. One can then calculate the entanglement entropy (the von Neumann entropy of $\rho_{\mathcal{A}}$)

$$\mathcal{S}(\rho_{\mathcal{A}}) = -\mathrm{tr}(\rho_{\mathcal{A}} \log \rho_{\mathcal{A}}), \tag{5.2}$$

---

[41]See section 5.4.

[42]The correlation length is finite since the system is assumed to possess a non-zero energy gap above its ground state.

which measures the correlations of region $\mathcal{A}$ with region $\mathcal{B}$.

$\mathcal{S}(\rho_{\mathcal{A}})$ takes the generic form

$$\mathcal{S}(\rho_{\mathcal{A}}) = \alpha|\partial\mathcal{A}| - \gamma, \tag{5.3}$$

where $|\partial\mathcal{A}|$ is the size of the boundary separating the two regions and α and γ are non-negative constants. $\alpha|\partial\mathcal{A}|$ represents the so-called *area law* contribution to the entanglement entropy (Eisert *et al.*, 2010), and is common to the ground states of gapped many-body quantum systems with local interactions. It arises since entanglement between the two regions can only exist in the vicinity of $\partial\mathcal{A}$, between degrees of freedom which are separated up to distances of the order of the correlation length. α is a non-universal quantity since it depends on the microscopic details of the system. On the other hand, $-\gamma$ is a universal quantity which is known as the *topological entanglement entropy*. When this is finite, the system is topologically ordered: γ is non-zero if and only if the system supports anyons, while $\gamma = 0$ is equivalent to the statement that the system does not support anyons. γ is determined entirely by the properties of the anyons that the system can host; in particular, it is insensitive to deformations of the system Hamiltonian which do not change the phase that the system resides in, which explains its universality. The fact that γ does not depend on the geometry of the partition tells us that it captures global or topological features of the entanglement in the ground state; when $\gamma \neq 0$, we interpret the system to possess an additional order which reduces the entanglement entropy.

However, as mentioned earlier, there are inequivalent notions of topological order, and it turns out that there are topologically ordered states for which γ vanishes. For instance, IQH states have a non-zero Chern number, yet the topological entropy vanishes since they do not support anyons. In a seminal paper (Li & Haldane, 2008), Li and Haldane showed that the entire spectrum of a reduced density matrix (such as $\rho_{\mathcal{A}}$ above) can often contain additional information, which is not revealed by the entanglement entropy. For many systems, this spectrum can be readily accessed by introducing the so-called *entanglement Hamiltonian* $\mathcal{H}_{\mathcal{A}}^{\mathrm{e}}$, a Hermitian operator which is defined as $\rho_{\mathcal{A}} \propto e^{-\mathcal{H}_{\mathcal{A}}^{\mathrm{e}}}$ and whose eigenvalues are known as the ES. It is known that the ES of non-interacting topological insulators and superconductors contains degeneracies (for appropriate spatial partitions), by virtue of these systems possessing gapless edge modes (Fidkowski, 2010; Qi *et al.*, 2012; Turner *et al.*, 2009). Therefore, knowledge of the ES of these systems allows one to infer the edge mode spectrum and thus, the topological phase that the system resides in [43].

Let us discuss how one goes about calculating the ES for the relatively simple case of non-interacting topological insulators (Legner & Neupert, 2013; Turner *et al.*, 2009). The

---

[43]To be exact, while gapless edge modes imply degeneracies in the ES, the converse is *not* always true: there are special cases where the system may be topologically trivial yet still possess degeneracies in the ES. This can happen for inversion symmetric insulators (Turner *et al.*, 2009), for instance.

Hamiltonian for such systems are of generic tight-binding form

$$\mathcal{H} = \sum_{m,n=1}^{N} a_m^\dagger h_{m,n} a_n \,, \tag{5.4}$$

where $a_m^\dagger$ are fermionic creation operators which create single-particle states in a single-particle Hilbert space (of dimension N), from which Fock space is built. The creation and annihilation operators obey the usual fermionic anti-commutation relations, while the indices m and n could refer to positions on a lattice, or encode multiple degrees of freedom such as position, spin, orbital and so on. We can partition the system into two parts, say $\mathcal{A}$ and $\mathcal{B}$, with the nature of this partitioning being unspecified for the moment. For example, the partitioning could be a cut in real space which splits the system in half – in which case $\mathcal{A}$ and $\mathcal{B}$ represent the degrees of freedom in the two halves – or it could divide the system into subsystems distinguished by different spin projections. With this partitioning, one can write the ground state $|\psi\rangle$ of (5.4) in the form of a *Schmidt decomposition*

$$|\psi\rangle = \sum_{\alpha} \frac{1}{\sqrt{\mathcal{Z}}} \exp\left(-\frac{E_\alpha^{\mathrm{e}}}{2}\right) |\alpha, \mathcal{A}\rangle |\alpha, \mathcal{B}\rangle \,, \tag{5.5}$$

where $\mathcal{Z} \equiv \sum_\alpha \exp\left(-E_\alpha^{\mathrm{e}}\right)$ ensures that $|\psi\rangle$ is normalized. $|\alpha, \mathcal{A}\rangle |\alpha, \mathcal{B}\rangle$ is a short-hand, which indicates that each state (labelled by α) in the decomposition is given by a product of an operator with no support on $\mathcal{B}$ and an operator with no support on $\mathcal{A}$ acting on the vacuum. By performing a partial trace over the degrees of freedom in $\mathcal{B}$, one arrives at the reduced density matrix of $\mathcal{A}$, from which, as discussed above, an entanglement Hamiltonian $\mathcal{H}_\mathcal{A}^{\mathrm{e}}$ can be defined:

$$\rho_\mathcal{A} = \mathrm{tr}_\mathcal{B} |\psi\rangle \langle\psi| \equiv \frac{1}{\mathcal{Z}} e^{-\mathcal{H}_\mathcal{A}^{\mathrm{e}}} \,. \tag{5.6}$$

$\{E_\alpha^{\mathrm{e}}\}$ are the eigenvalues of $\mathcal{H}_\mathcal{A}^{\mathrm{e}}$ and are thus the ES. It is of course natural to also refer to $\{E_\alpha^{\mathrm{e}}\}$ as the 'energies' of the entanglement Hamiltonian, but one should note that they have nothing to do with the physical energies of the system (the superscript 'e' denotes entanglement). Rather, they determine the weights of the states in the reduced density matrix, with low 'energy' eigenstates of $\mathcal{H}_\mathcal{A}^{\mathrm{e}}$ having greatest weight.

General arguments (see (Peschel, 2003) and references therein) tell us that the entanglement Hamiltonian of a free-fermion system (such as a band insulator) must also describe a free-fermion system. In other words, $\mathcal{H}_\mathcal{A}^{\mathrm{e}}$ must assume a tight-binding form

$$\mathcal{H}_\mathcal{A}^{\mathrm{e}} = \sum_{m,n=1}^{N} a_m^\dagger (h_\mathcal{A}^{\mathrm{e}})_{m,n} a_n \,, \tag{5.7}$$

where despite the sum being over all modes in the single-particle Hilbert space, only terms involving fermionic operators of $\mathcal{A}$ actually enter $\mathcal{H}_\mathcal{A}^{\mathrm{e}}$. Indeed, it has been shown by Peschel

(Peschel, 2003) that $h_{\mathcal{A}}^{e}$ is related to the restricted correlation matrix $\mathcal{C}_{\mathcal{A}} = \mathcal{P}_{\mathcal{A}}\mathcal{C}\mathcal{P}_{\mathcal{A}}$ by

$$h_{\mathcal{A}}^{e} = \log\left(\frac{\mathbb{1} - \mathcal{C}_{\mathcal{A}}}{\mathcal{C}_{\mathcal{A}}}\right) \tag{5.8}$$

(all matrices are $N \times N$), and thus the eigenvalues $\{\varepsilon_i\}$ of $h_{\mathcal{A}}^{e}$ (the single-particle entanglement 'energies' or spectrum) are related to the eigenvalues $\{\zeta_i\}$ of $\mathcal{C}_{\mathcal{A}}$ by

$$\varepsilon_i = \log\left(\frac{1 - \zeta_i}{\zeta_i}\right). \tag{5.9}$$

Above, $\mathcal{P}_{\mathcal{A}}$ projects onto subsystem $\mathcal{A}$ while $\mathcal{C}$ is the two-point correlation function with elements $\mathcal{C}_{m,n} = \langle\psi| a_m^\dagger a_n |\psi\rangle$.

Therefore, with knowledge of $\{\varepsilon_i\}$, the ES is given by

$$E_\alpha^{e} = \sum_{i=1}^{N} n_\alpha^i \varepsilon_i, \tag{5.10}$$

where $n_\alpha^i = 0, 1$ are the occupation numbers of the single-particle states. Since $\mathrm{tr}\mathcal{P}_{\mathcal{A}} < N$, $\mathcal{C}_{\mathcal{A}}$ will possess $N - \mathrm{tr}\mathcal{P}_{\mathcal{A}}$ trivial zero eigenvalues. These zero eigenvalues correspond to $\varepsilon_i = \infty$ and do not contribute to the ES, and are thus neglected in (5.10). On the other hand, zero eigenvalues of $h_{\mathcal{A}}^{e}$ ($\varepsilon_i = 0$) lead to degeneracies in the ES: if $\varepsilon_k = 0$, replacing $n_\alpha^k = 0$ by $n_{\alpha'}^k = 1$ results in $E_\alpha^{e} \to E_{\alpha'}^{e} = E_\alpha^{e}$. Such degeneracies tend to make the reduced density matrix more mixed and indicate higher entanglement between the subsystems.

To end this section, we briefly discuss features of the ES that result from some possible partitions. As alluded to above, a common partitioning is to split the system into two halves (Turner *et al.*, 2009). If the cut preserves the translational symmetries of the system in the directions parallel to the cut, the restricted correlation matrix will also retain these symmetries. As a result, its eigenvalues, and thus the single-particle ES, can be labelled by the lattice momenta along these directions. For free-fermion systems possessing gapless edge states, it is known that the single-particle ES mimics these dispersions (Fidkowski, 2010; Turner *et al.*, 2009). Each branch of gapless edge states results in a gapless branch (with the same chirality) of the single-particle ES, taking all values in $[-\infty, \infty]$ in the thermodynamic limit. The reason for this is quite simple: given (5.4), a topologically equivalent Hamiltonian is given by the replacement $h \to \mathbb{1}/2 - \mathcal{C}$. This is known as the *flat band* version of the original Hamiltonian, since its eigenvalues are $-1/2$ ($1/2$) for the single-particle states that are occupied (empty) in $|\psi\rangle$ [44]. Now, restricting (projecting) $\mathcal{C}$ to one half of the system $\mathcal{A}$ is tantamount to throwing away the degrees of freedom in $\mathcal{B}$, and thus simulates an edge being introduced into the system, which is the cut which separates the halves. Therefore, if the original Hamiltonian possesses gapless edge modes, the flat band version restricted to $\mathcal{A}$ will possess these as well, i.e. the spectrum of $\mathcal{C}_{\mathcal{A}}$ will be gapless. Since the spectrum of

---

[44]The eigenstates of the flat band Hamiltonian are the same as those of the original Hamiltonian.

$h_\mathcal{A}^{\mathrm{e}}$ is monotonically related to this spectrum (see (5.9)), the single-particle ES will thus be gapless as well.

Recently, an alternative partitioning which preserves full translational symmetry by tracing out a subset of local degrees of freedom – such as sublattice sites or spin orientations – has been investigated (Legner & Neupert, 2013). The authors found that for Chern insulators (Haldane, 1988) (lattice analogues of IQH states) and $\mathbb{Z}_2$ topological insulators (Kane & Mele, 2005) in a non-trivial topological phase, the ES (with respect to a sublattice cut) is gapless. In section 6.2, we explain how this *component ES* can be measured in cold atom experiments.

5.4 Detection of Chern numbers of two-component systems

In this section, we explain how the Chern number of simple two-component systems can be constructed in experiments with cold atoms in optical lattices, using the standard diagnostic technique of TOF images (Alba *et al.*, 2011; Pachos *et al.*, 2013). Examples of two-component systems which possess phases with non-trivial Chern numbers include *p*-wave superconductors (Bernevig & Hughes, 2013; Read & Green, 2000; Volovik, 2009) and the celebrated Haldane model (Haldane, 1988), the first example of a Chern insulator.

Consider a translationally invariant non-interacting system of fermions described by the Hamiltonian

$$\mathcal{H}_2 = \int_{\mathrm{BZ}} d^2 p \, \psi_{\vec{p}}^\dagger h_2(\vec{p}) \psi_{\vec{p}} \,. \tag{5.11}$$

The system has two components, which means that the spinor $\psi_{\vec{p}} = (a_{\vec{p}}, b_{\vec{p}})^T$ for some fermionic plane-wave annihilation operators, $a_{\vec{p}}$ and $b_{\vec{p}}$. $h_2(\vec{p})$ is thus a 2×2 matrix and is known as the *Bloch Hamiltonian*. To find the ground state of the system, one simply needs to diagonalize the Bloch Hamiltonian: $h_2(\vec{p}) \to \mathrm{diag}\,(E_1(\vec{p}), E_2(\vec{p}))$. The two eigenvalues at each point in the BZ – E_1 and E_2 – are known as the *band energies*, and we assume that $E_1(\vec{p}) > E_2(\vec{q})$ for arbitrary $\vec{p}$ and $\vec{q}$, i.e. the system is gapped.

Let us first take a look at insulators; for instance, $a_{\vec{p}}$ and $b_{\vec{p}}$ could correspond to the two sublattices of the Haldane model on a honeycomb lattice. Diagonalization yields creation operators $c_{1,\vec{p}}^\dagger$ and $c_{2,\vec{p}}^\dagger$ which create modes with lattice momentum [45] $\vec{p}$ and energies E_1 and E_2, respectively. The ground state of the system at half-filling [46] is thus given by

$$|\mathrm{gs}\rangle = \prod_{\vec{p} \in \mathrm{BZ}} c_{2,\vec{p}}^\dagger |0\rangle \,, \tag{5.12}$$

where $|0\rangle$ is the vacuum with respect to the *a* and *b* operators, i.e. $a_{\vec{p}}|0\rangle = b_{\vec{p}}|0\rangle = 0$ for all $\vec{p}$.

For a single-species or *p*-wave superconductor, $b_{\vec{p}} = a_{-\vec{p}}^\dagger$, which comes about through

---

[45] Below, we will refer to lattice momentum as momentum.

[46] I.e. the dimension of the single-particle Hilbert space is N and there are only $N/2$ particles in the system.

the Bogoliubov-de Gennes formalism (Bernevig & Hughes, 2013) which is used to diagonalize mean-field superconductors, such as the generic p-wave superconductor we are considering here. This formalism enforces a *particle-hole symmetry*, which implies that $E_2(\vec{p}) = -E_1(\vec{p})$. In this case, diagonalization yields creation operators $c_{\vec{p}}^\dagger$ which create quasiparticles [47] with momenta $\vec{p}$ and energies $2E_1$. The ground state of the system is the well known BCS wave function (Annett, 2004; Read & Green, 2000)

$$|\text{BCS}\rangle = \prod_{\vec{p}\in \text{BZ}/2} \left(u_{\vec{p}} + v_{\vec{p}} a_{\vec{p}}^\dagger a_{-\vec{p}}^\dagger \right) |0\rangle \,, \qquad (5.13)$$

where 'BZ/2' refers to the fact that the product should run over half of the BZ so that each time-reversed pair $(\vec{p}, -\vec{p})$ only enters once. The complex functions $u_{\vec{p}}$ and $v_{\vec{p}}$ satisfy $|u_{\vec{p}}|^2 + |v_{\vec{p}}|^2 = 1$, which ensures that $|\text{BCS}\rangle$ is normalized.

Both the insulating and superconducting ground states – (5.12) and (5.13), respectively – are given by a product of operators (with each operator labelled by $\vec{p}$) acting on the vacuum state. Below, we make use of this fact and write the ground state for both types of systems in the form $|\Phi\rangle = \prod_{\vec{p}} |\Phi_{\vec{p}}\rangle$. This is a slight abuse of notation since Fock space does not possess a tensor product structure. However, as far as topological properties are concerned, what matters is how the occupation numbers of the plane wave modes (which are governed by $u_{\vec{p}}$ and $v_{\vec{p}}$ in (5.13) for superconductors, for instance) vary across the BZ, and this information is what is contained in $|\Phi_{\vec{p}}\rangle$.

The Chern number of either system can be calculated from the formula (5.1), with $\mathcal{P}_{\vec{p}} = |\chi_{\vec{p}}\rangle \langle \chi_{\vec{p}}|$ being the projector onto the ground state of $h_2(\vec{p})$, $|\chi_{\vec{p}}\rangle$ (which has eigenvalue E_2). In appendix E we demonstrate the well known fact that for two-component systems, ν can be expressed as a *winding number* $\tilde{\nu}[\hat{\vec{s}}_{\vec{p}}]$

$$\nu = \frac{1}{4\pi} \int_{\text{BZ}} d^2 p \, \hat{\vec{s}}_{\vec{p}} \cdot \left(\partial_{p_x} \hat{\vec{s}}_{\vec{p}} \times \partial_{p_y} \hat{\vec{s}}_{\vec{p}} \right) \equiv \tilde{\nu}[\hat{\vec{s}}_{\vec{p}}] \,, \qquad (5.14)$$

which counts the number of times the normalized three-vector $\hat{\vec{s}}_{\vec{p}}$ winds around or covers the unit sphere as the BZ is spanned. $\hat{\vec{s}}_{\vec{p}}$ parametrizes the Bloch Hamiltonian through

$$h_2(\vec{p}) = -|\vec{s}| \hat{\vec{s}}_{\vec{p}} \cdot \vec{\sigma} \,, \qquad (5.15)$$

where $\vec{\sigma} = (X, Y, Z)$ is the vector of Pauli matrices, and can thus be regarded as the Bloch vector representation of $|\chi_{\vec{p}}\rangle$ [48]. It was shown in (Alba *et al.*, 2011) for Chern insulators (such as Haldane's model), and in (Pachos *et al.*, 2013) for topological superconductors, that the vector $\hat{\vec{s}}_{\vec{p}}$ can be constructed from physical observables associated with TOF measure-

---

[47]These quasiparticles are superpositions of particles and holes.

[48]For insulators, the expansion of $h_2(\vec{p})$ in (5.15) can in principle contain a term proportional to the identity matrix. We neglect this term since it merely adds a constant to the spectrum and does not alter any topological properties.

ments. As ν in (5.14) is fully determined by $\hat{\vec{s}}_{\vec{p}}$, the Chern number can thus be constructed from such measurements.

More precisely, by studying how the atom cloud expands as the trap is switched off, a set of TOF images can be obtained, which amount to measuring density operators of the form $a_{\vec{p}}^{\dagger} a_{\vec{p}}$ and $b_{\vec{p}}^{\dagger} b_{\vec{p}}$. As these correspond to different species, they can be measured independently by releasing only one species from the trap at a time. It can be easily shown that $\hat{\vec{s}}_{\vec{p}}$ can be written either as the ground state (of $h_2(\vec{p}) - |\chi_{\vec{p}}\rangle$) expectation value of $\vec{\sigma}$, or as the ground state (of $\mathcal{H}_2 - |\Phi\rangle$) expectation value of the Fock space representation of $\vec{\sigma}$, $\psi_{\vec{p}}^{\dagger} \vec{\sigma} \psi_{\vec{p}}$:

$$\hat{\vec{s}}_{\vec{p}} = \langle \chi_{\vec{p}} | \vec{\sigma} | \chi_{\vec{p}} \rangle = \langle \Phi | \psi_{\vec{p}}^{\dagger} \vec{\sigma} \psi_{\vec{p}} | \Phi \rangle = \langle \Phi_{\vec{p}} | \psi_{\vec{p}}^{\dagger} \vec{\sigma} \psi_{\vec{p}} | \Phi_{\vec{p}} \rangle \ . \tag{5.16}$$

$s_{\vec{p}}^z$ is thus given directly by TOF images, while the other components of $\hat{\vec{s}}_{\vec{p}}$ can be measured via suitable Hamiltonian manipulations (Alba *et al.*, 2011; Pachos *et al.*, 2013).

For a system with more than two components – for instance additional spin or internal degrees of freedom – the straightforward path from physical observables to the construction of ν no longer holds. The Bloch Hamiltonian for such a system is no longer a 2×2 matrix, and thus cannot be expanded in the Pauli matrix basis $\{X, Y, Z\}$. While the Hamiltonian can be expanded in a basis of higher dimensional matrices and parametrized by a vector $\hat{\vec{v}}_{\vec{p}}$, this vector will have more than three components (Bernevig & Hughes, 2013). As a result, the fundamental definition of the Chern number (5.1) no longer reduces to the simple winding number expression (5.14). While the components of $\hat{\vec{v}}_{\vec{p}}$ can still in principle be obtained from TOF images following Hamiltonian manipulations, there is no longer a recipe to construct ν from them.

In the next chapter, we generalize the method to extract Chern numbers from TOF images to four-component systems. We also discuss how this experimental technique allows one to access the ES with respect to component bi-partitions (Legner & Neupert, 2013).

CHAPTER 6

Detection of the Chern number and entanglement in four-component systems

As discussed in the previous chapter, cold atom experiments are a promising route to the preparation and measurement of topological phases. To realize such phases, delicate interactions such as spin-orbit coupling, non-Abelian gauge fields or p-wave pairing are often required, which necessitates the use of many species of atoms and/or internal states. As a result, since measurement schemes usually rely on single-species observables [49], there is often no way of verifying the existence of topological phases.

This chapter deals with how single-species observables suffice to construct the Chern number of four-component systems. We demonstrate that ν decomposes into contributions arising from subsystems; these contributions are *subsystem winding numbers* which are physically observable, just like the winding number (5.14) of two-component systems. We examine two interesting four-component systems to illustrate this method. More specifically, we show that the phase diagrams of the quantum spin-Hall insulator (QSHI) (Kane & Mele, 2005) and a staggered topological superconductor (Pachos *et al.*, 2013) are accurately reproduced, as long as the subsystem components are not highly entangled. Furthermore, the degree of this entanglement can be inferred using the very same operators used to construct the subsystem winding numbers. This means that our method enables one to probe entanglement between different degrees of freedom and measure the ES with respect to bi-partitions between these degrees of freedom. The contents of this chapter are based on (de Lisle *et al.*, 2014).

---

[49]By single-species observables, we mean observables of the form $\psi_{\vec{p}}^{\dagger} \vec{\sigma} \psi_{\vec{p}}$ introduced in section 5.4, where $\psi_{\vec{p}}$ is a two-component spinor. The z-component of this observable is the difference of two density operators corresponding to different species; the other components can be measured by rotating them to the z-axis (by manipulating the Hamiltonian) and then measuring the z-component.

6.1 Decomposition of the Chern number into subsystem winding numbers

In this section, we show analytically that the Chern number of four-component systems decomposes into a sum of subsystem winding numbers, which are physically observable. We demonstrate this in detail first for topological insulators, and then for topological superconductors, for which the arguments carry over with minor modifications.

6.1.1 Decomposition for topological insulators

Let us consider an insulator with four distinct types of fermions, whose annihilation operators are denoted by a_1, a_2, b_1 and b_2. The grouping or bi-partitioning of the components into a and b type fermions is physically motivated, and could correspond to different spin orientations or sublattices, for instance. Assuming translational invariance with respect to these operators, the system Hamiltonian can be written as

$$\mathcal{H}_4 = \int_{\mathrm{BZ}} d^2 p\, \psi_{\vec{p}}^\dagger h_4(\vec{p}) \psi_{\vec{p}}, \quad \psi_{\vec{p}} = \begin{pmatrix} a_{1,\vec{p}} \\ a_{2,\vec{p}} \\ b_{1,\vec{p}} \\ b_{2,\vec{p}} \end{pmatrix}, \tag{6.1}$$

where the Bloch Hamiltonian $h_4(\vec{p})$ is a 4×4 matrix. As discussed in section 5.4, the ground state of the system can be written in the form

$$|\Phi\rangle = \prod_{\vec{p} \in \mathrm{BZ}} \left(\sum_{n_{1,\vec{p}}^a, n_{2,\vec{p}}^a, n_{1,\vec{p}}^b, n_{2,\vec{p}}^b = 0,1} \alpha_{n_{1,\vec{p}}^a, n_{2,\vec{p}}^a, n_{1,\vec{p}}^b, n_{2,\vec{p}}^b} |n_{1,\vec{p}}^a, n_{2,\vec{p}}^a, n_{1,\vec{p}}^b, n_{2,\vec{p}}^b\rangle \right) \equiv \prod_{\vec{p} \in \mathrm{BZ}} |\Phi_{\vec{p}}\rangle, \tag{6.2}$$

with Fock states

$$|n_{1,\vec{p}}^a, n_{2,\vec{p}}^a, n_{1,\vec{p}}^b, n_{2,\vec{p}}^b\rangle \equiv (a_{1,\vec{p}}^\dagger)^{n_{1,\vec{p}}^a} (a_{2,\vec{p}}^\dagger)^{n_{2,\vec{p}}^a} (b_{1,\vec{p}}^\dagger)^{n_{1,\vec{p}}^b} (b_{2,\vec{p}}^\dagger)^{n_{2,\vec{p}}^b} |0\rangle. \tag{6.3}$$

$n_{i,\vec{p}}^{a,b} = 0,1$ are the mode occupation numbers while $|0\rangle$ refers to the vacuum state of all modes. To ensure that the ground state in (6.2) is normalized, the coefficients $\alpha_{n_{1,\vec{p}}^a, n_{2,\vec{p}}^a, n_{1,\vec{p}}^b n_{2,\vec{p}}^b}$ must satisfy $\sum_{n_{1,\vec{p}}^a, n_{2,\vec{p}}^a, n_{1,\vec{p}}^b n_{2,\vec{p}}^b = 0,1} |\alpha_{n_{1,\vec{p}}^a, n_{2,\vec{p}}^a, n_{1,\vec{p}}^b n_{2,\vec{p}}^b}|^2 = 1$.

Since the system conserves particle number, i.e. $[\mathcal{H}_4, \mathcal{N}] = 0$, where $\mathcal{N} = \sum_{\vec{p}, \alpha=1,2} (a_{\alpha,\vec{p}}^\dagger a_{\alpha,\vec{p}} + b_{\alpha,\vec{p}}^\dagger b_{\alpha,\vec{p}})$ is the total particle number operator, $\mathcal{H}_4$ consists of sectors labelled by different total particle numbers. Therefore, at half-filling, $|\Phi_{\vec{p}}\rangle$ can only consist of Fock states that satisfy the condition $\sum_{\alpha=1,2} (n_{\alpha,\vec{p}}^a + n_{\alpha,\vec{p}}^b) = 2$. A complete basis for each momentum component $|\Phi_{\vec{p}}\rangle$ of the ground state is thus given by

$$\{|1100\rangle, |1010\rangle, |1001\rangle, |0110\rangle, |0101\rangle, |0011\rangle\}. \tag{6.4}$$

$|\Phi_{\vec{p}}\rangle$ can be written as a sum of two states living in two orthogonal ('even' and 'odd')

subspaces

$$|\Phi_{\vec{p}}\rangle = A\,|\Phi(n_1^a + n_2^a = \text{even}; n_1^b + n_2^b = \text{even})\rangle + B\,|\Phi(n_1^a + n_2^a = \text{odd}; n_1^b + n_2^b = \text{odd})\rangle$$
$$\equiv A\,|\Phi_{\text{e}}\rangle + B\,|\Phi_{\text{o}}\rangle\,, \tag{6.5}$$

where we have suppressed the $\vec{p}$ dependence on the right-hand side for ease of readability. The populations $n_1^a + n_2^a$ and $n_1^b + n_2^b$ are either both even or both odd, $|\Phi_{\text{e}}\rangle$ and $|\Phi_{\text{o}}\rangle$ are normalized and orthogonal to each other, while A and B satisfy $|A|^2 + |B|^2 = 1$ to ensure normalization. The partitioning of the state in this manner facilitates our derivation.

We now Schmidt decompose both the even and odd parts of (6.5) with respect to the a and b subsystems:

$$|\Phi_{\text{e}}\rangle = \cos\theta_{\text{e}}\,|a_{\text{e}}\rangle\,|b_{\text{e}}\rangle + \sin\theta_{\text{e}}\,|\tilde{a}_{\text{e}}\rangle\,|\tilde{b}_{\text{e}}\rangle$$
$$|\Phi_{\text{o}}\rangle = \cos\theta_{\text{o}}\,|a_{\text{o}}\rangle\,|b_{\text{o}}\rangle + \sin\theta_{\text{o}}\,|\tilde{a}_{\text{o}}\rangle\,|\tilde{b}_{\text{o}}\rangle\,, \tag{6.6}$$

where $\theta_{\text{e}}, \theta_{\text{o}} \in [0, \pi/2]$ such that all the Schmidt coefficients are non-negative. It is understood that the states $|a_{\text{e/o}}\rangle$, $|b_{\text{e/o}}\rangle$, $|\tilde{a}_{\text{e/o}}\rangle$ and $|\tilde{b}_{\text{e/o}}\rangle$ – which are written in the occupation number basis – have the creation operators ordered as in (6.3). These states are normalized and obey the orthogonality conditions $\langle a_{\text{e/o}}|\tilde{a}_{\text{e/o}}\rangle = \langle b_{\text{e/o}}|\tilde{b}_{\text{e/o}}\rangle = 0$, as one can see from

$$|a_{\text{o}}\rangle = \left(\alpha_{01}a_{2,\vec{p}}^\dagger + \alpha_{10}a_{1,\vec{p}}^\dagger\right)|0\rangle\,, \quad |\tilde{a}_{\text{o}}\rangle = \left(\alpha_{10}^* a_{2,\vec{p}}^\dagger - \alpha_{01}^* a_{1,\vec{p}}^\dagger\right)|0\rangle\,,$$
$$|b_{\text{o}}\rangle = \left(\beta_{01}b_{2,\vec{p}}^\dagger + \beta_{10}b_{1,\vec{p}}^\dagger\right)|0\rangle\,, \quad |\tilde{b}_{\text{o}}\rangle = \left(\beta_{10}^* b_{2,\vec{p}}^\dagger - \beta_{01}^* b_{1,\vec{p}}^\dagger\right)|0\rangle \tag{6.7}$$

and

$$|a_{\text{e}}\rangle = e^{i\phi_a}\,|0\rangle\,, \qquad\qquad |\tilde{a}_{\text{e}}\rangle = e^{i\tilde{\phi}_a}a_{1,\vec{p}}^\dagger a_{2,\vec{p}}^\dagger\,|0\rangle\,,$$
$$|b_{\text{e}}\rangle = e^{i\phi_b}b_{1,\vec{p}}^\dagger b_{2,\vec{p}}^\dagger\,|0\rangle\,, \quad |\tilde{b}_{\text{e}}\rangle = e^{i\tilde{\phi}_b}\,|0\rangle\,, \tag{6.8}$$

where $|\alpha_{01}|^2 + |\alpha_{10}|^2 = |\beta_{01}|^2 + |\beta_{10}|^2 = 1$. The phases $\phi_{a/b}$ and $\tilde{\phi}_{a/b}$ are in general non-zero. However, after multiplying $|\Phi_{\vec{p}}\rangle$ by a global phase of $e^{-i(\phi_a + \phi_b)}$ [50], we can transfer them to the odd subspace through the $U(1)$ gauge transformation $a_{1,\vec{p}}^\dagger \to e^{-i(\tilde{\phi}_a + \tilde{\phi}_b - \phi_a - \phi_b)}a_{1,\vec{p}}^\dagger \equiv e^{i\varphi}a_{1,\vec{p}}^\dagger$. These phases can therefore be absorbed into α_{01} and α_{10} [51]. As a result, the only $\vec{p}$ dependence in $|\Phi_{\text{e}}\rangle$ is in its Schmidt coefficients, $\cos\theta_{\text{e}}$ and $\sin\theta_{\text{e}}$.

Before we evaluate the Chern number of the ground state (6.2) using the Berry phase

---

[50] One can see from the Berry phase representation of ν which we discuss below (see (6.9)) that, such a gauge transformation results in $\langle\Phi_{\vec{p}}|\vec{\nabla}|\Phi_{\vec{p}}\rangle \to \langle\Phi_{\vec{p}}|\vec{\nabla}|\Phi_{\vec{p}}\rangle - i\vec{\nabla}(\phi_a + \phi_b)$. This extra gradient term vanishes upon using Stokes' theorem.

[51] Explicitly, after multiplying $|\Phi_{\vec{p}}\rangle$ by a phase $e^{-i(\varphi/2)}$, we can make the replacements $\alpha_{01} \to e^{-i(\varphi/2)}\alpha_{01}$ and $\alpha_{10} \to e^{i(\varphi/2)}\alpha_{10}$.

representation

$$\nu = -\frac{i}{2\pi} \oint_{\partial BZ} \langle \Phi_{\vec{p}} | \vec{\nabla} | \Phi_{\vec{p}} \rangle \cdot d\vec{p}, \tag{6.9}$$

where $\vec{\nabla} = (\partial_{p_x}, \partial_{p_y})$ and ∂BZ refers to the boundary of the BZ, let us show that (6.9) and (5.1) are equivalent. Diagonalization of $h_4(\vec{p})$ in (6.1) yields the creation operators $c_1^\dagger$, $c_2^\dagger$, $c_3^\dagger$, and $c_4^\dagger$ (suppressing the $\vec{p}$ label), with the latter two corresponding to the two lowest energy bands. We can write these as

$$\begin{aligned} c_3^\dagger &= \alpha a_1^\dagger + \beta a_2^\dagger + \gamma b_1^\dagger + \delta b_2^\dagger \\ c_4^\dagger &= \varepsilon a_1^\dagger + \eta a_2^\dagger + \mu b_1^\dagger + \omega b_2^\dagger, \end{aligned} \tag{6.10}$$

with the vectors $|\chi_3\rangle = (\alpha, \beta, \gamma, \delta)^T$ and $|\chi_4\rangle = (\varepsilon, \eta, \mu, \omega)^T$ being the two lowest energy eigenvectors of $h_4(\vec{p})$. As a result, $|\Phi_{\vec{p}}\rangle = c_3^\dagger c_4^\dagger |0\rangle$, which means that $|\Phi_{\vec{p}}\rangle$ can be equally well represented by a Slater determinant of $|\chi_3\rangle$ and $|\chi_4\rangle$ [52]:

$$|\Phi_{\vec{p}}\rangle \leftrightarrow \frac{1}{\sqrt{2}} \left(|\chi_3\rangle \otimes |\chi_4\rangle - |\chi_4\rangle \otimes |\chi_3\rangle \right). \tag{6.11}$$

Substituting this alternative representation into (6.9) yields

$$\nu = -\frac{i}{2\pi} \oint_{\partial BZ} \left(\langle \chi_3 | \vec{\nabla} | \chi_3 \rangle + \langle \chi_4 | \vec{\nabla} | \chi_4 \rangle \right) \cdot d\vec{p}, \tag{6.12}$$

which is precisely what one obtains if one evaluates the projector representation of ν, (5.1), with $\mathcal{P}_{\vec{p}} = |\chi_3\rangle\langle\chi_3| + |\chi_4\rangle\langle\chi_4|$ and uses Stokes' theorem. The representations (5.1) and (6.9) are thus equivalent, and this equivalence holds in general.

Let us now evaluate the Chern number. We note that A and B can be taken to be real and non-negative, which is achieved by absorbing possible complex phases into the states $|a_{e/o}\rangle |b_{e/o}\rangle$ and $|\tilde{a}_{e/o}\rangle |\tilde{b}_{e/o}\rangle$. Plugging (6.5) into (6.9) one finds

$$\nu = -\frac{i}{2\pi} \oint_{\partial BZ} \left(A^2 \langle \Phi_e | \vec{\nabla} | \Phi_e \rangle + B^2 \langle \Phi_o | \vec{\nabla} | \Phi_o \rangle \right) \cdot d\vec{p}, \tag{6.13}$$

where the terms $A\vec{\nabla}A$ and $B\vec{\nabla}B$ do not contribute since $A\vec{\nabla}A + B\vec{\nabla}B = \vec{\nabla}(A^2 + B^2)/2 = 0$. The even subspace contribution to the integral vanishes because $\cos\theta_e \vec{\nabla}\cos\theta_e + \sin\theta_e \vec{\nabla}\sin\theta_e = \vec{\nabla}(\cos^2\theta_e + \sin^2\theta_e)/2 = 0$ (recall that the only $\vec{p}$ dependence in $|\Phi_e\rangle$ is in $\cos\theta_e$ and $\sin\theta_e$). Turning our attention to the odd subspace contribution, $\langle i_o | \vec{\nabla} | i_o \rangle = -\langle \tilde{i}_o | \vec{\nabla} | \tilde{i}_o \rangle$, which stems from $\vec{\nabla} \left(|\alpha_{01}|^2 + |\alpha_{10}|^2 \right) = \vec{\nabla} \left(|\beta_{01}|^2 + |\beta_{10}|^2 \right) = 0$. Furthermore, since the terms involving gradients of the Schmidt coefficients disappear (for the same reason that the even versions

---

[52] In other words, an anti-symmetrized tensor product of $|\chi_3\rangle$ and $|\chi_4\rangle$, which reflects the anti-commutation property of the creation operators.

disappear), we arrive at

$$\nu = -\frac{i}{2\pi} \sum_{i=a,b} \oint_{\partial \mathrm{BZ}} S_{\vec{p}} \langle i_{\mathrm{o}}|\vec{\nabla}|i_{\mathrm{o}}\rangle \cdot d\vec{p}, \qquad S_{\vec{p}} = B^2 T, \qquad (6.14)$$

where $T = \cos^2 \theta_{\mathrm{o}} - \sin^2 \theta_{\mathrm{o}}$ is a measure of entanglement between the a and b subsystems [53].

Equation (6.14) reveals that the Chern number is a sum of exclusive contributions from the a or b subsystems. Due to the presence of S [54], these contributions are *not* in general Berry phases which can be evaluated as winding numbers of the vectors $\hat{\vec{s}}_a(\vec{p})$ and $\hat{\vec{s}}_b(\vec{p})$, associated with the 2D states $|a_{\mathrm{o}}\rangle$ and $|b_{\mathrm{o}}\rangle$ (see (6.7)), respectively. ν decomposes into a sum of Berry phase contributions if and only if $|S| = 1$, which occurs when $|T| = 1$, implying that the subsystems are unentangled. However, as we further discuss in section 6.1.2, as long as $S \neq 0$, the Chern number can be calculated using the right-hand side of (6.14) with $|S| = 1$. This method fails only when $S \to 0$, i.e. when the system is maximally entangled [55].

6.1.2 Subsystem winding numbers as physical observables

The observables for the a and b subsystems take the same form as the observables for a two-component system (see (5.16)):

$$
\begin{aligned}
\Sigma_a^x &= a_{1,\vec{p}}^\dagger a_{2,\vec{p}} + a_{2,\vec{p}}^\dagger a_{1,\vec{p}}, & \Sigma_a^y &= -ia_{1,\vec{p}}^\dagger a_{2,\vec{p}} + ia_{2,\vec{p}}^\dagger a_{1,\vec{p}}, & \Sigma_a^z &= a_{1,\vec{p}}^\dagger a_{1,\vec{p}} - a_{2,\vec{p}}^\dagger a_{2,\vec{p}} \\
\Sigma_b^x &= b_{1,\vec{p}}^\dagger b_{2,\vec{p}} + b_{2,\vec{p}}^\dagger b_{1,\vec{p}}, & \Sigma_b^y &= -ib_{1,\vec{p}}^\dagger b_{2,\vec{p}} + ib_{2,\vec{p}}^\dagger b_{1,\vec{p}}, & \Sigma_b^z &= b_{1,\vec{p}}^\dagger b_{1,\vec{p}} - b_{2,\vec{p}}^\dagger b_{2,\vec{p}}.
\end{aligned}
$$
$$(6.15)$$

The ground state expectation values of these operators, $\vec{\Sigma}_{i,\vec{p}} = \left(\Sigma_i^x, \Sigma_i^y, \Sigma_i^z \right)$, is easily calculated to be

$$
\begin{aligned}
\langle \Phi_{\vec{p}} | \vec{\Sigma}_{i,\vec{p}} | \Phi_{\vec{p}} \rangle &= B^2 \left(\cos^2 \theta_{\mathrm{o}} \langle i_{\mathrm{o}} | \vec{\Sigma}_{i,\vec{p}} | i_{\mathrm{o}} \rangle + \sin^2 \theta_{\mathrm{o}} \langle \tilde{i}_{\mathrm{o}} | \vec{\Sigma}_{i,\vec{p}} | \tilde{i}_{\mathrm{o}} \rangle \right) \\
&= S \langle i_{\mathrm{o}} | \vec{\Sigma}_{i,\vec{p}} | i_{\mathrm{o}} \rangle,
\end{aligned}
\qquad (6.16)
$$

---

[53] To be precise, T is only a measure of entanglement in the 'odd part' of $|\Phi_{\vec{p}}\rangle$, $|\Phi_{\mathrm{o}}\rangle$. Below, when we talk of the degree of entanglement in the 'system', we mean the entanglement present in $|\Phi_{\mathrm{o}}\rangle$, unless stated otherwise.

[54] We will suppress the $\vec{p}$ dependence of $S_{\vec{p}}$ for the most part.

[55] Of course, $B \to 0$ with T remaining finite also results in $S \to 0$, i.e. it appears that $S \to 0$ does not necessarily imply that the system is maximally entangled. However, it appears that in most cases, B should remain non-zero throughout the BZ. Only in certain extreme (and topologically trivial) cases – such as when a large energy imbalance forces the entire population into subsystem a or b – can B possibly vanish. This leads us to believe that in general, $S \to 0$ implies that $T \to 0$. We note that for superconducting systems (see section 6.1.3 and (6.28)), $S = A^2 T \to 0$ implies that $T \to 0$, since A *cannot* vanish. This is apparent from equations (6.35) and (6.36) and the discussion in section 6.2 regarding the superconducting ground state of the entanglement Hamiltonian.

where we have used the traceless property of the $\vec{\Sigma}_{i,\vec{p}}$ operators which implies $\langle \tilde{i}_{\mathrm{o}} | \vec{\Sigma}_{i,\vec{p}} | \tilde{i}_{\mathrm{o}} \rangle = -\langle i_{\mathrm{o}} | \vec{\Sigma}_{i,\vec{p}} | i_{\mathrm{o}} \rangle$. If we define the normalized three-vector $\langle i_{\mathrm{o}} | \vec{\Sigma}_{i,\vec{p}} | i_{\mathrm{o}} \rangle$ to be

$$\langle i_{\mathrm{o}} | \vec{\Sigma}_{i,\vec{p}} | i_{\mathrm{o}} \rangle \equiv \hat{\vec{s}}_i(\vec{p}) \,, \tag{6.17}$$

we obtain

$$\langle \Phi_{\vec{p}} | \vec{\Sigma}_{a,\vec{p}} | \Phi_{\vec{p}} \rangle = S \hat{\vec{s}}_a(\vec{p}), \tag{6.18}$$

$$\langle \Phi_{\vec{p}} | \vec{\Sigma}_{b,\vec{p}} | \Phi_{\vec{p}} \rangle = S \hat{\vec{s}}_b(\vec{p}), \tag{6.19}$$

i.e. the observables (6.15) allow an experimentalist to measure the vectors $S\hat{\vec{s}}_{a/b}(\vec{p})$, at least in principle. Furthermore, since the norm of these vectors is equal to $|S|$, the degree of entanglement between the subsystems can be probed by using the operators (6.15).

We would like to express the Chern number (6.14) in terms of the measurable quantities that we have discussed, so that the single-species observables (6.15) suffice to measure ν. As it stands, the elements of (6.14) cannot be determined from these observables; for instance, the sign of S cannot be determined using (6.15). On the right-hand side of (6.14), let us set $|S| = 1$ and assume that the sign of S, $\mathrm{sgn}(S)$, does not change along the integration contour, so that it can be taken outside the integral. The right-hand side thus becomes

$$-\frac{i}{2\pi} \sum_{i=a,b} \mathrm{sgn}(S) \oint_{\partial \mathrm{BZ}} \langle i_{\mathrm{o}} | \vec{\nabla} | i_{\mathrm{o}} \rangle \cdot d\vec{p} = \mathrm{sgn}(S) \sum_{i=a,b} \tilde{\nu}[\hat{\vec{s}}_i] \,, \tag{6.20}$$

where equality follows from the fact that the Berry phase of $|i_{\mathrm{o}}\rangle$ can be expressed as the winding number of the Bloch vector characterizing $|i_{\mathrm{o}}\rangle$ [56], $\hat{\vec{s}}_i$, which is defined in (6.17). We *postulate* that ν can be calculated from (6.20).

The right-hand side of (6.20) is in fact experimentally accessible, using the observables we are considering. From (6.18) and (6.19), it is clear that while $\hat{\vec{s}}_i(\vec{p})$ is *not* observable, $\mathrm{sgn}(S)\hat{\vec{s}}_i(\vec{p})$ *is* observable. This is because only the magnitude of S can be determined, while its sign is inaccessible. Therefore, the winding numbers $\tilde{\nu}[\mathrm{sgn}(S)\hat{\vec{s}}_i]$ are also observable. Assuming that $\mathrm{sgn}(S)$ remains constant (and non-zero) in the BZ, the following holds:

$$\sum_{i=a,b} \tilde{\nu}[\mathrm{sgn}(S)\hat{\vec{s}}_i] = \mathrm{sgn}(S) \sum_{i=a,b} \tilde{\nu}[\hat{\vec{s}}_i] \,. \tag{6.21}$$

In other words, the sum of the subsystem winding numbers, (6.20), that we postulate to yield the Chern number, is *physically observable*. Indeed, the examples of section 6.3 show that the method works even for $|S| \neq 1$: ν is returned as long as the system is not maximally entangled, or $S \nrightarrow 0$. Our method only breaks down when $S \to 0$, which implies that no

---

[56] As explained in section 6.1.1, the Berry phase and projector representations of ν are equivalent, and appendix E demonstrates that for 2D systems (such as $|i_{\mathrm{o}}\rangle$), the projector and winding number representations are equivalent.

information about the vectors $\hat{\vec{s}}_i(\vec{p})$ can be inferred. We will now show that with small modifications, a similar decomposition holds for topological superconductors.

6.1.3 Decomposition for topological superconductors

The generalization to topological superconductors is straightforward. We take the Hamiltonian to be of the same form as (6.1), with the basis given now by $\psi_{\vec{p}} = \left(a_{\vec{p}}, a_{-\vec{p}}^\dagger, b_{\vec{p}}, b_{-\vec{p}}^\dagger \right)^T$. The many-body ground state of the system can again be written as (6.2) (with BZ $\to$ BZ/2) with the Fock states

$$|n_{\vec{p}}^a, n_{-\vec{p}}^a, n_{\vec{p}}^b, n_{-\vec{p}}^b\rangle = (a_{\vec{p}}^\dagger)^{n_{\vec{p}}^a}(a_{-\vec{p}}^\dagger)^{n_{-\vec{p}}^a}(b_{\vec{p}}^\dagger)^{n_{\vec{p}}^b}(b_{-\vec{p}}^\dagger)^{n_{-\vec{p}}^b}|0\rangle . \qquad (6.22)$$

Superconductors conserve only the parity, Π, of the total number of particles in the system, i.e. $[\mathcal{H}_4, \Pi] = 0$ with

$$\Pi = \exp\left(i\pi \sum_{\vec{p}} \left[a_{\vec{p}}^\dagger a_{\vec{p}} + b_{\vec{p}}^\dagger b_{\vec{p}} \right] \right) = \exp\left(i\pi \sum_{\vec{p}} a_{\vec{p}}^\dagger a_{\vec{p}} \right) \exp\left(i\pi \sum_{\vec{p}} b_{\vec{p}}^\dagger b_{\vec{p}} \right) \equiv \Pi_a \Pi_b, \quad (6.23)$$

where Π_a and Π_b are the subsystem parities. When the subsystems are coupled, Π_a and Π_b are not independently conserved. Since the ground state of a superconductor resides in the even (total) parity sector [57], the subsystem parities are correlated such that $\Pi_a = \Pi_b$. Furthermore, the ground state is a condensate of Cooper-pairs which have zero total momentum, and so the Fock states which enter (6.2) must reflect this. These considerations imply that $|\Phi_{\vec{p}}\rangle$ can be expanded in the basis

$$\{|0000\rangle, |0011\rangle, |1100\rangle, |1111\rangle, |0110\rangle, |1001\rangle\} . \qquad (6.24)$$

As in the insulating case (see (6.5)), the basis for $|\Phi_{\vec{p}}\rangle$ can be split into even and odd occupation subspaces:

$$|\Phi_{\vec{p}}\rangle = A|\Phi_\mathrm{e}\rangle + B|\Phi_\mathrm{o}\rangle . \qquad (6.25)$$

A Schmidt decomposition on $|\Phi_\mathrm{e/o}\rangle$ with respect to the subsystems a and b yields expressions which have the same form as (6.6), but with the Schmidt bases now being given by

$$|a_\mathrm{e}\rangle = \left(\alpha_{00} + \alpha_{11} a_{\vec{p}}^\dagger a_{-\vec{p}}^\dagger \right)|0\rangle, \quad |\tilde{a}_\mathrm{e}\rangle = \left(\alpha_{11}^* - \alpha_{00}^* a_{\vec{p}}^\dagger a_{-\vec{p}}^\dagger \right)|0\rangle,$$
$$|b_\mathrm{e}\rangle = \left(\beta_{00} + \beta_{11} b_{\vec{p}}^\dagger b_{-\vec{p}}^\dagger \right)|0\rangle, \quad |\tilde{b}_\mathrm{e}\rangle = \left(\beta_{11}^* - \beta_{00}^* b_{\vec{p}}^\dagger b_{-\vec{p}}^\dagger \right)|0\rangle, \qquad (6.26)$$

---

[57] See the ground state (5.13), for instance.

and

$$|a_{\mathrm{o}}\rangle = e^{i\phi_a} a^{\dagger}_{-\vec{p}}|0\rangle, \quad |\tilde{a}_{\mathrm{o}}\rangle = e^{i\tilde{\phi}_a} a^{\dagger}_{\vec{p}}|0\rangle,$$
$$|b_{\mathrm{o}}\rangle = e^{i\phi_b} b^{\dagger}_{\vec{p}}|0\rangle, \quad |\tilde{b}_{\mathrm{o}}\rangle = e^{i\tilde{\phi}_b} b^{\dagger}_{-\vec{p}}|0\rangle. \tag{6.27}$$

Since $|\alpha_{00}|^2 + |\alpha_{11}|^2 = |\beta_{00}|^2 + |\beta_{11}|^2 = 1$, the above states are all normalized and subject to the same orthogonality conditions as their insulating counterparts.

Similar to the case of topological insulators, suitable gauge transformations can transfer the odd subspace phases to the even subspace. The decomposition of the Chern number via the Berry phase representation proceeds in similar steps to the insulating case. The only difference is that it is now the odd subspace contribution that vanishes in (6.13), with the Chern number now being given by

$$\nu = -\frac{i}{2\pi} \sum_{i=a,b} \oint_{\partial\mathrm{BZ}} S\langle i_{\mathrm{e}}|\vec{\nabla}|i_{\mathrm{e}}\rangle \cdot d\vec{p}, \qquad S = A^2 T, \tag{6.28}$$

with $T = \cos^2\theta_{\mathrm{e}} - \sin^2\theta_{\mathrm{e}}$ being a measure of entanglement between the subsystems.

The subsystem observables $\vec{\Sigma}_{i,\vec{p}} = \left(\Sigma_i^x, \Sigma_i^y, \Sigma_i^z\right)$ are now defined by

$$\begin{aligned}
\Sigma_a^x &= a^{\dagger}_{\vec{p}} a^{\dagger}_{-\vec{p}} + a_{-\vec{p}} a_{\vec{p}}, & \Sigma_a^y &= -ia^{\dagger}_{\vec{p}} a^{\dagger}_{-\vec{p}} + ia_{-\vec{p}} a_{\vec{p}}, & \Sigma_a^z &= a^{\dagger}_{\vec{p}} a_{\vec{p}} - a_{-\vec{p}} a^{\dagger}_{-\vec{p}}, \\
\Sigma_b^x &= b^{\dagger}_{\vec{p}} b^{\dagger}_{-\vec{p}} + b_{-\vec{p}} b_{\vec{p}}, & \Sigma_b^y &= -ib^{\dagger}_{\vec{p}} b^{\dagger}_{-\vec{p}} + ib_{-\vec{p}} b_{\vec{p}}, & \Sigma_b^z &= b^{\dagger}_{\vec{p}} b_{\vec{p}} - b_{-\vec{p}} b^{\dagger}_{-\vec{p}},
\end{aligned} \tag{6.29}$$

and so the ground state expectation value of $\vec{\Sigma}_{i,\vec{p}}$ is

$$\begin{aligned}
\langle\Phi_{\vec{p}}|\vec{\Sigma}_{i,\vec{p}}|\Phi_{\vec{p}}\rangle &= A^2 \left(\cos^2\theta_{\mathrm{e}} \langle i_{\mathrm{e}}|\vec{\Sigma}_{i,\vec{p}}|i_{\mathrm{e}}\rangle + \sin^2\theta_{\mathrm{e}} \langle\tilde{i}_{\mathrm{e}}|\vec{\Sigma}_{i,\vec{p}}|\tilde{i}_{\mathrm{e}}\rangle\right) \\
&= S\langle i_{\mathrm{e}}|\vec{\Sigma}_{i,\vec{p}}|i_{\mathrm{e}}\rangle \\
&\equiv S\hat{\vec{s}}_i(\vec{p}), \tag{6.30}
\end{aligned}$$

i.e. the vectors $S\hat{\vec{s}}_{a/b}(\vec{p})$ are observable. Once again, this allows $|S|$ to be measured, and thus the degree of entanglement between subsystems can be probed for superconducting systems by using the observables (6.29). Furthermore, using the argument presented for insulators, (6.28) becomes a sum of subsystem winding numbers (right-hand side of (6.20)) which are observable. For a superconducting model that we examine in 6.3.2, the sum of these winding numbers indeed yields ν, as long as the system [58] is not maximally entangled.

6.2 Detection of the component entanglement spectrum

We found above that since the entanglement measure T is proportional to the observable $|S|$, the degree to which the subsystems are entangled can be probed experimentally. We now

---

[58]For superconductors, entanglement of the 'system' refers to entanglement of $|\Phi_{\mathrm{e}}\rangle$, unless stated otherwise.

show that one can go further and use these same observables to construct the component ES (Legner & Neupert, 2013) of non-interacting insulators and superconductors.

We first consider the insulating case. The two-point correlation function (which was introduced in section 5.3) becomes block diagonal when expressed in momentum space

$$\bar{\mathbb{C}} = \bigoplus_{\vec{p} \in \text{BZ}} \bar{\mathbb{C}}(\vec{p}) \,, \tag{6.31}$$

where each block $\bar{\mathbb{C}}(\vec{p})$ is a 4×4 matrix labelled by $\vec{p}$. These blocks have matrix elements $\bar{\mathbb{C}}_{i,j}(\vec{p})$ where $i,j = 1,2,3,4$ and $1 \leftrightarrow a_1$, $2 \leftrightarrow a_2$, $3 \leftrightarrow b_1$, $4 \leftrightarrow b_2$; for instance, $\bar{\mathbb{C}}_{2,3}(\vec{p}) = \langle \Phi | a_{2,\vec{p}}^\dagger b_{1,\vec{p}} | \Phi \rangle$. The projector onto subsystem a also assumes a block diagonal structure in $\vec{p}$ space

$$\bar{\mathcal{P}}_a = \bigoplus_{\vec{p} \in \text{BZ}} \bar{\mathcal{P}}_a(\vec{p}) \,, \quad \bar{\mathcal{P}}_a(\vec{p}) = \text{diag}(1,1,0,0) \,, \tag{6.32}$$

and thus the restricted correlation matrix is given by

$$\bar{\mathbb{C}}_a = \bar{\mathcal{P}}_a \bar{\mathbb{C}} \bar{\mathcal{P}}_a = \bigoplus_{\vec{p} \in \text{BZ}} \bar{\mathbb{C}}_a(\vec{p}) \,. \tag{6.33}$$

It is easy to see that $S s_a^z(\vec{p}) = \left(\bar{\mathbb{C}}_a(\vec{p})\right)_{11} - \left(\bar{\mathbb{C}}_a(\vec{p})\right)_{22}$, and similarly for the x- and y-components. A simple calculation reveals that the (non-trivial) eigenvalues of $\bar{\mathbb{C}}_a(\vec{p})$ are $\zeta_\pm = \left(N_a(\vec{p}) \pm |S|\right)/2$, where we have defined the occupation in subsystem a to be $N_a(\vec{p}) \equiv \langle \Phi | a_{1,\vec{p}}^\dagger a_{1,\vec{p}} + a_{2,\vec{p}}^\dagger a_{2,\vec{p}} | \Phi \rangle$. Substituting this into (5.9) yields the single-particle ES or 'energies' at each momenta

$$\varepsilon_\pm(\vec{p}) = \log \left(\frac{N_b(\vec{p}) \mp |S|}{N_a(\vec{p}) \pm |S|} \right) \,, \tag{6.34}$$

where the occupation in subsystem b is $N_b(\vec{p}) = 2 - N_a(\vec{p})$, since we are considering systems at half-filling. Our observables thus give direct access to the component ES. The entanglement gap closes if $\varepsilon_+ = \varepsilon_-$ for some $\vec{p}$ [59]. It is straightforward to verify that this is satisfied only when $|S| = 0$, i.e. when the subsystems are maximally entangled and our detection scheme becomes unreliable.

While a similar analytic derivation between the ES and the observables is more involved for paired fermion systems, due to (5.9) being replaced by a more complicated relation (Peschel, 2003), one can qualitatively understand that a similar relation must also hold for such systems. The $\vec{p}$-th component of ρ_a is

$$\rho_a(\vec{p}) = A^2 \left(\cos^2 \theta_\text{e} |a_\text{e}\rangle \langle a_\text{e}| + \sin^2 \theta_\text{e} |\tilde{a}_\text{e}\rangle \langle \tilde{a}_\text{e}| \right) + B^2 \left(\cos^2 \theta_\text{o} |a_\text{o}\rangle \langle a_\text{o}| + \sin^2 \theta_\text{o} |\tilde{a}_\text{o}\rangle \langle \tilde{a}_\text{o}| \right) \,, \tag{6.35}$$

---

[59] This is a 'direct' gap closure; in principle, 'indirect' gap closures where $\varepsilon_+(\vec{p}) = \varepsilon_-(\vec{q})$ for $\vec{p} \neq \vec{q}$ can also exist. The gap is thus formally given by $\min_{\vec{p}} \varepsilon_+ - \max_{\vec{p}} \varepsilon_-$.

with ρ_a being a product of these components over $\vec{p}$. The state with greatest weight in ρ_a is the ground state of the entanglement Hamiltonian, and since this Hamiltonian is of superconducting form, the ground state must reside in the even parity sector. This means that the largest eigenvalue of ρ_a is

$$\prod_{\vec{p}} A^2 \max(\cos^2\theta_e, \sin^2\theta_e). \qquad (6.36)$$

$|S| = A^2|\cos^2\theta_e - \sin^2\theta_e|$ vanishes when $\cos^2\theta_e = \sin^2\theta_e$ [60], and when this happens, the largest eigenvalue of ρ_a becomes degenerate. In other words, as for insulators, when the subsystems are maximally entangled, the entanglement gap closes [61]. Indeed, we will numerically show in section 6.3.2 that there is exact agreement between the observable $|S| \to 0$ and the entanglement gap closing for superconducting systems as well.

6.3 Case studies

We now demonstrate the validity of our analytic arguments by examining two distinct topological models: the QSHI (Kane & Mele, 2005) and a staggered topological superconductor (Pachos *et al.*, 2013). In both cases, the phase diagrams are accurately reproduced by subsystem winding numbers, with any discrepancies coinciding with regions of high entanglement between the subsystems.

6.3.1 Example I: The quantum spin-Hall insulator

The first example we consider is the QSHI defined on a honeycomb lattice (Kane & Mele, 2005). With this model, Kane and Mele showed that time-reversal symmetric topological insulators can exist in principle. In contrast to phases which break time-reversal symmetry, such as IQH states, the QSHI supports non-chiral edge states. Namely, an edge state which propagates in a certain direction is accompanied by its time-reversed partner which moves in the opposite direction. There are an odd number of such 'Kramers pairs' in the non-trivial quantum spin-Hall (QSH) phase and an even number in the trivial insulating phase.

The Hamiltonian of this model is given by

$$\mathcal{H}_{KM} = t\sum_{\langle i,j\rangle} c_i^\dagger c_j + \lambda_\nu \sum_i \varepsilon_i c_i^\dagger c_i + i\lambda_{SO} \sum_{\langle\langle i,j\rangle\rangle} \nu_{ij} c_i^\dagger Z c_j + i\lambda_R \sum_{\langle i,j\rangle} c_i^\dagger \left(\vec{\sigma}\times\hat{\vec{d}}_{ij}\right)_z c_j, \qquad (6.37)$$

where $c_i = (c_{i,\uparrow}, c_{i,\downarrow})^T$ denotes the two spin degrees of freedom of a spin-half particle at lattice site i. The first term describes nearest neighbour tunnelling with hopping amplitude

---

[60] As mentioned earlier, A must be non-zero since the ground state of the entanglement Hamiltonian must belong to the even parity sector.

[61] Recall the discussion in section 5.3 where we explained that zeros in the single-particle ES imply degeneracies in the ES. Assuming that the converse holds, and using the particle-hole symmetry $\varepsilon_- = -\varepsilon_+$ of superconductors, degeneracies in the ES imply entanglement gap closure.
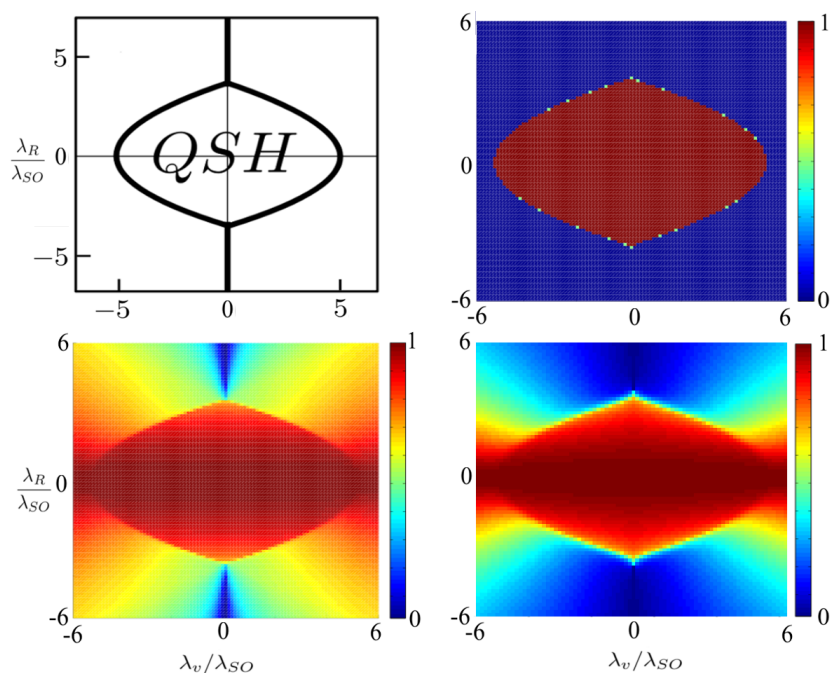
Figure 6.1: *Top left*: Theoretical phase diagram of (6.37) in the parameter space $(\lambda_v/\lambda_{SO}, \lambda_R/\lambda_{SO})$. The trivial phase corresponds to $\nu_S = 0$, while the QSH phase corresponds to $\nu_S = 1$. *Top right*: Phase diagram computed from $(\tilde{\nu}_\uparrow - \tilde{\nu}_\downarrow)/2 \mod 2$. *Bottom left*: The minimum of the subsystem entanglement measure across the BZ, $\min_{\vec{p}}|S|$. $\min_{\vec{p}}|S| \to 0$ indicates maximal entanglement whereas $\min_{\vec{p}}|S| \to 1$ indicates minimal entanglement. We see that in the QSH phase, the spin components are either completely or effectively decoupled. *Bottom right*: The gap of the ES of the spin-up subsystem. This gap is defined to be $\min_{\vec{p}}\zeta_+ - \max_{\vec{p}}\zeta_-$ and closes when $|S| = 0$, as noted in section 6.2.

t, while the second term is a sublattice energy imbalance, where $\varepsilon_i = \pm 1$ depends on which sublattice i belongs to and λ_v sets the magnitude of the imbalance. Both these terms are spin-conserving. The third term is an 'intrinsic' spin-orbit coupling of strength λ_{SO}, in the form of next-nearest neighbour hopping, and conserves only the z-component of spin. In it, $v_{ij} = (2/\sqrt{3})\,\mathrm{sgn}\left(\hat{\vec{d}}_1 \times \hat{\vec{d}}_2\right)_z$ where $\hat{\vec{d}}_1$ and $\hat{\vec{d}}_2$ are unit vectors along the two bonds a particle traverses in going from j to i. The last term is a Rashba spin-orbit coupling of strength λ_R, in the form of nearest neighbour hopping, with $\hat{\vec{d}}_{ij}$ being a unit vector from site j to i. This last term breaks Z conservation and was introduced to model realistic solid-state environments.

After Fourier transforming (6.37), it assumes the form of (6.1) in the basis $\psi_{\vec{p}} = (a_{\uparrow,\vec{p}}, a_{\downarrow,\vec{p}}, b_{\uparrow,\vec{p}}, b_{\downarrow,\vec{p}})^T$, where a and b denote the two sublattice degrees of freedom in the unit cell of the honeycomb lattice [62]. While the Chern number is zero for time-reversal symmetric systems (Avron *et al.*, 1988), Kane and Mele showed that $\mathcal{H}_{KM}$ supports trivial insulating and QSH phases, which are distinguished by a bulk $\mathbb{Z}_2$ valued topological

---

[62] $a_{\uparrow,\vec{p}}$ is the Fourier transform of $c_{i \in a,\uparrow}$, with the other components of $\psi_{\vec{p}}$ being defined in an analogous manner.

invariant (Kane & Mele, 2005) [63]. Moreover, the $\mathbb{Z}_2$ invariant was shown to be related to the so-called spin Chern number ν_S (Sheng *et al.*, 2006), which is determined by spin-up/down Chern numbers $\nu_{\uparrow/\downarrow}$. More precisely, the $\mathbb{Z}_2$ invariant is given by $\nu_S = (\nu_\uparrow - \nu_\downarrow)/2 \mod 2$. The phase diagram as a function of λ_R and λ_v (in units of λ_{SO}) is shown in the top left panel of figure 6.1.

The spin Chern number has a natural counterpart in our construction if we identify the spin-up and spin-down components as the two subsystems with respect to which the ground state is Schmidt decomposed. Let us define the $\uparrow$-spin observables to be

$$\Sigma_\uparrow^x \;=\; a_{\uparrow,\vec{p}}^\dagger b_{\uparrow,\vec{p}} + b_{\uparrow,\vec{p}}^\dagger a_{\uparrow,\vec{p}}, \quad \Sigma_\uparrow^y \;=\; -ia_{\uparrow,\vec{p}}^\dagger b_{\uparrow,\vec{p}} + ib_{\uparrow,\vec{p}}^\dagger a_{\uparrow,\vec{p}}, \quad \Sigma_\uparrow^z \;=\; a_{\uparrow,\vec{p}}^\dagger a_{\uparrow,\vec{p}} - b_{\uparrow,\vec{p}}^\dagger b_{\uparrow,\vec{p}}$$
$$(6.38)$$

and similarly for the $\downarrow$-spin component. By evaluating the ground state expectation values of these operators, one can construct the vectors $S\hat{\vec{s}}_\uparrow(\vec{p})$ and $S\hat{\vec{s}}_\downarrow(\vec{p})$, and thus the subsystem winding numbers $\tilde{\nu}[\text{sgn}(S)\hat{\vec{s}}_{\uparrow/\downarrow}] \equiv \tilde{\nu}_{\uparrow/\downarrow}$. When $\lambda_R = 0$, Z is conserved, and so the subsystems are decoupled with $|S| = 1$. In this case, the winding numbers $\tilde{\nu}_{\uparrow/\downarrow}$ are *bona fide* Chern numbers, and thus $(\tilde{\nu}_\uparrow - \tilde{\nu}_\downarrow)/2 \mod 2$ coincides with ν_S, as expected. In fact, the top right panel of figure 6.1 reveals that even when $\lambda_R \neq 0$ i.e. the subsystems are coupled, the difference of the winding numbers still yields the correct value of ν_S with high precision. The bottom left panel of the same figure shows that the subsystem entanglement measure $|S|$ remains large within the QSH phase, which confirms that the spin components are minimally entangled in this phase. We take this as confirming the reliability of our method for non-maximally entangled states.

The entanglement gap of the spin-up subsystem is shown in the bottom right panel of figure 6.1. Since $\varepsilon_\pm \in [-\infty, \infty]$, the gap is defined to be $\min_{\vec{p}}\zeta_+ - \max_{\vec{p}}\zeta_-$ where $\zeta_\pm \in [0,1]$; from (5.9), if this gap closes, $\min_{\vec{p}}\varepsilon_+ - \max_{\vec{p}}\varepsilon_-$ vanishes as well. It is clear to see that when $|S| = 0$, the gap closes, as expected from section 6.2. An alternative partitioning is to treat the two sublattices as subsystems. It was found in (Legner & Neupert, 2013) that in the QSH phase, the corresponding sublattice ES (the eigenvalues $\zeta_\pm$) covers the entire interval $[0,1]$, although the converse does not hold. Therefore, if using our observables one finds that the sublattice ES does not cover the entire interval $[0,1]$, one can deduce that the system is topologically trivial.

6.3.2 *Example II: A staggered topological superconductor*

The second example we consider is a recently introduced staggered topological superconductor (Pachos *et al.*, 2013) which supports phases with Chern numbers $\nu = 0, \pm 1$ and ± 2. The interest in this model stems from the fact that it is adiabatically connected to Kitaev's celebrated honeycomb model (Kitaev, 2006a). In particular, detection of the $\nu = \pm 2$ phases

---

[63]When the $\mathbb{Z}_2$ invariant is equal to zero (trivial phase), there are an even number of the above-mentioned Kramers pairs, whereas when it is equal to one (non-trivial phase) there are an odd number.
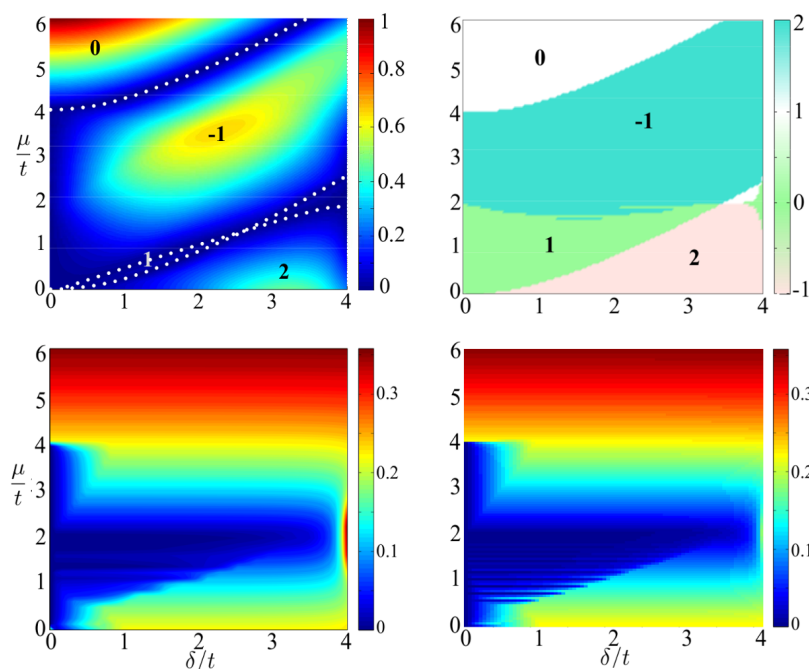
Figure 6.2: *Top left*: The phase diagram of (6.39) in $(\delta/t, \mu/t)$ space computed via the Berry phase (the numbers within the phase diagram are the Chern numbers of the corresponding phase). The colour encodes the magnitude of the spectral gap, while the dashed lines indicate the phase boundaries. *Top right*: The phase diagram computed from the sum of the winding numbers of the *a* and *b* sublattices. *Bottom left*: The sublattice entanglement measure as characterized by $\min_{\vec{p}}|S|$. *Bottom right*: The gap of the ES corresponding to either sublattice. Here, the gap is defined to be $\min_{\vec{p}}|1/2 - \eta_+| = \min_{\vec{p}}|1/2 - \eta_-|$ (see main text for more details). There is good correspondence between $|S| \to 0$ and the gap closing.

– which are known to emerge from the collective interactions of Majorana modes bound to a vortex lattice (Lahtinen *et al.*, 2012) – would provide unambiguous evidence for the existence of Majorana modes.

The model is defined on a square lattice and described by the Hamiltonian

$$\mathcal{H}_{SC} = \sum_j \left[(\mu - \delta)a_j^\dagger a_j + (\mu + \delta)b_j^\dagger b_j + t\left(ia_j^\dagger b_j - ib_j^\dagger a_{j+\hat{x}} + a_j^\dagger a_{j+\hat{y}} + b_j^\dagger b_{j+\hat{y}}\right) \right.$$
$$\left. + \Delta\left(a_j^\dagger b_j^\dagger + b_j^\dagger a_{j+\hat{x}}^\dagger + a_j^\dagger a_{j+\hat{y}}^\dagger + b_j^\dagger b_{j+\hat{y}}^\dagger\right) + \text{H.c.} \right], \tag{6.39}$$

where *j* denotes the positions of the unit cell, which consists of two adjacent (square lattice) sites in the *x*-direction, and $\hat{x}$ and $\hat{y}$ are the primitive lattice translation vectors. The two sites of the unit cell are distinguished by a staggered offset $\pm\delta$ in the chemical potential, and a staggered nearest-neighbour hopping amplitude $\pm it$ in the *x*-direction. These sites can thus be regarded as two sublattice degrees of freedom, at which spinless fermions can be created by the operators $a_j^\dagger$ and $b_j^\dagger$. The fermions are subject to (nearest-neighbour) *s*-wave pairing of strength Δ.

We partition the system into the *a* and *b* sublattices; the relevant operators to evaluate

the corresponding subsystem winding numbers are thus given by (6.29). The phase diagram constructed from the winding numbers is shown in the top right panel of figure 6.2, and in general faithfully reproduces the true phase diagram in the top left panel. Discrepancies between the two occur only in regions where the sublattices are highly entangled, as can be seen from the plot of $\min_{\vec{p}}|S|$ in the bottom left panel of figure 6.2. Thus, as expected from section 6.2, the decomposition breaks down when $|S| \to 0$; results in these regimes should therefore be treated with caution. Nonetheless, we note that the discrepancies in the phase diagrams are only in the sign of ν, which is sufficient to distinguish all distinct types of topological phases up to their chiralities.

In section 5.3, we saw that for an insulator, $\varepsilon_{\pm}$ are determined by the spectrum of the restricted flat band Hamiltonian of the insulator. This holds for superconductors as well, with $\varepsilon_{\pm}$ being determined by the eigenvalues $1/2 - \eta_{\pm}$ of the restricted flat band Bloch Hamiltonian

$$\mathbb{1}/2 - \bar{\mathcal{P}}_i \mathcal{P}(\vec{p}) \bar{\mathcal{P}}_i \,, \tag{6.40}$$

where $\mathcal{P}(\vec{p})$ is the projector onto the two lowest energy bands (with energy $-1/2$) and $\bar{\mathcal{P}}_i$ is the projector onto subsystem i. The exact relationship between the two sets of eigenvalues is not needed for our purposes. We simply note that the particle-hole symmetry of (6.40) implies that $1/2 - \eta_+ = -(1/2 - \eta_-)$ and thus $\varepsilon_+ = -\varepsilon_-$. Entanglement gap closure therefore corresponds to $1/2 - \eta_{\pm} = 0$ and $\varepsilon_{\pm} = 0$. The entanglement gap – defined as $\min_{\vec{p}}|1/2 - \eta_+| = \min_{\vec{p}}|1/2 - \eta_-|$ – for either sublattice is shown in the bottom right panel of figure 6.2. We see that gap closures are in excellent agreement with $|S| \to 0$, as argued in section 6.2, with slight mismatches and discontinuities in the plot of the gap resulting from the coarse-graining of parameter space and the BZ. The significance or otherwise of a gapless component ES for a topological superconductor (beyond indicating maximal subsystem entanglement) is unclear at present.

6.4 Summary and discussion

This chapter has dealt with the problem of measuring the Chern number of topological four-component insulators and superconductors. To solve this problem, we have presented an analytic decomposition of the Chern number into a sum of subsystem winding numbers, which can be measured using single-species observables. To test the veracity of the decomposition, subsystem winding numbers were used to construct the phase diagrams of the QSHI and a staggered superconductor. In both cases, the results agree favourably with the true phase diagrams. Our method is tailored for cold atom experiments, where multiple atomic species and/or internal states are often used to synthesize the pairing terms, spin-orbit couplings and gauge fields required to create topological phases (Béri & Cooper, 2011; Bermudez *et al.*, 2010a,b; Goldman *et al.*, 2010; Kubasiak *et al.*, 2010; Mazza *et al.*, 2012). Being able to separately measure the TOF images of the individual components or species (Alba *et al.*, 2011; Pachos *et al.*, 2013) is sufficient to construct the subsystem

winding numbers, and thus the Chern number.

The accuracy of our method is limited only by the entanglement between the components with respect to which the observables are defined. In the limit of maximal entanglement, BZ discretization errors become significant and thus the winding numbers, despite remaining integers, become unreliable. Fortunately, the observables that are used to construct the winding numbers can also probe the degree of entanglement, and thus assess the reliability of the results. In our case studies, all discrepancies can be explained in terms of high entanglement occurring in the corresponding regions of parameter space. The fact that our decomposition method makes no *a priori* assumptions on the nature of the components – i.e. a decomposition exists for any partition – means that in practice, an experimentalist would have some freedom when using our method. Of course, for 'best' results, one should employ observables associated with components that are as close to being unentangled as possible, if indeed this can be gauged.

With the help of analytics and numerics, we revealed a connection between subsystem entanglement and the translation symmetric component ES (Legner & Neupert, 2013). In particular, we found that entanglement gap closure implies maximal entanglement and vice versa. Indeed, our work provides a rare example of entanglement (spectrum) properties that can be probed experimentally.

Conclusions

In this second part of the thesis, we have presented a method of detecting the Chern number and entanglement properties of 2D topological four-component insulators and superconductors. Our scheme is applicable to cold atom experiments, and is notable for its relative simplicity since it only relies on the standard tool of TOF imaging. In fact, the method is quite general and could conceivably be applied to other experimental setups, such as solid-state experiments or simulations of topological phases (Roushan *et al.*, 2014). The only requirement is that single-species observables should be accessible.

An open question is the generalization of our method to systems with more than four components, a possible direction being to employ a multipartite Schmidt decomposition (Carteret *et al.*, 2000). We note that attempting to prove that the Chern number decomposes for such systems may be a non-trivial task, since employing a general multipartite Schmidt decomposition while respecting symmetries and constraints appears to be an involved affair. Another possible route is to perform convoluted bipartite Schmidt decompositions, although this hardly seems to be any easier. Numerical investigations might be the best bet to see whether a decomposition holds more generally; if so, it would be interesting to see what sort of correlations in the system lead to the method breaking down. Another topic worthy of future study is to see whether other entanglement (spectrum) properties – in particular those related to other types of system partitions (Hsieh & Fu, 2013) – can be accessed through measurements.

It is interesting to speculate whether the method (or generalizations of it) could be applied to extract the invariants and entanglement spectra characterizing three-dimensional topological insulators and superconductors (Bernevig & Hughes, 2013; Qi & Zhang, 2011). Such invariants are determined by integrals over momentum space (as for the Chern number), and it is plausible that the information contained in TOF images may suffice to construct them. Another worthwhile direction of study is to see whether the existence of interacting topological phases can be verified. Hybrid methods such as TOF imaging supplemented with *in situ* measurements (Wang *et al.*, 2013) – or even novel tools – are perhaps needed to attack this problem.

Appendices

APPENDIX A

Some capacitance matrices and their inverses

Here, we collect the (transformed) capacitance matrices and inverses of an array of length two ($\mathcal{C}'_{4\times4}$ and $\mathcal{C}'^{-1}_{4\times4}$), length three ($\mathcal{C}'_{6\times6}$ and $\mathcal{C}'^{-1}_{6\times6}$) and length four ($\mathcal{C}'_{8\times8}$ and $\mathcal{C}'^{-1}_{8\times8}$). Open boundary conditions are assumed for all cases. From these examples, we infer the important features of $\mathcal{C}'^{-1}$ for an arbitrary sized array to approximate (2.1) as (2.7). The important thing to note about the inverses is that, the elements which couple the '$+$' components only fall off arithmetically with distance by a fraction of C_1^{-1}, while those which couple the '$-$' components fall off geometrically with distance by a factor $\mathcal{O}(C_1/C_I)$. Below, $a \equiv C_1{}^2 - 2C_I{}^2$ and $b \equiv C_1{}^4 - 12C_1{}^2C_I{}^2 + 16C_I{}^4$.

A. Some capacitance matrices and their inverses

$$
\mathcal{C}'_{4\times4} \;\approx\;
\begin{pmatrix}
2C_1 & 0 & -C_1 & 0 \\
0 & 2C_I & 0 & -C_1 \\
-C_1 & 0 & 2C_1 & 0 \\
0 & -C_1 & 0 & 2C_I
\end{pmatrix}
\qquad
\mathcal{C}'^{-1}_{4\times4} \;\approx\;
\begin{pmatrix}
\frac{2}{3C_1} & 0 & \frac{1}{3C_1} & 0 \\
0 & -\frac{2C_I}{(C_1{}^2-4C_I{}^2)} & 0 & -\frac{C_1}{(C_1{}^2-4C_I{}^2)} \\
\frac{1}{3C_1} & 0 & \frac{2}{3C_1} & 0 \\
0 & -\frac{C_1}{(C_1{}^2-4C_I{}^2)} & 0 & -\frac{2C_I}{(C_1{}^2-4C_I{}^2)}
\end{pmatrix}
$$

$$
\mathcal{C}'_{6\times6} \;\approx\;
\begin{pmatrix}
2C_1 & 0 & -C_1 & 0 & 0 & 0 \\
0 & 2C_I & 0 & -C_1 & 0 & 0 \\
-C_1 & 0 & 2C_1 & 0 & -C_1 & 0 \\
0 & -C_1 & 0 & 2C_I & 0 & -C_1 \\
0 & 0 & -C_1 & 0 & 2C_1 & 0 \\
0 & 0 & 0 & -C_1 & 0 & 2C_I
\end{pmatrix}
$$

$$
\mathcal{C}'^{-1}_{6\times6} \;\approx\;
\begin{pmatrix}
\frac{3}{4C_1} & 0 & \frac{1}{2C_1} & 0 & \frac{1}{4C_1} & 0 \\
0 & \frac{1}{4C_I}-\frac{C_I}{2a} & 0 & -\frac{C_1}{2a} & 0 & -\frac{C_1{}^2}{4C_I a} \\
\frac{1}{2C_1} & 0 & \frac{1}{C_1} & 0 & \frac{1}{2C_1} & 0 \\
0 & -\frac{C_1}{2a} & 0 & -\frac{C_I}{a} & 0 & -\frac{C_1}{2a} \\
\frac{1}{4C_1} & 0 & \frac{1}{2C_1} & 0 & \frac{3}{4C_1} & 0 \\
0 & -\frac{C_1{}^2}{4C_I a} & 0 & -\frac{C_1}{2a} & 0 & \frac{1}{4C_I}-\frac{C_I}{2a}
\end{pmatrix}
$$

$$
\mathcal{C}'_{8\times8} \;\approx\;
\begin{pmatrix}
2C_1 & 0 & -C_1 & 0 & 0 & 0 & 0 & 0 \\
0 & 2C_I & 0 & -C_1 & 0 & 0 & 0 & 0 \\
-C_1 & 0 & 2C_1 & 0 & -C_1 & 0 & 0 & 0 \\
0 & -C_1 & 0 & 2C_I & 0 & -C_1 & 0 & 0 \\
0 & 0 & -C_1 & 0 & 2C_1 & 0 & -C_1 & 0 \\
0 & 0 & 0 & -C_1 & 0 & 2C_I & 0 & -C_1 \\
0 & 0 & 0 & 0 & -C_1 & 0 & 2C_1 & 0 \\
0 & 0 & 0 & 0 & 0 & -C_1 & 0 & 2C_I
\end{pmatrix}
$$

$$
\mathcal{C}'^{-1}_{8\times8} \;\approx\;
\begin{pmatrix}
\frac{4}{5C_1} & 0 & \frac{3}{5C_1} & 0 & \frac{2}{5C_1} & 0 & \frac{1}{5C_1} & 0 \\
0 & -\frac{4C_I\left(C_1{}^2-2C_I{}^2\right)}{b} & 0 & -\frac{C_1\left(C_1{}^2-4C_I{}^2\right)}{b} & 0 & \frac{2C_1{}^2C_I}{b} & 0 & \frac{C_1{}^3}{b} \\
\frac{3}{5C_1} & 0 & \frac{6}{5C_1} & 0 & \frac{4}{5C_1} & 0 & \frac{2}{5C_1} & 0 \\
0 & -\frac{C_1\left(C_1{}^2-4C_I{}^2\right)}{b} & 0 & -\frac{2C_I\left(C_1{}^2-4C_I{}^2\right)}{b} & 0 & \frac{4C_1C_I{}^2}{b} & 0 & \frac{2C_1{}^2C_I}{b} \\
\frac{2}{5C_1} & 0 & \frac{4}{5C_1} & 0 & \frac{6}{5C_1} & 0 & \frac{3}{5C_1} & 0 \\
0 & \frac{2C_1{}^2C_I}{b} & 0 & \frac{4C_1C_I{}^2}{b} & 0 & -\frac{2C_I\left(C_1{}^2-4C_I{}^2\right)}{b} & 0 & -\frac{C_1\left(C_1{}^2-4C_I{}^2\right)}{b} \\
\frac{1}{5C_1} & 0 & \frac{2}{5C_1} & 0 & \frac{3}{5C_1} & 0 & \frac{4}{5C_1} & 0 \\
0 & \frac{C_1{}^3}{b} & 0 & \frac{2C_1{}^2C_I}{b} & 0 & -\frac{C_1\left(C_1{}^2-4C_I{}^2\right)}{b} & 0 & -\frac{4C_I\left(C_1{}^2-2C_I{}^2\right)}{b}
\end{pmatrix}
$$

$$\tag{A.1}$$

APPENDIX B

Effective Hamiltonians via degenerate perturbation theory

Following the discussion in (Gottfried & Yan, 2003), we give some details on how to derive an effective Hamiltonian via degenerate perturbation theory. We adopt the conventions used by Gottfried and Yan, although the final result is slightly different. Consider a Hamiltonian $\mathcal{H}$ which is the sum of two parts:

$$\mathcal{H} = \mathcal{H}_0 + \lambda \mathcal{H}_1, \tag{B.1}$$

where $\mathcal{H}_0$ is the unperturbed Hamiltonian, which is assumed to have a complete set of known eigenstates and eigenvalues, and $\mathcal{H}_1$ is the perturbation. Even if the perturbation is small, it will have a big effect on unperturbed states that have neighbours with energies close by, which is the case for a degenerate or nearly degenerate spectrum. When this is so, non-degenerate perturbation theory has to be modified, since the eigenstates and eigenvalues calculated with it diverge.

Let us assume that the spectrum of $\mathcal{H}_0$ contains a degenerate or nearly degenerate subspace $\mathfrak{D}$ spanned by $\{|\alpha\rangle\}$. Since the problem is to find the perturbed spectrum in $\mathfrak{D}$, all that needs to be said about the states $\{|\mu\rangle\}$ outside of $\mathfrak{D}$ is that they are 'far away' from $\mathfrak{D}$, in the sense that

$$|\lambda \langle \alpha | \mathcal{H}_1 | \mu \rangle | \ll |E_\alpha - E_\mu|. \tag{B.2}$$

Within $\mathfrak{D}$ there is no such constraint on the matrix elements of the perturbation. The eigenstates $\{|a\rangle\}$ of $\mathcal{H}$ which correspond to $\mathfrak{D}$ satisfy

$$(\mathcal{H} - E_a) |a\rangle = 0, \tag{B.3}$$

and can be expanded as

$$|a\rangle = \sum_\alpha c_\alpha |\alpha\rangle + \sum_\mu d_\mu |\mu\rangle, \tag{B.4}$$

B. Effective Hamiltonians via degenerate perturbation theory

where $\{c_\alpha\}$ are expected to be $\mathcal{O}(1)$, while $\{d_\mu\}$ are expected to be $\mathcal{O}(\lambda)$. Taking the inner product of (B.3) with $|\beta\rangle \in \mathfrak{D}$ and with $|\mu\rangle \notin \mathfrak{D}$ yields the equations

$$c_\beta(E_\beta - E_a) + \lambda \sum_\alpha c_\alpha \langle\beta|\mathcal{H}_1|\alpha\rangle + \lambda \sum_\mu d_\mu \langle\beta|\mathcal{H}_1|\mu\rangle = 0, \tag{B.5}$$

$$d_\mu(E_\mu - E_a) + \lambda \sum_\alpha c_\alpha \langle\mu|\mathcal{H}_1|\alpha\rangle + \lambda \sum_\nu d_\nu \langle\mu|\mathcal{H}_1|\nu\rangle = 0. \tag{B.6}$$

The last term of (B.6) is $\mathcal{O}(\lambda^2)$, and so rearranging this equation for d_μ and plugging into (B.5) gives us

$$c_\beta(E_\beta - E_a) + \sum_\alpha c_\alpha \left(\lambda \langle\beta|\mathcal{H}_1|\alpha\rangle + \lambda^2 \sum_\mu \frac{\langle\beta|\mathcal{H}_1|\mu\rangle \langle\mu|\mathcal{H}_1|\alpha\rangle}{E_a - E_\mu} \right) = 0, \tag{B.7}$$

to second order in λ.

Since $\sum_\alpha c_\alpha \langle\beta|\mathcal{H}_0|\alpha\rangle = c_\beta E_\beta$, the above can be rewritten as

$$\sum_\alpha c_\alpha \underbrace{\left(\langle\beta|\mathcal{H}_0|\alpha\rangle + \lambda \langle\beta|\mathcal{H}_1|\alpha\rangle + \lambda^2 \sum_\mu \frac{\langle\beta|\mathcal{H}_1|\mu\rangle \langle\mu|\mathcal{H}_1|\alpha\rangle}{\bar{E} - E_\mu} \right)}_{\equiv \langle\beta|\mathcal{H}_{\text{eff}}|\alpha\rangle} = c_\beta E_a, \tag{B.8}$$

where $\bar{E}$ is some mean energy in $\mathfrak{D}$, and the error in replacing E_a with $\bar{E}$ is negligible. The motivation for the definition of the effective Hamiltonian $\mathcal{H}_{\text{eff}}$ above is that, (B.8) looks just like an eigenvalue problem restricted to the subspace $\mathfrak{D}$. Since the matrix elements of $\mathcal{H}_{\text{eff}}$ only ever correspond to states in $\mathfrak{D}$, we can define $\mathcal{H}_{\text{eff}}$ to be (setting $\lambda = 1$)

$$\mathcal{H}_{\text{eff}} \equiv \mathcal{P}\mathcal{H}\mathcal{P} + \mathcal{P}\mathcal{H}_1 \frac{1 - \mathcal{P}}{\bar{E} - \mathcal{H}_0} \mathcal{H}_1 \mathcal{P}, \tag{B.9}$$

where $\mathcal{P} = \sum_\alpha |\alpha\rangle\langle\alpha|$ projects onto $\mathfrak{D}$, and $\bar{E}$ should not coincide with any of the eigenvalues in $\mathfrak{D}$. This definition of $\mathcal{H}_{\text{eff}}$ differs from that in (Gottfried & Yan, 2003), in which the first term on the right in (B.9) is $\mathcal{P}\mathcal{H}_1\mathcal{P}$. Our choice seems to be a more natural definition, since as $\mathcal{H}_1 \to 0$, $\mathcal{H}_{\text{eff}} \to \mathcal{P}\mathcal{H}_0\mathcal{P}$ above, whereas Gottfried and Yan's effective Hamiltonian tends to zero.

APPENDIX C

An effective Hamiltonian for Kitaev's current mirror qubit

In this appendix, we derive a low energy effective Hamiltonian for the system analysed by Kitaev. We start by decomposing (2.7) as

$$\mathcal{H}_{\text{KCMQ}} \approx \mathcal{H}_{\text{KCMQ}}^0 + \mathcal{H}_{\text{KCMQ}}^J, \tag{C.1}$$

where

$$\mathcal{H}_{\text{KCMQ}}^0 = \mathcal{O}(E_1) \sum_x n_+(x)^2 + E_I \sum_x n_-(x)^2 + \mathcal{O}(E_1) \sum_{x;y>0} n_+(x) n_+(x+y) \tag{C.2}$$

is the free term and

$$\mathcal{H}_{\text{KCMQ}}^J = -2E_J \sum_x \cos\left[\varphi_+(x+1) - \varphi_+(x)\right] \cos\left[\varphi_-(x+1) - \varphi_-(x)\right] \tag{C.3}$$

is the perturbation. The free part is clearly in a diagonal form, and it has a non-degenerate ground state given by $n_+(x) = n_-(x) = 0 \, \forall x$, while since $E_1 \gg E_I$, its lowest excited states are given by $n_+(x) = 0$, $n_-(x) = 0, \pm 2 \, \forall x$. Since only the low energy dynamics of the system concern us, degenerate perturbation theory allows us to project $\mathcal{H}_{\text{KCMQ}}$ onto the subspace $\mathfrak{D}$, spanned by the ground and lowest excited states, to arrive at an effective Hamiltonian.

Denoting the basis by $\{|n_+(1), n_-(1), n_+(2), n_-(2), \ldots, n_+(L), n_-(L)\rangle\}$ (the length of the array is L and we assume periodic boundary conditions), we can write the ground state as $|\text{gs}\rangle \equiv |0, 0, \ldots, 0, 0\rangle$, and thus form the projector $\mathcal{P}$ onto $\mathfrak{D}$:

$$\mathcal{P} \equiv \underbrace{|\text{gs}\rangle \langle \text{gs}|}_{\mathcal{P}_0} + \sum_{\{n_-(x)\} \equiv n_-(x) = 0, \pm 2} \underbrace{|0, n_-(1), \ldots, 0, n_-(L)\rangle \langle 0, n_-(1), \ldots, 0, n_-(L)|}_{\mathcal{P}_{\{n_-(x)\}}}. \tag{C.4}$$

It is understood that the sum does not contain the term $n_-(x) = 0 \, \forall x$. With this projector,

C. An effective Hamiltonian for Kitaev's current mirror qubit

we can form an effective Hamiltonian using the definition (B.9)

$$\mathcal{H}_{\text{KCMQ}}^{\text{eff}} \equiv \mathcal{P}\mathcal{H}_{\text{KCMQ}}\mathcal{P} + \mathcal{P}\mathcal{H}_{\text{KCMQ}}^{J} \frac{1 - \mathcal{P}}{\bar{E} - \mathcal{H}_{\text{KCMQ}}^{0}} \mathcal{H}_{\text{KCMQ}}^{J}\mathcal{P}, \tag{C.5}$$

where $\bar{E}$ is the mean energy of $\mathfrak{D}$ and is very small compared to E_1. The tunnelling perturbation can be written in terms of charge raising (lowering) operators $b_j^{\dagger}(x)$ ($b_j(x)$) – where $j \in \{+, -\}$ – by defining

$$\underbrace{e^{i\varphi_j(x)}}_{b_j(x)} |\ldots, n_j(x), \ldots\rangle = |\ldots, n_j(x) - 1, \ldots\rangle, \tag{C.6}$$

$$\underbrace{e^{-i\varphi_j(x)}}_{b_j^{\dagger}(x)} |\ldots, n_j(x), \ldots\rangle = |\ldots, n_j(x) + 1, \ldots\rangle. \tag{C.7}$$

Since $\cos\left[\varphi_j(x+1) - \varphi_j(x)\right] = \frac{1}{2}\left(e^{i\varphi_j(x+1)}e^{-i\varphi_j(x)} + e^{-i\varphi_j(x+1)}e^{i\varphi_j(x)}\right)$, (C.3) becomes

$$\mathcal{H}_{\text{KCMQ}}^{J} = -\frac{E_J}{2} \sum_x b_+(x+1)b_+^{\dagger}(x) \left(b_-(x+1)b_-^{\dagger}(x) + \text{H.c.}\right) + \text{H.c.}. \tag{C.8}$$

The first term to be examined in (C.5) is $\mathcal{P}\mathcal{H}_{\text{KCMQ}}^{0}\mathcal{P}$, and inspection reveals this to be

$$\mathcal{P}\mathcal{H}_{\text{KCMQ}}^{0}\mathcal{P} = E_I \sum_{\{n_-(x)\}} \left(\sum_x n_-(x)^2\right) \mathcal{P}_{\{n_-(x)\}}. \tag{C.9}$$

This term simply measures the energy of the system in the absence of a tunnelling perturbation. $\mathcal{P}\mathcal{H}_{\text{KCMQ}}^{J}\mathcal{P}$ is next on the list to look at, and applying the perturbation on the ground state gives

$$\mathcal{H}_{\text{KCMQ}}^{J}|\text{gs}\rangle \propto \sum_x |\ldots, n_+(x) = -1, n_-(x) = 1, 1, -1, \ldots\rangle + |\ldots, -1, -1, 1, 1, \ldots\rangle$$
$$+ |\ldots, 1, 1, -1, -1, \ldots\rangle + |\ldots, 1, -1, -1, 1, \ldots\rangle, \tag{C.10}$$

where $\ldots$ refers to $0, 0, \ldots, 0$. $\mathcal{P}_0\mathcal{H}_{\text{KCMQ}}^{J}|\text{gs}\rangle$ and $\mathcal{P}_{\{n_-(x)\}}\mathcal{H}_{\text{KCMQ}}^{J}|\text{gs}\rangle$ clearly vanish, and similar analysis of $\mathcal{P}\mathcal{H}_{\text{KCMQ}}^{J}\sum_{\{n_-(x)\}}\mathcal{P}_{\{n_-(x)\}}$ shows that it vanishes as well, which means that

$$\mathcal{P}\mathcal{H}_{\text{KCMQ}}^{J}\mathcal{P} = 0. \tag{C.11}$$

Since (C.11) vanishes, the second order term in (C.5) simplifies to

$$\mathcal{P}\mathcal{H}_{\text{KCMQ}}^{J} \frac{1 - \mathcal{P}}{\bar{E} - \mathcal{H}_{\text{KCMQ}}^{0}} \mathcal{H}_{\text{KCMQ}}^{J}\mathcal{P} = \mathcal{P}\mathcal{H}_{\text{KCMQ}}^{J}(\bar{E} - \mathcal{H}_{\text{KCMQ}}^{0})^{-1}\mathcal{H}_{\text{KCMQ}}^{J}\mathcal{P}. \tag{C.12}$$

Writing $\sum_x \mathcal{O}(E_1) n_+(x)^2 + E_I n_-(x)^2$ as

$$\sum_{\{n_j(x)\}} \left(\sum_{j,x} k_j n_j(x)^2 \right) \underbrace{|n_+(1), n_-(1), \ldots, n_+(L), n_-(L)\rangle \langle n_+(1), n_-(1), \ldots, n_+(L), n_-(L)|}_{\mathfrak{Q}_{\{n_j(x)\}}},$$

(C.13)

where $k_+ \equiv \mathcal{O}(E_1)$ and $k_- \equiv E_I$, and $\mathcal{O}(E_1) \sum_{x;y>0} n_+(x) n_+(x+y)$ as

$$\sum_{\{n_j(x)\}} \left(\mathcal{O}(E_1) \sum_{x;y>0} n_+(x) n_+(x+y) \right) \mathfrak{Q}_{\{n_j(x)\}},$$

(C.14)

one can see that

$$(\bar{E} - \mathcal{H}_{\text{KCMQ}}^0)^{-1} = \sum_{\{n_j(x)\}} \left(\bar{E} - \sum_{j,x} k_j n_j(x)^2 - \mathcal{O}(E_1) \sum_{x;y>0} n_+(x) n_+(x+y) \right)^{-1} \mathfrak{Q}_{\{n_j(x)\}}.$$

(C.15)

In the above, the inverse exists as long as we do not encounter 0^{-1}; we can always tweak $\bar{E}$ to ensure that this is so.

To determine $\mathcal{P} \mathcal{H}_{\text{KCMQ}}^J (\bar{E} - \mathcal{H}_{\text{KCMQ}}^0)^{-1} \mathcal{H}_{\text{KCMQ}}^J \mathcal{P}$ we work our way from right to left. $\mathcal{H}_{\text{KCMQ}}^J \mathcal{P}_0$ has already been worked out in (C.10), while $\mathcal{H}_{\text{KCMQ}}^J \sum_{\{n_-(x)\}} \mathcal{P}_{\{n_-(x)\}}$ is given by

$$\mathcal{H}_{\text{KCMQ}}^J \sum_{\{n_-(x)\}} \mathcal{P}_{\{n_-(x)\}} = -\frac{E_J}{2} \sum_{\{n_-(x)\}} \sum_x \left(|\ldots, 1, n_-(x)+1, -1, n_-(x+1)-1, \ldots\rangle \right.$$
$$+ |\ldots, 1, n_-(x)-1, -1, n_-(x+1)+1, \ldots\rangle + |\ldots, -1, n_-(x)-1, 1, n_-(x+1)+1, \ldots\rangle$$
$$\left. + |\ldots, -1, n_-(x)+1, 1, n_-(x+1)-1, \ldots\rangle \right) \langle \{n_-(x)\}|,$$

(C.16)

where the meaning of $\ldots$ should be self-explanatory. Before we examine the effect of $(\bar{E} - \mathcal{H}_{\text{KCMQ}}^0)^{-1}$ acting on these two terms, we introduce the following notation to keep things as uncluttered as possible:

$$|\{n_j(x)\}\rangle' \equiv (\bar{E} - \mathcal{H}_{\text{KCMQ}}^0)^{-1} |\{n_j(x)\}\rangle$$
$$= \left(\bar{E} - \sum_{j,x} k_j n_j(x)^2 - \mathcal{O}(E_1) \sum_{x;y>0} n_+(x) n_+(x+y) \right)^{-1} |\{n_j(x)\}\rangle.$$

Thus,

$$(\bar{E} - \mathcal{H}_{\text{KCMQ}}^0)^{-1} \mathcal{H}_{\text{KCMQ}}^J \mathcal{P}_0 = -\frac{E_J}{2} \sum_x \left(|\ldots, n_+(x) = -1, n_-(x) = 1, 1, -1, \ldots\rangle' \right.$$
$$+ |\ldots, -1, -1, 1, 1, \ldots\rangle' + |\ldots, 1, 1, -1, -1, \ldots\rangle' + |\ldots, 1, -1, -1, 1, \ldots\rangle' \right) \langle \text{gs}|, \quad \text{(C.17)}$$

C. An effective Hamiltonian for Kitaev's current mirror qubit

and

$$(\bar{E} - \mathcal{H}^0_{\text{KCMQ}})^{-1} \mathcal{H}^J_{\text{KCMQ}} \sum_{\{n_-(x)\}} \mathcal{P}_{\{n_-(x)\}} =$$

$$-\frac{E_J}{2} \sum_{\{n_-(x)\}} \sum_x \big(|\ldots, 1, n_-(x)+1, -1, n_-(x+1)-1, \ldots\rangle'$$

$$+ |\ldots, 1, n_-(x)-1, -1, n_-(x+1)+1, \ldots\rangle' + |\ldots, -1, n_-(x)-1, 1, n_-(x+1)+1, \ldots\rangle'$$

$$+ |\ldots, -1, n_-(x)+1, 1, n_-(x+1)-1, \ldots\rangle' \big) \langle \{n_-(x)\}| \, . \tag{C.18}$$

One should keep in mind that '…' refers to different things in equations (C.17) and (C.18).

$\mathcal{P}\mathcal{H}^J_{\text{KCMQ}}$ has already been worked out since it is equal to $\left(\mathcal{H}^J_{\text{KCMQ}}\mathcal{P}\right)^\dagger$, and multiplying $\mathcal{P}_0 \mathcal{H}^J_{\text{KCMQ}}$ with (C.17) yields

$$\mathcal{P}_0 \mathcal{H}^J_{\text{KCMQ}} (\bar{E} - \mathcal{H}^0_{\text{KCMQ}})^{-1} \mathcal{H}^J_{\text{KCMQ}} \mathcal{P}_0 = \frac{E_J^2}{4} 4L \left(\bar{E} - \mathcal{O}(E_1) - 2E_I\right)^{-1} \mathcal{P}_0$$

$$\sim -L \frac{E_J^2}{E_1} \mathcal{P}_0 \, , \tag{C.19}$$

where the factor of $4L$ arises since at each position x only four overlaps survive, and there are L instances of this (we also use $(\bar{E} - \mathcal{O}(E_1) - 2E_I)^{-1} \sim -E_1^{-1}$). Next, we look at the action of $\mathcal{P}_0 \mathcal{H}^J_{\text{KCMQ}}$ on (C.18). If we focus on $\langle \ldots, n_+(x) = 1, n_-(x) = 1, -1, -1, \ldots|$ first, we see that its overlap with $|\ldots, 1, n_-(x)+1, -1, n_-(x+1)-1, \ldots\rangle'$ cannot survive since the configuration $n_-(x) = 0 \, \forall x$ was excluded from the sum over $\{n_-(x)\}$. On the other hand, its overlap with $|\ldots, 1, n_-(x)-1, -1, n_-(x+1)+1, \ldots\rangle'$ is finite if $n_-(x) = -n_-(x+1) = 2$ with all other $n_-(x)$ being zero. Since all other overlaps with $\langle \ldots, n_+(x) = 1, n_-(x) = 1, -1, -1, \ldots|$ vanish, we see that it contributes

$$(\bar{E} - \mathcal{O}(E_1) - 2E_I)^{-1} \frac{E_J^2}{4} |\text{gs}\rangle \sum_x \langle 0, 0, \ldots, 0, n_-(x) = 2, 0, n_-(x+1) = -2, \ldots, 0, 0| \, .$$

Similar analysis of the other terms shows that

$$\mathcal{P}_0 \mathcal{H}^J_{\text{KCMQ}} (\bar{E} - \mathcal{H}^0_{\text{KCMQ}})^{-1} \mathcal{H}^J_{\text{KCMQ}} \sum_{\{n_-(x)\}} \mathcal{P}_{\{n_-(x)\}}$$

$$\sim -\frac{E_J^2}{2E_1} |\text{gs}\rangle \sum_x \langle 0, 0, \ldots, 0, n_-(x) = 2, 0, -2, \ldots, 0, 0| + \langle 0, 0, \ldots, 0, n_-(x) = -2, 0, 2, \ldots, 0, 0| \, . \tag{C.20}$$

$n_+(x) = 0, n_-(x) = \pm 2$ correspond to neutral excitations which we will call excitons. They consist of an excess Cooper-pair at one island and a deficit of a Cooper-pair at the other island at the same position x. (C.20) thus describes the 'annihilation' of an exciton with an adjacent 'exciton-hole' to produce the 'vacuum' (i.e. the ground state). $\sum_{\{n_-(x)\}} \mathcal{P}_{\{n_-(x)\}} \mathcal{H}^J_{\text{KCMQ}}$ multiplied with (C.17) gives the inverse of the process just described, namely, the creation
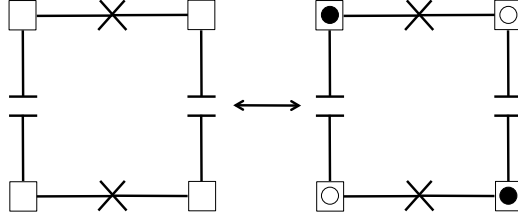
Figure C.1: A picture showing the effect of (C.20) and (C.21). An unfilled square represents a neutral island, a filled circle represents an excess Cooper-pair while an unfilled circle depicts the deficit of a Cooper-pair.

of an exciton and exciton-hole pair from the vacuum:

$$\sum_{\{n_-(x)\}} \mathcal{P}_{\{n_-(x)\}} \mathcal{H}_{\text{KCMQ}}^J (\bar{E} - \mathcal{H}_{\text{KCMQ}}^0)^{-1} \mathcal{H}_{\text{KCMQ}}^J \mathcal{P}_0 \sim$$

$$-\frac{E_J^2}{2E_1} \sum_x \left(|0,0,\ldots,0,n_-(x) = 2,0,-2,\ldots,0,0\rangle + |0,0,\ldots,0,n_-(x) = -2,0,2,\ldots,0,0\rangle \right) \langle \text{gs}| \, .$$

(C.21)

The processes described by (C.20) and (C.21) are shown in figure C.1.

Finally, we look at $\sum_{\{n_-(x)\}} \mathcal{P}_{\{n_-(x)\}} \mathcal{H}_{\text{KCMQ}}^J$ acting on (C.18). The overlap between $\langle \ldots, 1, n_-(x)+1, -1, n_-(x+1)-1, \ldots |$ and $|\ldots, 1, n_-(x)+1, -1, n_-(x+1)-1, \ldots\rangle'$ yields

$$\frac{E_J^2}{4} \underbrace{\left(\bar{E} - \mathcal{O}(E_1) - E_I \left[(n_-(x)+1)^2 + (n_-(x+1)-1)^2 + \sum_{y \neq x,x+1} n_-(y)^2 \right] \right)^{-1}}_{\sim -E_1^{-1}} \mathcal{P}_{\{n_-(x)\}},$$

where we are assuming that $E_I \left[(n_-(x)+1)^2 + (n_-(x+1)-1)^2 + \sum_{y \neq x,x+1} n_-(y)^2 \right]$ is negligible in comparison to E_1. There are L instances of the above, corresponding to the L different positions where $n_+ = 1$. The same analysis with the terms $\langle \ldots, 1, n_-(x)-1, -1, n_-(x+1)+1, \ldots |$, $\langle \ldots, -1, n_-(x)+1, 1, n_-(x+1)-1, \ldots |$ and $\langle \ldots, -1, n_-(x)-1, 1, n_-(x+1)+1, \ldots |$ leads to the same outcome as described above (i.e. along with the factor of L there is also a factor of 4 as well), and so these contributions result in the term

$$-L \frac{E_J^2}{E_1} \sum_{\{n_-(x)\}} \mathcal{P}_{\{n_-(x)\}} \, .$$

(C.22)

The above and the scaled ground state projector (C.19) result in a multiple of the identity operator on the subspace $\mathfrak{D}$ (i.e. it is an energy constant in the effective Hamiltonian), which we can ignore.

The other terms that arise from $\sum_{\{n_-(x)\}} \mathcal{P}_{\{n_-(x)\}} \mathcal{H}_{\text{KCMQ}}^J$ acting on (C.18) represent the propagation of excitons and exciton-holes, as well as the creation and annihilation of exciton and exciton-hole pairs. Since it would be lengthy to show explicitly how all these terms arise, just the result will be quoted. Along with the terms in equations (C.20) and (C.21),

C. An effective Hamiltonian for Kitaev's current mirror qubit

the net result is an exciton tunnelling term

$$-\frac{E_J^2}{2E_1}\sum_x b_-(x+1)^2 b_-^\dagger(x)^2 + \text{H.c.} = -\frac{E_J^2}{2E_1}\sum_x e^{i2\varphi_-(x+1)} e^{-i2\varphi_-(x)} + \text{H.c.}$$

$$= -E_J^{\text{ex}}\sum_x \cos\left[2\varphi_-(x+1) - 2\varphi_-(x)\right], \tag{C.23}$$

where the Josephson energy for excitons is defined as $E_J^{\text{ex}} \equiv E_J^2/E_1$. Putting this together with $\mathcal{P}\mathcal{H}_{\text{KCMQ}}^0\mathcal{P}$ (equation (C.9)) which we write as $E_I\sum_x n_-(x)^2$, and making the change of variables $\varphi_-'(x) \equiv 2\varphi_-(x)$ and $n_-'(x) \equiv n_-(x)/2$ (so that $[\varphi_-'(x), n_-'(y)] = i\delta_{xy}$), we finally end up with the effective Hamiltonian

$$\mathcal{H}_{\text{KCMQ}}^{\text{eff}} = 4E_I\sum_x n_-'(x)^2 - E_J^{\text{ex}}\sum_x \cos\left[\varphi_-'(x+1) - \varphi_-'(x)\right]. \tag{C.24}$$

$\mathcal{H}_{\text{KCMQ}}^{\text{eff}}$ describes a chain of Josephson junctions with excitons as the tunnelling objects. The junctions have a charging and Josephson energy of $4E_I$ and E_J^{ex}, respectively, while $\varphi_-'(x)$ and $n_-'(x)$ are the phase of the macroscopic exciton wave function and the number of excitons at position x, respectively.

APPENDIX D

The Villain approximation

The Villain approximation (José *et al.*, 1977; Villain, 1975) is a transparent means of seeing the existence of vortices in the 2D XY model. Here, we follow the derivation in (Herbut, 2007). Let us take the spins (or phases) $\{\vec{s}_i = (\cos\phi_i, \sin\phi_i)\}$ of the model to reside on the sites $\{i\}$ of a 2D square lattice. Each phase is ferromagnetically coupled to its nearest neighbours through a term $-J\vec{s}_i \cdot \vec{s}_j = -J\cos(\phi_i - \phi_j)$, where $J > 0$. The system's partition function is thus ($k = 1$)

$$\mathcal{Z}_{\text{XY}} = \prod_i \int_0^{2\pi} \frac{d\phi_i}{2\pi} \exp\left(\frac{J}{T} \sum_{i,\mu} \cos(\phi_{i+\hat{\mu}} - \phi_i) \right), \tag{D.1}$$

where $\hat{\mu} = \hat{x}, \hat{y}$ are the two lattice unit vectors. In the Villain approximation, $\mathcal{Z}_{\text{XY}}$ is approximated by [64]

$$\mathcal{Z}_{\text{XY}} \approx \mathcal{Z}_{\text{V}} = \prod_i \int_0^{2\pi} \frac{d\phi_i}{2\pi} \prod_{i,\mu} \sum_{m_i^\mu = -\infty}^{\infty} \exp\left(-\frac{J}{2T} \sum_{i,\mu} (\phi_{i+\hat{\mu}} - \phi_i - 2\pi m_i^\mu)^2 \right), \tag{D.2}$$

where the integer-valued variables m_i^μ are associated with each link connecting the sites i and $i + \hat{\mu}$. The motivation for this approximation is that the phases can be integrated out without sacrificing their 2π periodicity, due to the summation over integers. (D.2) can be rewritten, by making use of the Gaussian integral identity

$$\int_{-\infty}^{\infty} dx \, e^{-\frac{a}{2}x^2 + zx} = \sqrt{\frac{2\pi}{a}} \exp\left(\frac{z^2}{2a} \right), \tag{D.3}$$

---

[64]In general, J/T in (D.2) should be replaced with $f(J/T)$ (Fazio & Van der Zant, 2001; José *et al.*, 1977), but the stated form is a good approximation for low temperatures.

D. The Villain approximation

which holds for $a > 0$ and arbitrary z. Identifying $a \equiv T/J$ and $z \equiv -i(\phi_{i+\hat{\mu}} - \phi_i - 2\pi m_i^{\mu})$, we see that

$$
\mathcal{Z}_V = \prod_i \int_0^{2\pi} \frac{d\phi_i}{2\pi} \prod_{i,\mu} \sum_{m_i^{\mu}=-\infty}^{\infty} \int_{-\infty}^{\infty} dx_i^{\mu} \exp\left(-\frac{T}{2J} \sum_{i,\mu} (x_i^{\mu})^2 - i \sum_{i,\mu} (\phi_{i+\hat{\mu}} - \phi_i - 2\pi m_i^{\mu}) x_i^{\mu} \right),
$$
(D.4)

up to constants, and after employing the Poisson resummation formula

$$
\sum_{m_i^{\mu}=-\infty}^{\infty} \exp\left(i2\pi m_i^{\mu} x_i^{\mu} \right) = \sum_{n_i^{\mu}=-\infty}^{\infty} \delta(x_i^{\mu} - n_i^{\mu}),
$$
(D.5)

we arrive at

$$
\mathcal{Z}_V = \prod_i \int_0^{2\pi} \frac{d\phi_i}{2\pi} \prod_{i,\mu} \sum_{n_i^{\mu}=-\infty}^{\infty} \exp\left(-\frac{T}{2J} \sum_{i,\mu} (n_i^{\mu})^2 - i \sum_{i,\mu} n_i^{\mu} (\phi_{i+\hat{\mu}} - \phi_i) \right).
$$
(D.6)

The phase integrals can now be performed, which leads to the (finite difference) divergenceless condition for each vector field $\vec{n}_i = (n_i^x, n_i^y)$, namely $\vec{\nabla} \cdot \vec{n}_i = n_i^x - n_{i-\hat{x}}^x + n_i^y - n_{i-\hat{y}}^y = 0$. These conditions can be solved by introducing variables that reside on the dual lattice, which consists of the set of points at the centres of the elementary squares of the original lattice. Some further manipulations lead to the emergence of vortex degrees of freedom, in much the same way that they emerge in section 3.2.

Winding number representation of the Chern number for two-component systems

The ground state, $|\chi_{\vec{p}}\rangle$, of a 2D Bloch Hamiltonian such as $h_2(\vec{p})$ in (5.11) can be represented by a normalized Bloch vector, $\hat{\vec{s}}_{\vec{p}}$, which lies on the Bloch sphere. As a result, the projector onto $|\chi_{\vec{p}}\rangle$ can be written as

$$\mathcal{P}_{\vec{p}} = |\chi_{\vec{p}}\rangle\langle\chi_{\vec{p}}| = \frac{1}{2}\left(I + \hat{\vec{s}}_{\vec{p}} \cdot \vec{\sigma}\right), \tag{E.1}$$

where I is the 2D identity matrix and $\vec{\sigma} = (X, Y, Z)$ is the vector of Pauli matrices, since $\hat{\vec{s}}_{\vec{p}} \cdot \vec{\sigma} |\chi_{\vec{p}}\rangle = |\chi_{\vec{p}}\rangle$. Substituting this representation of the projector into the expression for ν, (5.1), and employing the identities

$$(\vec{a} \cdot \vec{\sigma})(\vec{b} \cdot \vec{\sigma}) = \vec{a} \cdot \vec{b} I + i\left(\vec{a} \times \vec{b}\right) \cdot \vec{\sigma}, \tag{E.2}$$

for two three-vectors $\vec{a}$ and $\vec{b}$, and

$$\mathrm{tr}\left(\sigma^{\alpha}\sigma^{\beta}\right) = 2\delta^{\alpha\beta}, \qquad \alpha, \beta = 1, 2, 3, \tag{E.3}$$

we obtain

$$\begin{aligned}
\nu &= -\frac{i}{2\pi}\int_{\mathrm{BZ}} d^2p \, \mathrm{tr}\left(\mathcal{P}_{\vec{p}}\left[\partial_{p_x}\mathcal{P}_{\vec{p}}, \partial_{p_y}\mathcal{P}_{\vec{p}}\right]\right) \\
&= -\frac{i}{16\pi}\int_{\mathrm{BZ}} d^2p \, \mathrm{tr}\left(\left[I + \hat{\vec{s}}_{\vec{p}} \cdot \vec{\sigma}\right]\left[\partial_{p_x}\hat{\vec{s}}_{\vec{p}} \cdot \vec{\sigma}, \partial_{p_y}\hat{\vec{s}}_{\vec{p}} \cdot \vec{\sigma}\right]\right) \\
&= \frac{1}{4\pi}\int_{\mathrm{BZ}} d^2p \, \hat{\vec{s}}_{\vec{p}} \cdot \left(\partial_{p_x}\hat{\vec{s}}_{\vec{p}} \times \partial_{p_y}\hat{\vec{s}}_{\vec{p}}\right) \\
&\equiv \tilde{\nu}[\hat{\vec{s}}_{\vec{p}}].
\end{aligned} \tag{E.4}$$

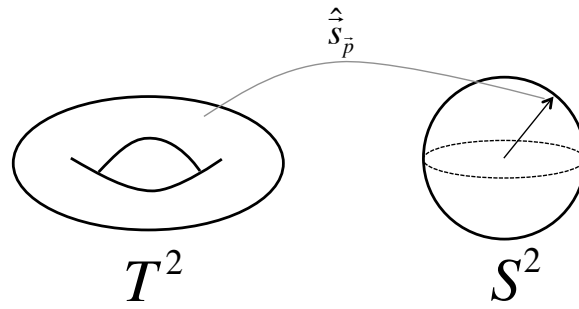**E. Winding number representation of the Chern number for two-component systems**

Figure E.1: The winding number (E.4) is equal to the number of times the map $\hat{\vec{s}}_{\vec{p}} : T^2 \to S^2$ covers the unit 2-sphere as the BZ is spanned.

Since $\hat{\vec{s}}_{\vec{p}} : T^2 \to S^2$ is a map from the toroidal BZ to the unit 2-sphere, as shown in figure E.1, the Chern number for two-component systems can be thought of as a *winding number*, which we denote as $\tilde{v}[\hat{\vec{s}}_{\vec{p}}]$. The winding number counts the number of times $\hat{\vec{s}}_{\vec{p}}$ winds around or covers S^2 as the BZ is spanned.

References

ABANIN, D.A. & DEMLER, E. (2012). Measuring entanglement entropy of a generic many-body system with a quantum switch. *Physical review letters*, **109**, 020504. 67

ABANIN, D.A., KITAGAWA, T., BLOCH, I. & DEMLER, E. (2013). Interferometric approach to measuring band topology in 2d optical lattices. *Phys. Rev. Lett.*, **110**, 165304. 67

AHARONOV, Y. & BOHM, D. (1959). Significance of electromagnetic potentials in the quantum theory. *Physical Review*, **115**, 485. 49

AHARONOV, Y. & CASHER, A. (1984). Topological quantum effects for neutral particles. *Physical Review Letters*, **53**, 319–321. 49

AIDELSBURGER, M., ATALA, M., LOHSE, M., BARREIRO, J., PAREDES, B. & BLOCH, I. (2013). Realization of the hofstadter hamiltonian with ultracold atoms in optical lattices. *Physical review letters*, **111**, 185301. 66

ALBA, E., FERNANDEZ-GONZALVO, X., MUR-PETIT, J., PACHOS, J.K. & GARCIA-RIPOLL, J.J. (2011). Seeing topological order in time-of-flight measurements. *Phys. Rev. Lett.*, **107**, 235301. 2, 66, 72, 73, 74, 88

ALICEA, J. (2012). New directions in the pursuit of majorana fermions in solid state systems. *Reports on Progress in Physics*, **75**, 076501. 66

AMICO, L., FAZIO, R., OSTERLOH, A. & VEDRAL, V. (2008). Entanglement in many-body systems. *Reviews of Modern Physics*, **80**, 517. 5

ANDERSON, P.W. (1984). *Basic notions of condensed matter physics*, vol. 55. Benjamin/Cummings Publishing Company, Advanced Book Program. 65

ANNETT, J.F. (2004). *Superconductivity, superfluids, and condensates*, vol. 67. Oxford University Press Oxford. 6, 73

ANNETT, J.F., GYORFFY, B.L. & SPILLER, T.P. (2002). Superconducting devices for quantum computation. In *Exotic States in Quantum Nanostructures*, 165–212, Springer. 15

ATALA, M., AIDELSBURGER, M., BARREIRO, J.T., ABANIN, D., KITAGAWA, T., DEMLER, E. & BLOCH, I. (2013). Direct measurement of the zak phase in topological bloch bands. *Nature Physics*, **9**, 795–800. 66

AVRON, J., SEILER, R. & SIMON, B. (1983). Homotopy and quantization in condensed matter physics. *Physical review letters*, **51**, 51. 67

AVRON, J., SADUN, L., SEGERT, J. & SIMON, B. (1988). Topological invariants in fermi systems with time-reversal invariance. *Physical review letters*, **61**, 1329. 85

AVRON, J.E., OSADCHY, D. & SEILER, R. (2003). A topological look at the quantum hall effect. *Physics Today*, **56**, 38–42. 65

BARDEEN, J., COOPER, L.N. & SCHRIEFFER, J.R. (1957). Theory of superconductivity. *Physical Review*, **108**, 1175. 9

BARENDS, R., KELLY, J., MEGRANT, A., VEITIA, A., SANK, D., JEFFREY, E., WHITE, T., MUTUS, J., FOWLER, A., CAMPBELL, B. *et al.* (2014). Superconducting quantum circuits at the surface code threshold for fault tolerance. *Nature*, **508**, 500–503. 18

BELL, M.T., PARAMANANDAM, J., IOFFE, L.B. & GERSHENSON, M.E. (2014). Protected josephson rhombus chains. *Physical review letters*, **112**, 167001. 18

BENNETT, C.H., BRASSARD, G. *et al.* (1984). Quantum cryptography: Public key distribution and coin tossing. In *Proceedings of IEEE International Conference on Computers, Systems and Signal Processing*, vol. 175, New York. 5

BEREZINSKII, V. (1971). Destruction of long-range order in one-dimensional and two-dimensional systems having a continuous symmetry group i. classical systems. *Sov. Phys. JETP*, **32**, 493–500. 30

BÉRI, B. & COOPER, N. (2011). Z 2 topological insulators in ultracold atomic gases. *Physical review letters*, **107**, 145301. 88

BERMUDEZ, A., GOLDMAN, N., KUBASIAK, A., LEWENSTEIN, M. & MARTIN-DELGADO, M.A. (2010a). Topological phase transitions in the non-abelian honeycomb lattice. *New J. Phys.*, **12**, 033041. 88

BERMUDEZ, A., MAZZA, L., RIZZI, M., GOLDMAN, N., LEWENSTEIN, M. & MARTIN-DELGADO, M.A. (2010b). Wilson fermions and axion electrodynamics in optical lattices. *Phys. Rev. Lett.*, **105**, 190404. 88

BERNEVIG, B.A. & HUGHES, T.L. (2013). *Topological Insulators and Topological Superconductors*. Princeton University Press, Oxford. 65, 66, 67, 68, 72, 73, 74, 90

BLAIS, A., HUANG, R.S., WALLRAFF, A., GIRVIN, S. & SCHOELKOPF, R.J. (2004). Cavity quantum electrodynamics for superconducting electrical circuits: An architecture for quantum computation. *Physical Review A*, **69**, 062320. 12

BOUCHIAT, V., VION, D., JOYEZ, P., ESTEVE, D. & DEVORET, M. (1998). Quantum coherence with a single cooper pair. *Physica Scripta*, **1998**, 165. 12

BRAVYI, S. & KITAEV, A. (2005). Universal quantum computation with ideal clifford gates and noisy ancillas. *Physical Review A*, **71**, 022316. 48

BROOKS, P., KITAEV, A. & PRESKILL, J. (2013). Protected gates for superconducting qubits. *Physical Review A*, **87**, 052306. 26, 48, 49, 52, 53, 57, 58, 59

BÜTTIKER, M. (1987). Zero-current persistent potential drop across small-capacitance josephson junctions. *Physical Review B*, **36**, 3548. 12

CAMINO, F., ZHOU, W. & GOLDMAN, V. (2005). Realization of a laughlin quasiparticle interferometer: observation of fractional statistics. *Physical Review B*, **72**, 075342. 21

CARTERET, H., HIGUCHI, A. & SUDBERY, A. (2000). Multipartite generalization of the schmidt decomposition. *Journal of Mathematical Physics*, **41**, 7932–7939. 90

CHIORESCU, I., NAKAMURA, Y., HARMANS, C.M. & MOOIJ, J. (2003). Coherent quantum dynamics of a superconducting flux qubit. *Science*, **299**, 1869–1871. 12, 17, 18

CHOI, M. (1994). Quantum hall effect in ideal superconducting arrays at zero temperature. *Physical Review B*, **50**, 10088. 39

CHOI, M.S., CHOI, M., CHOI, T. & LEE, S.I. (1998). Cotunneling transport and quantum phase transitions in coupled josephson-junction chains with charge frustration. *Physical review letters*, **81**, 4240. 21, 22, 42

CLARKE, J. & WILHELM, F.K. (2008). Superconducting quantum bits. *Nature*, **453**, 1031–1042. 6, 12, 27

CSERTI, J. (2000). Application of the lattice greens function for calculating the resistance of an infinite network of resistors. *American Journal of Physics*, **68**, 896–906. 36

DAS, A., RONEN, Y., MOST, Y., OREG, Y., HEIBLUM, M. & SHTRIKMAN, H. (2012). Zero-bias peaks and splitting in an al-inas nanowire topological superconductor as a signature of majorana fermions. *Nature Physics*, **8**, 887–895. 66

DAUPHIN, A. & GOLDMAN, N. (2013). Extracting the chern number from the dynamics of a fermi gas: Implementing a quantum hall bar for cold atoms. *Phys. Rev. Lett.*, **111**, 135302. 67

DE, S. & SPILLER, T. (2014). A protected vortex exciton qubit. *arXiv preprint arXiv:1405.4446*. i, 1, 2, 29, 48

DE LISLE, J., DE, S., ALBA, E., BULLIVANT, A., GARCIA-RIPOLL, J.J., LAHTINEN, V. & PACHOS, J.K. (2014). Detection of chern numbers and entanglement in topological two-species systems through subsystem winding numbers. *New Journal of Physics*, **16**, 083022. i, 2, 75

DEMPSTER, J., FU, B., FERGUSON, D.G., SCHUSTER, D. & KOCH, J. (2014). Understanding degenerate ground states of a protected quantum circuit in the presence of disorder. *arXiv preprint arXiv:1402.7310*. 26, 45, 61

DENG, M., YU, C., HUANG, G., LARSSON, M., CAROFF, P. & XU, H. (2012). Anomalous zero-bias conductance peak in a nb–insb nanowire–nb hybrid device. *Nano letters*, **12**, 6414–6419. 66

DEUTSCH, D. (1985). Quantum theory, the church-turing principle and the universal quantum computer. *Proceedings of the Royal Society of London. A. Mathematical and Physical Sciences*, **400**, 97–117. 5

DEVORET, M. & SCHOELKOPF, R. (2013). Superconducting circuits for quantum information: an outlook. *Science*, **339**, 1169–1174. 6

DIVINCENZO, D.P. (2000). The physical implementation of quantum computation. *Fortschritte der Physik*, **48**, 771–783. 7

DOUÇOT, B. & IOFFE, L. (2012). Physical implementation of protected qubits. *Reports on Progress in Physics*, **75**, 072001. 1, 12

DOUÇOT, B. & VIDAL, J. (2002). Pairing of cooper pairs in a fully frustrated josephson-junction chain. *Physical review letters*, **88**, 227005. 27, 45

EINARSSON, T. (1990). Fractional statistics on a torus. *Physical review letters*, **64**, 1995. 66

EISERT, J., CRAMER, M. & PLENIO, M.B. (2010). Colloquium: Area laws for the entanglement entropy. *Reviews of Modern Physics*, **82**, 277. 69

ELION, W., WACHTERS, J., SOHN, L. & MOOIJ, J. (1993). Observation of the aharonov-casher effect for vortices in josephson-junction arrays. *Physical review letters*, **71**, 2311–2314. 45, 49

FAORO, L. & IOFFE, L.B. (2008). Microscopic origin of low-frequency flux noise in josephson circuits. *Physical review letters*, **100**, 227005. 17

FAZIO, R. & SCHÖN, G. (1991). Charge and vortex dynamics in arrays of tunnel junctions. *Physical Review B*, **43**, 5307. xi, 31, 37, 40

FAZIO, R. & VAN DER ZANT, H. (2001). Quantum phase transitions and vortex dynamics in superconducting networks. *Physics Reports*, **355**, 235–334. 39, 40, 103

FEIGEL'MAN, M.V., IOFFE, L.B., GESHKENBEIN, V.B. & BLATTER, G. (2000). Andreev spectroscopy for superconducting phase qubits. *Journal of Low Temperature Physics*, **118**, 805–816. 17

FERGUSON, D.G., HOUCK, A. & KOCH, J. (2013). Symmetries and collective excitations in large superconducting circuits. *Physical Review X*, **3**, 011003. 54

FEYNMAN, R.P. (1982). Simulating physics with computers. *International journal of theoretical physics*, **21**, 467–488. 5

FIDKOWSKI, L. (2010). Entanglement spectrum of topological insulators and superconductors. *Physical review letters*, **104**, 130502. 69, 71

FOWLER, A.G., MARIANTONI, M., MARTINIS, J.M. & CLELAND, A.N. (2012). Surface codes: Towards practical large-scale quantum computation. *Physical Review A*, **86**, 032324. 5, 18

FRIEDMAN, J.R., PATEL, V., CHEN, W., TOLPYGO, S. & LUKENS, J.E. (2000). Quantum superposition of distinct macroscopic states. *nature*, **406**, 43–46. 12, 15, 17

GIRVIN, S.M. (2011). Superconducting qubits and circuits: Artificial atoms coupled to microwave photons. *École dété Les Houches*. 12

GLADCHENKO, S., OLAYA, D., DUPONT-FERRIER, E., DOUÇOT, B., IOFFE, L.B. & GERSHENSON, M.E. (2008). Superconducting nanocircuits for topologically protected qubits. *Nature Physics*, **5**, 48–53. 12, 18, 27, 45, 67

GOLDMAN, N., SATIJA, I., NIKOLIC, P., BERMUDEZ, A., MARTIN-DELGADO, M.A., LEWENSTEIN, M. & SPIELMAN, I.B. (2010). Realistic time-reversal invariant topological insulators with neutral atoms. *Phys. Rev. Lett.*, **105**, 255302. 88

GOLDMAN, N., ANISIMOVAS, E., GERBIER, F., ÖHBERG, P., SPIELMAN, I. & JUZELIŪNAS, G. (2013). Measuring topology in a laser-coupled honeycomb lattice: from chern insulators to topological semi-metals. *New Journal of Physics*, **15**, 013025. 67

GORKOV, L.P. (1959). Microscopic derivation of the ginzburg-landau equations in the theory of superconductivity. *Sov. Phys. JETP*, **9**, 1364–1367. 9

GOTTESMAN, D. (2009). An introduction to quantum error correction and fault-tolerant quantum computation. In *Quantum Information Science and Its Contributions to Mathematics, Proceedings of Symposia in Applied Mathematics*, vol. 68, 13–58. 18

GOTTESMAN, D., KITAEV, A. & PRESKILL, J. (2001). Encoding a qubit in an oscillator. *Physical Review A*, **64**, 012310. 57

GOTTFRIED, K. & YAN, T.M. (2003). *Quantum mechanics: fundamentals*. Springer. 95, 96

HALDANE, F.D.M. (1988). Model for a quantum hall effect without landau levels: Condensed-matter realization of the "parity anomaly". *Phys. Rev. Lett.*, **61**, 2015–2018. 72

HASAN, M.Z. & KANE, C.L. (2010). *Colloquium* : Topological insulators. *Rev. Mod. Phys.*, **82**, 3045–3067. 65, 68

HATSUGAI, Y. (1993). Chern number and edge states in the integer quantum hall effect. *Physical review letters*, **71**, 3697. 66, 68

HAYDEN, P. & PRESKILL, J. (2007). Black holes as mirrors: quantum information in random subsystems. *Journal of High Energy Physics*, **2007**, 120. 5

HERBUT, I. (2007). *A modern approach to critical phenomena*. Cambridge University Press. 29, 103

HSIEH, T.H. & FU, L. (2013). Bulk entanglement spectrum reveals quantum criticality within a topological state. *arXiv preprint arXiv:1305.1949*. 90

IOFFE, L. & FEIGELMAN, M. (2002). Possible realization of an ideal quantum computer in josephson junction array. *Physical Review B*, **66**, 224503. 12, 18, 27, 45

IOFFE, L., FEIGEL'MAN, M., IOSELEVICH, A., IVANOV, D., TROYER, M. & BLATTER, G. (2002). Topologically protected quantum bits using josephson junction arrays. *Nature*, **415**, 503–506. 12, 18

IVANOV, D.A. (2001). Non-abelian statistics of half-quantum vortices in p-wave superconductors. *Physical review letters*, **86**, 268. 66

JOSÉ, J.V., KADANOFF, L.P., KIRKPATRICK, S. & NELSON, D.R. (1977). Renormalization, vortices, and symmetry-breaking perturbations in the two-dimensional planar model. *Physical Review B*, **16**, 1217. 32, 103

JOSEPHSON, B.D. (1962). Possible new effects in superconductive tunnelling. *Physics Letters*, **1**, 251–253. 9

KANE, C.L. & MELE, E.J. (2005). Z_2 topological order and the quantum spin hall effect. *Phys. Rev. Lett.*, **95**, 146802. 2, 66, 72, 75, 84, 86

KITAEV, A. (2006a). Anyons in an exactly solved model and beyond. *Ann. of Phys.*, **321**, 1. 68, 86

KITAEV, A. (2006b). Protected qubit based on a superconducting current mirror. *arXiv preprint cond-mat/0609441*. iv, 1, 2, 12, 19, 21, 26, 45, 47, 48, 61

KITAEV, A. (2009). Periodic table for topological insulators and superconductors. *AIP Conference Proceedings*, **1134**. 66

KITAEV, A. & PRESKILL, J. (2006). Topological entanglement entropy. *Phys. Rev. Lett.*, **96**, 110404. 66, 68

KITAEV, A.Y. (1997). Fault-tolerant quantum computation by anyons. *arXiv preprint quant-ph/9707021*. 18

KITAEV, A.Y. (2001). Unpaired majorana fermions in quantum wires. *Physics-Uspekhi*, **44**, 131. 66

KITAEV, A.Y. (2003). Fault-tolerant quantum computation by anyons. *Annals of Physics*, **303**, 2–30. 1, 5, 18

KLITZING, K.V., DORDA, G. & PEPPER, M. (1980). New method for high-accuracy determination of the fine-structure constant based on quantized hall resistance. *Phys. Rev. Lett.*, **45**, 494–497. 65

KOCH, J., TERRI, M.Y., GAMBETTA, J., HOUCK, A.A., SCHUSTER, D., MAJER, J., BLAIS, A., DEVORET, M.H., GIRVIN, S.M. & SCHOELKOPF, R.J. (2007a). Charge-insensitive qubit design derived from the cooper pair box. *Physical Review A*, **76**, 042319. 12

KOCH, R.H., DIVINCENZO, D.P. & CLARKE, J. (2007b). Model for 1/f flux noise in squids and qubits. *Physical review letters*, **98**, 267003. 17

KOGUT, J.B. (1979). An introduction to lattice gauge theory and spin systems. *Reviews of Modern Physics*, **51**, 659. 37, 38

KOHMOTO, M. (1985). Topological invariant and the quantization of the hall conductance. *Annals of Physics*, **160**, 343 – 354. 65, 66, 67

KÖNIG, M., WIEDMANN, S., BRÜNE, C., ROTH, A., BUHMANN, H., MOLENKAMP, L.W., QI, X.L. & ZHANG, S.C. (2007). Quantum spin hall insulator state in hgte quantum wells. *Science*, **318**, 766–770. 66

KOSTERLITZ, J.M. & THOULESS, D.J. (1973). Ordering, metastability and phase transitions in two-dimensional systems. *Journal of Physics C: Solid State Physics*, **6**, 1181. 30

KUBASIAK, A., MASSIGNAN, P. & LEWENSTEIN, M. (2010). Topological superfluids on a lattice with non-abelian gauge fields. *EPL (Europhysics Letters)*, **92**, 46004. 88

LADD, T.D., JELEZKO, F., LAFLAMME, R., NAKAMURA, Y., MONROE, C. & OBRIEN, J.L. (2010). Quantum computers. *Nature*, **464**, 45–53. 5

LAHTINEN, V., LUDWIG, A.W., PACHOS, J.K. & TREBST, S. (2012). Topological liquid nucleation induced by vortex-vortex interactions in kitaev's honeycomb model. *Physical Review B*, **86**, 075115. 87

LAMBERT, N., CHEN, Y.N., CHENG, Y.C., LI, C.M., CHEN, G.Y. & NORI, F. (2013). Quantum biology. *Nature Physics*, **9**, 10–18. 5

LANDAU, L. (1937). Zur theorie der phasenumwandlungen ii. *Phys. Z. Sowjetunion*, **11**, 26–35. 65

LANDAU, L. & LIFSHITZ, E. (1958). *Statistical Physics: Course of Theoretical Physics/Translated from the Russian by E. Peierls and RF Peierls*. Pergamon Press. 65

LAUGHLIN, R.B. (1983). Anomalous quantum hall effect: an incompressible quantum fluid with fractionally charged excitations. *Physical Review Letters*, **50**, 1395–1398. 65

LEGGETT, A. (1980). Macroscopic quantum systems and the quantum theory of measurement. *Progress of Theoretical Physics Supplement*, **69**, 80–100. 6

LEGNER, M. & NEUPERT, T. (2013). Relating the entanglement spectrum of noninteracting band insulators to their quantum geometry and topology. *Phys. Rev. B*, **88**, 115114. 2, 69, 72, 74, 83, 86, 89

LEINAAS, J.M. & MYRHEIM, J. (1977). On the theory of identical particles. *Il Nuovo Cimento B Series 11*, **37**, 1–23. 18

LEVIN, M. & WEN, X.G. (2006). Detecting topological order in a ground state wave function. *Phys. Rev. Lett.*, **96**, 110405. 66, 68

LI, H. & HALDANE, F.D.M. (2008). Entanglement spectrum as a generalization of entanglement entropy: Identification of topological order in non-abelian fractional quantum hall effect states. *Phys. Rev. Lett.*, **101**, 010504. 2, 66, 67, 69

LLOYD, S. (1996). Universal quantum simulators. *Science*, **273**, 1073–1078. 5

MAKHLIN, Y., SCHÖN, G. & SHNIRMAN, A. (2001). Quantum-state engineering with josephson-junction devices. *Reviews of modern physics*, **73**, 357. 12

MANUCHARYAN, V.E., KOCH, J., GLAZMAN, L.I. & DEVORET, M.H. (2009). Fluxonium: Single cooper-pair circuit free of charge offsets. *Science*, **326**, 113–116. 12, 54

MARTINIS, J.M., NAM, S., AUMENTADO, J. & URBINA, C. (2002). Rabi oscillations in a large josephson-junction qubit. *Physical Review Letters*, **89**, 117901. 12

MATVEEV, K., LARKIN, A. & GLAZMAN, L. (2002). Persistent current in superconducting nanorings. *Physical review letters*, **89**, 096802. 25

MAZZA, L., BERMUDEZ, A., GOLDMAN, N., RIZZI, M., MARTIN-DELGADO, M.A. & LEWENSTEIN, M. (2012). An optical-lattice-based quantum simulator for relativistic field theories and topological insulators. *New Journal of Physics*, **14**, 015007. 88

MIYAKE, H., SIVILOGLOU, G.A., KENNEDY, C.J., BURTON, W.C. & KETTERLE, W. (2013). Realizing the harper hamiltonian with laser-assisted tunneling in optical lattices. *Physical review letters*, **111**, 185302. 66

MOOIJ, J., ORLANDO, T., LEVITOV, L., TIAN, L., VAN DER WAL, C.H. & LLOYD, S. (1999). Josephson persistent-current qubit. *Science*, **285**, 1036–1039. 12, 17

MOURIK, V., ZUO, K., FROLOV, S., PLISSARD, S., BAKKERS, E. & KOUWENHOVEN, L. (2012). Signatures of majorana fermions in hybrid superconductor-semiconductor nanowire devices. *Science*, **336**, 1003–1007. 21, 66

NAKAMURA, Y., CHEN, C. & TSAI, J. (1997). Spectroscopy of energy-level splitting between two macroscopic quantum states of charge coherently superposed by josephson coupling. *Physical review letters*, **79**, 2328. 14

NAKAMURA, Y., PASHKIN, Y.A. & TSAI, J. (1999). Coherent control of macroscopic quantum states in a single-cooper-pair box. *Nature*, **398**, 786–788. 12, 15

NAYAK, C., SIMON, S.H., STERN, A., FREEDMAN, M. & DAS SARMA, S. (2008). Non-abelian anyons and topological quantum computation. *Rev. Mod. Phys.*, **80**, 1083–1159. 5, 18, 65

NIELSEN, M.A. & CHUANG, I.L. (2010). *Quantum computation and quantum information*. Cambridge university press. 6

PACHOS, J.K. (2012). *Topological Quantum Computation*. Cambridge University Press, Cambridge. 5, 18, 65, 68

PACHOS, J.K., ALBA, E., LAHTINEN, V. & GARCIA-RIPOLL, J.J. (2013). Seeing majorana fermions in time-of-flight images of staggered spinless fermions coupled by *s*-wave pairing. *Phys. Rev. A*, **88**, 013622. 2, 67, 72, 73, 74, 75, 84, 86, 88

PALADINO, E., GALPERIN, Y., FALCI, G. & ALTSHULER, B. (2014). 1/f noise: Implications for solid-state quantum information. *Reviews of Modern Physics*, **86**, 361. 15, 17

PEOTTA, S., GIBERTINI, M., DOLCINI, F., TADDEI, F., POLINI, M., IOFFE, L., FAZIO, R. & MACDONALD, A. (2011). Josephson current in a four-terminal superconductor/exciton-condensate/superconductor system. *Physical Review B*, **84**, 184528. 27

PESCHEL, I. (2003). Calculation of reduced density matrices from correlation functions. *J. Phys. A: Math. Gen.*, **36**, L205. 70, 71, 83

POP, I.M., PROTOPOPOV, I., LECOCQ, F., PENG, Z., PANNETIER, B., BUISSON, O. & GUICHARD, W. (2010). Measurement of the effect of quantum phase slips in a josephson junction chain. *Nature Physics*, **6**, 589–592. 25

PRICE, H.M. & COOPER, N.R. (2012). Mapping the berry curvature from semiclassical dynamics in optical lattices. *Phys. Rev. A*, **85**, 033620. 67

QI, X.L. & ZHANG, S.C. (2011). Topological insulators and superconductors. *Rev. Mod. Phys.*, **83**, 1057–1110. 65, 90

QI, X.L., KATSURA, H. & LUDWIG, A.W. (2012). General relationship between the entanglement spectrum and the edge state spectrum of topological quantum states. *Physical review letters*, **108**, 196402. 69

RAUSSENDORF, R. & HARRINGTON, J. (2007). Fault-tolerant quantum computation with high threshold in two dimensions. *Physical review letters*, **98**, 190504. 5, 18

READ, N. & GREEN, D. (2000). Paired states of fermions in two dimensions with breaking of parity and time-reversal symmetries and the fractional quantum hall effect. *Physical Review B*, **61**, 10267. 66, 67, 68, 72, 73

REZNIK, B. & AHARONOV, Y. (1989). Question of the nonlocality of the aharonov-casher effect. *Physical Review D*, **40**, 4178. 49

ROKHINSON, L.P., LIU, X. & FURDYNA, J.K. (2012). The fractional ac josephson effect in a semiconductor-superconductor nanowire as a signature of majorana particles. *Nature Physics*, **8**, 795–799. 66

ROUSHAN, P., NEILL, C., CHEN, Y., KOLODRUBETZ, M., QUINTANA, C., LEUNG, N., FANG, M., BARENDS, R., CAMPBELL, B., CHEN, Z. *et al.* (2014). Observation of topological transitions in interacting quantum circuits. *arXiv preprint arXiv:1407.1585.* 67, 90

RYU, S. & HATSUGAI, Y. (2002). Topological origin of zero-energy edge states in particle-hole symmetric systems. *Physical review letters*, **89**, 077002. 66

SCHNYDER, A.P., RYU, S., FURUSAKI, A. & LUDWIG, A.W.W. (2008). Classification of topological insulators and superconductors in three spatial dimensions. *Phys. Rev. B*, **78**, 195125. 66

SCHRIEFFER, J.R. (1999). *Theory of superconductivity, Advanced book classics*. Perseus Books, Reading. 6

SCHUMACHER, B. (1995). Quantum coding. *Physical Review A*, **51**, 2738. 5

SHENG, D.N., WENG, Z.Y., SHENG, L. & HALDANE, F.D.M. (2006). Quantum spin-hall effect and topologically invariant chern numbers. *Phys. Rev. Lett.*, **97**, 036808. 86

SHOR, P.W. (1994). Algorithms for quantum computation: discrete logarithms and factoring. In *Foundations of Computer Science, 1994 Proceedings., 35th Annual Symposium on*, 124–134, IEEE. 5

SHOR, P.W. (1995). Scheme for reducing decoherence in quantum computer memory. *Physical review A*, **52**, R2493. 5, 8, 17

SHOR, P.W. (1996). Fault-tolerant quantum computation. In *Foundations of Computer Science, 1996. Proceedings., 37th Annual Symposium on*, 56–65, IEEE. 5, 8, 17

SHOR, P.W. (1997). Polynomial-time algorithms for prime factorization and discrete logarithms on a quantum computer. *SIAM journal on computing*, **26**, 1484–1509. 5

SPILLER, T.P., MUNRO, W.J., BARRETT, S.D. & KOK, P. (2005). An introduction to quantum information processing: applications and realizations. *Contemporary Physics*, **46**, 407–436. 6

SPIŠÁK, D. (1993). Self-consistent mean-field study of the anisotropic two-dimensional *xy* model. *Physica B: Condensed Matter*, **190**, 407–412. 41

STEANE, A.M. (1996). Error correcting codes in quantum theory. *Physical Review Letters*, **77**, 793. 5, 8, 17

STERN, A. (1994). Quantum hall fluid of vortices in a two-dimensional array of josephson junctions. *Physical Review B*, **50**, 10092. 32

STONE, M. (1992). *Quantum Hall Effect*. World Scientific Publishing Co., Inc. 66, 67

SWANSON, M. (1992). *Path Integrals and Quantum Processes*. Academic Press. 31

THOULESS, D.J., KOHMOTO, M., NIGHTINGALE, M.P. & DEN NIJS, M. (1982). Quantized hall conductance in a two-dimensional periodic potential. *Phys. Rev. Lett.*, **49**, 405–408. 65, 66, 67

TINKHAM, M. (2004). *Introduction to superconductivity*. Dover, 2nd edn. 6, 11, 38, 52

TSUI, D.C., STORMER, H.L. & GOSSARD, A.C. (1982). Two-dimensional magnetotransport in the extreme quantum limit. *Physical Review Letters*, **48**, 1559. 65

TURNER, A.M., ZHANG, Y. & VISHWANATH, A. (2009). Band topology of insulators via the entanglement spectrum. *arXiv preprint arXiv:0909.3119*. 69, 71

VAN DER WAL, C.H., TER HAAR, A., WILHELM, F., SCHOUTEN, R., HARMANS, C., ORLANDO, T., LLOYD, S. & MOOIJ, J. (2000). Quantum superposition of macroscopic persistent-current states. *Science*, **290**, 773–777. 12, 17

VAN WEES, B. (1990). Aharonov-bohm–type effect for vortices in josephson-junction arrays. *Physical review letters*, **65**, 255. 49

VAN WEES, B. (1991). Duality between cooper-pair and vortex dynamics in two-dimensional josephson-junction arrays. *Physical Review B*, **44**, 2264. 39

VERLINDE, E. & VERLINDE, H. (2013). Black hole entanglement and quantum error correction. *Journal of High Energy Physics*, **2013**, 1–34. 5

VILLAIN, J. (1975). Theory of one-and two-dimensional magnets with an easy magnetization plane. ii. the planar, classical, two-dimensional magnet. *Journal de Physique*, **36**, 581–590. 32, 103

VION, D., AASSIME, A., COTTET, A., JOYEZ, P., POTHIER, H., URBINA, C., ESTEVE, D. & DEVORET, M.H. (2002). Manipulating the quantum state of an electrical circuit. *Science*, **296**, 886–889. 12, 15, 18

VOLOVIK, G.E. (2009). *The universe in a helium droplet*, vol. 117. Oxford University Press. 67, 72

WALLRAFF, A., SCHUSTER, D.I., BLAIS, A., FRUNZIO, L., HUANG, R.S., MAJER, J., KUMAR, S., GIRVIN, S.M. & SCHOELKOPF, R.J. (2004). Strong coupling of a single photon to a superconducting qubit using circuit quantum electrodynamics. *Nature*, **431**, 162–167. 12, 18

WANG, D.S., FOWLER, A.G. & HOLLENBERG, L.C. (2011). Surface code quantum computing with error rates over 1%. *Physical Review A*, **83**, 020302. 18

WANG, L., SOLUYANOV, A.A. & TROYER, M. (2013). Proposal for direct measurement of topological invariants in optical lattices. *Phys. Rev. Lett.*, **110**, 166802. 67, 90

WEN, X.G. (1995). Topological orders and edge excitations in fractional quantum hall states. *Advances in Physics*, **44**, 405–473. 65

WEN, X.G. (2004). *Quantum Field Theory of Many-Body Systems*. Oxford University Press. 65

WEN, X.G. & NIU, Q. (1990). Ground-state degeneracy of the fractional quantum hall states in the presence of a random potential and on high-genus riemann surfaces. *Physical Review B*, **41**, 9377. 66

WILCZEK, F. (1982). Magnetic flux, angular momentum, and statistics. *Physical Review Letters*, **48**, 1144. 18

WILLETT, R.L., PFEIFFER, L.N. & WEST, K. (2009). Measurement of filling factor 5/2 quasiparticle interference with observation of charge e/4 and e/2 period oscillations. *Proceedings of the National Academy of Sciences*, **106**, 8853–8858. 21

WOOTTERS, W.K. & ZUREK, W.H. (1982). A single quantum cannot be cloned. *Nature*, **299**, 802–803. 17

XIANG, Z.L., ASHHAB, S., YOU, J. & NORI, F. (2013). Hybrid quantum circuits: Superconducting circuits interacting with other quantum systems. *Reviews of Modern Physics*, **85**, 623. 6

ZAGOSKIN, A. & BLAIS, A. (2008). Superconducting qubits. *arXiv preprint arXiv:0805.0164*. 12

ZAK, J. (1989). Berrys phase for energy bands in solids. *Physical review letters*, **62**, 2747. 66